INFORMATION TO USERS

The most advanced technology has been used to photograph and reproduce this manuscript from the microfilm master. UMI films the text directly from the original or copy submitted. Thus, some thesis and dissertation copies are in typewriter face, while others may be from any type of computer printer.

The quality of this reproduction is dependent upon the quality of the copy submitted. Broken or indistinct print, colored or poor quality illustrations and photographs, print bleedthrough, substandard margins, and improper alignment can adversely affect reproduction.

In the unlikely event that the author did not send UMI a complete manuscript and there are missing pages, these will be noted. Also, if unauthorized copyright material had to be removed, a note will indicate the deletion.

Oversize materials (e.g., maps, drawings, charts) are reproduced by sectioning the original, beginning at the upper left-hand corner and continuing from left to right in equal sections with small overlaps. Each original is also photographed in one exposure and is included in reduced form at the back of the book.

Photographs included in the original manuscript have been reproduced xerographically in this copy. Higher quality 6" x 9" black and white photographic prints are available for any photographs or illustrations appearing in this copy for an additional charge. Contact UMI directly to order.

U·M·I

University Microfilms International
A Bell & Howell Information Company
300 North Zeeb Road, Ann Arbor, MI 48106-1346 USA
313/761-4700 800/521-0600

Order Number 9108194

Sound propagation in complex fluids

Ye, Ling, Ph.D.

City University of New York, 1990

U·M·I

300 N. Zeeb Rd.
Ann Arbor, MI 48106

A

SOUND PROPAGATION IN COMPLEX FLUIDS

by

LING YE

A dissertation submitted to the Graduate Faculty in Physics in partial fulfillment of the requirements for the degree of Doctor of Philosophy, The City University of New York.

1990

This manuscript has been read and accepted for the Graduate Faculty in Physics in satisfaction of the dissertation requirement for the degree of Doctor of Philosophy.

July 6 1990
Date

Robert Genack
Chair of Examining Committee

July 23, 1990
Date

Joseph B. Krieger
Executive Officer

Dr. D. A. Weitz

Dr. N. Garcia

Dr. L. A. Ferrari

Dr. H. Z. Cummins

Supervisory Committee

The City University of New York

Abstract

SOUND PROPAGATION IN COMPLEX FLUIDS

by

LING YE

Advisers: Drs. David A. Weitz and Azi Z. Genack

In this thesis the sound propagation in complex fluids is studied. The complex fluid systems we study include AOT micelles, AOT microemulsions, a quaternary microemulsion and PMMA hard sphere colloids. We show that the sound propagation is modified by the properties of the dispersed phase in the system, the rigidity and the size of the droplets, and the interaction between the droplets. Therefore, measurements of the sound velocity as a function of the droplet concentration and the frequency allow us to study the contribution of the structural correlations to the elastic behavior of the system.

In the micelle and microemulsion systems, the size of the spherical droplets are small compared with the wavelength of the sound. In the AOT micelles and microemulsions, an attractive interaction between the droplets leads to the formation of short-lived connecting network. Due to the rigidity of the dispersed phase, the network can support shear, which contributes to the longitudinal elastic modulus of the system. Therefore, measurements results of the sound velocity as a function of the droplet volume fraction in the MHz-GHz frequency regime indicate a pronounced viscoelastic behavior. We find that the additional increase of the

elastic modulus at high frequency due to the rigidity of the networks exhibits a power-law scaling, which suggests a dynamic rigidity percolation in the system. The variation of the strength of the attractive interaction, achieved by changing the oil solvent or by varying the droplet size in the microemulsions, leads to a change in the viscoelastic behavior, since the characteristic time of the interaction between droplets is changed. By contrast, in the quaternary microemulsion, the repulsive interaction between droplets is dominant. We find that increasing the repulsive interaction by adding ionic charges to the system has no effect on the observed elastic behavior. The measurements of the sound velocity as a function of droplet volume fraction in the MHz-GHz frequency regime indicate that the elastic behavior in this microemulsion system may be strongly affected by the interaction between alcohol and water molecules, since it exhibits a behavior that is reminiscent of a binary mixture of water and alcohol.

In the PMMA hard sphere colloids, the wavelength of the sound is comparable to the size of the solid spheres. We find two novel propagating acoustic excitations. One has a velocity intermediate between that of the fluid and the solid phases, and is interpreted as an acoustic wave propagating through the composite medium of fluid and solid spheres. The second has a velocity slower than both that of the solid and the fluid phases and is interpreted as a propagating interfacial wave.

Acknowledgements

I would like to thank those with whom I have worked and from whom I have learned a great deal during my thesis research at Exxon, as well as my graduate course at Queens college of CUNY.

I have received most benefits, as a student who wants to learn physics, from my thesis supervisor, Dr. Dave Weitz. He has never stopped encouraging me to enjoy physics by solving one tough problem after another in my research work, and finally led me to where I can recognize my way to being a physicist. I would like to thank Dr. Ping Sheng and Dr. John Huang for those fruitful discussions and suggestions during the years I have worked in Exxon. I also like to thank Dr. Cummins, who was a member of my dissertation committee and was a great help to me with his experience in Brillouin scattering.

I want to thank Dr. Genack, Dr. Garcia, Dr. Ferrari and Dr. Laza of Queens college. Not only did they teach me in graduate courses, but they also helped me to start my life in this country.

Finally, I wish to thank my husband, Qiqing Yu, who always fully understands and supports me.

This thesis is dedicated to my mother, Xiusi Hou, from whom I know what is love in the life.

Annandale, New Jersey

July, 1990

CONTENTS

LIST OF FIGURES

Chapter 1

INTRODUCTION

Light scattering from thermally excited sound waves, or Brillouin scattering, is a powerful method for investigating sound wave propagation in liquids and solids, and for measuring the elastic properties of liquids and solids.[1–3] Research on pure liquids has demonstrated that these measurements can yield valuable information, including the elastic modulus and transport coefficients of the materials.[4,5] For molecular fluids, Brillouin scattering, which probes hypersonic wave propagation, can be combined with ultrasonic techniques to measure the frequency dispersion of the sound wave propagation and to study the relaxational processes in the fluids.[6] Moreover, if the frequency is high enough, some liquids may respond elastically to the perturbation, allowing one to study their viscoelastic behavior. A fluid is viscoelastic, if, above a certain frequency, it has insufficient time to flow in response to the applied strain rate, and thus reacts elastically in the same way as a solid does.

While simple fluids, molecular fluids and viscoelastic fluids have all been studied extensively using Brillouin scattering, considerably less attention has been devoted to complex fluids, which possess structure on length scales larger than the molecules that make up the fluid. This thesis is primarily concerned with the study of sound wave propagation in complex fluids, including in micelle[7] and microemulsion systems[8] and in suspensions of PMMA colloids[9] which behave as hard spheres. All of these systems consist of spherical particles dispersed in a continuous medium. The acoustic measurements discussed here probe the contribution of the dynamic structure to the elastic properties of a system, and investigate the nature of sound wave propagation in an inhomogeneous material. We are interested in how the sound propagation is affected by the existence of the dispersed

medium in complex fluids.

In 1922, Brillouin predicted[10] that the scattered light from a homogeneous fluid contains a doublet with a frequency shift due to the thermally induced sound waves in the system. The density fluctuations in the liquid scatter the light. They are induced by both entropy and pressure fluctuations. The entropy fluctuations lead to a nonpropagating mode, centered about the zero frequency shift in the spectrum. The pressure fluctuations lead to two propagating modes which are shifted in frequency and reflect the longitudinal sound waves in the fluid.

The Brillouin scattering technique has since been widely used to study hypersonic waves in simple liquids.[3] A typical Brillouin spectrum measured in our experiments for a simple liquid is shown in Fig. 1.1. It is composed of three Lorentzian peaks: the central or Rayleigh peak and the Brillouin doublet. The Rayleigh peak results from the nonpropagating entropy fluctuations, and reflects a mode due to the diffusion of heat. Thus the width of the central peak is determined by the thermal diffusivity. The Brillouin peaks have a frequency shift, ω, which is the frequency difference between the incident photon and the scattered photon, and is equal to the frequency of the thermally excited sound wave in the system, $|\omega| = qv$, where q is the scattering wave vector, and v is the velocity of sound in the liquid. The width of the peak is determined by the attenuation of the sound wave, which depends on the longitudinal viscosity $\eta_l = \eta_v + \frac{4}{3}\eta_s$ with η_v and η_s being the bulk and the shear viscosities, respectively. Therefore, measurements of the Brillouin peak can, in principle, determine both the sound velocity and the viscosity. Furthermore, the sound velocity is related to the elastic properties of the fluid by $v = \sqrt{\frac{\beta}{\rho}}$, where β is the longitudinal elastic modulus, and ρ is the density. This allows the measurement of elastic properties of the material by those techniques.

For a simple liquid, the dielectric constant, ϵ, in thermal equilibrium is in

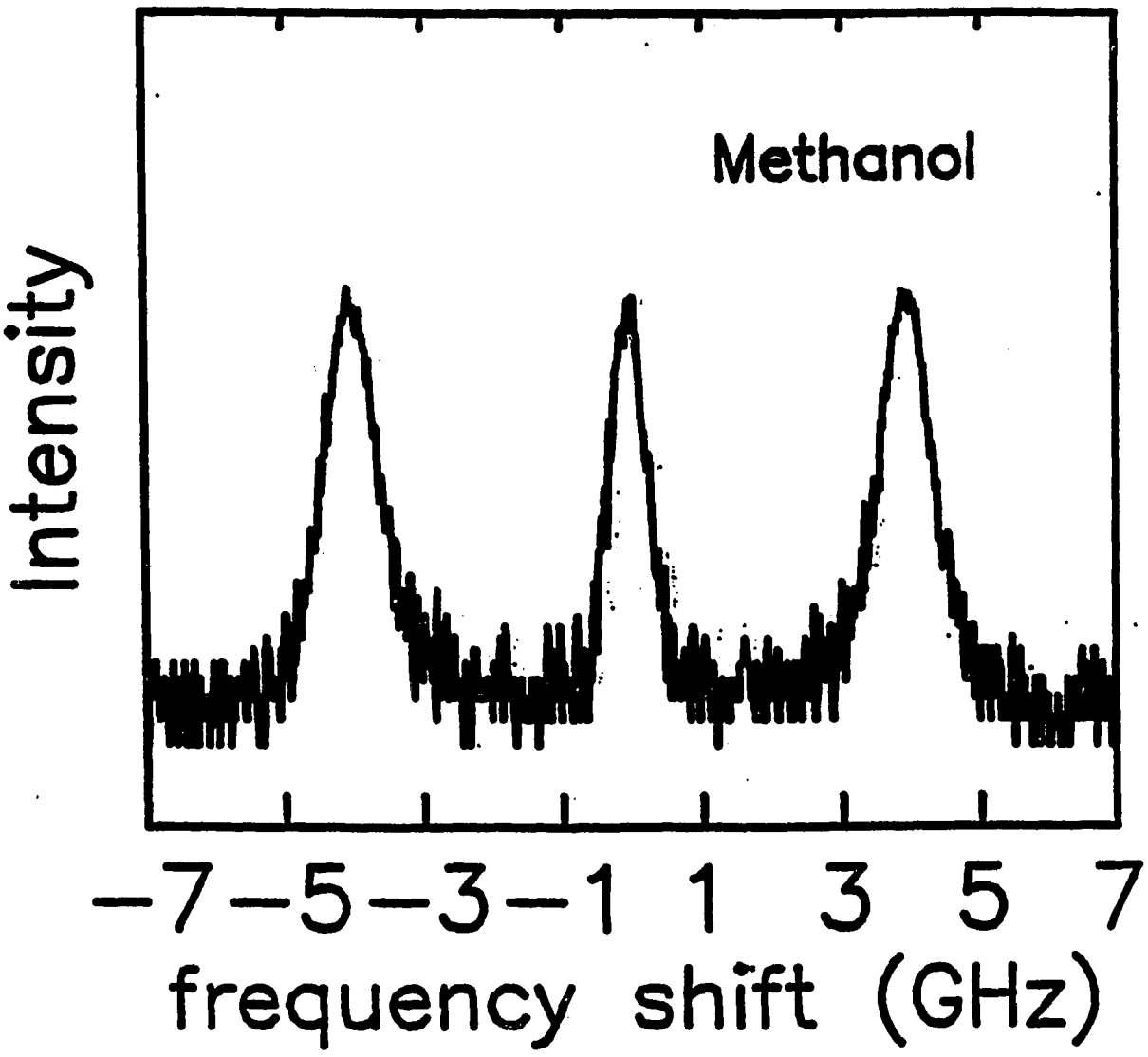

1.1 Brillouin spectrum of simple liquid methanol in 90°, with green light at 514.5Å.

general a function of the density ρ_0 and temperature T_0: $\varepsilon = \varepsilon(\rho_0, T_0)$. The local fluctuations of density and temperature lead to fluctuations in the dielectric constant given by

$$\delta\varepsilon(\mathbf{r},t) = (\frac{\partial\varepsilon}{\partial\rho})_T \delta\rho(\mathbf{r},t) + (\frac{\partial\varepsilon}{\partial T})_\rho \delta T(\mathbf{r},t) \tag{1.1}$$

The first term in eq.1.1 reflects the isothermal fluctuations of $\varepsilon(\mathbf{r},t)$ due to density fluctuations, and the second term reflects the fluctuations of $\varepsilon(\mathbf{r},t)$ at constant density due to temperature fluctuations. Experimentally, it is found[11] that $(\frac{\partial\varepsilon}{\partial T})_\rho \simeq 0$, thus the fluctuations in ε are primarily from density fluctuations. This leads to a direct correlation between density fluctuations and fluctuations in the scattered light. The intensity of the scattered light from the liquid is given by the time correlation function of the Fourier transform of $\varepsilon(\mathbf{r},t)$

$$\begin{aligned} I^s_{if}(\mathbf{q},\omega) &= < \delta\varepsilon^*_{if}(\mathbf{q},\omega)\delta\varepsilon_{if}(\mathbf{q},\omega) > \\ &\simeq (\mathbf{n}_i \cdot \mathbf{n}_f)^2 \left(\frac{\partial\varepsilon}{\partial\rho}\right)^2_T S_{\rho\rho}(\mathbf{q},\omega) \end{aligned} \tag{1.2}$$

Where $\mathbf{n}$ is a unit vector in the direction of light propagation, and i, f denote the initial and final states, respectively. The spectral density of the autocorrelation function of density fluctuations, $S_{\rho\rho}$, in eq. (1.2) is given by

$$S_{\rho\rho}(\mathbf{q},\omega) = \frac{1}{2\pi}\int_{-\infty}^{+\infty} dt\, e^{-i\omega t} < \delta\rho^*(\mathbf{q},0)\delta\rho(\mathbf{q},t) > \tag{1.3}$$

According to thermodynamic theory, one can represent the density fluctuations by entropy fluctuations and pressure fluctuations:

$$\delta\rho = (\frac{\partial\rho}{\partial S})_P \delta S + (\frac{\partial\rho}{\partial P})_S \delta P \tag{1.4}$$

Since S and P are statistically independent, eq. (1.2)-(1.4) result in

$$I^s_{if}(q,\omega) = (\mathbf{n}_i \cdot \mathbf{n}_f)^2 \left(\frac{\partial\varepsilon}{\partial\rho}\right)^2_T \left[\left(\frac{\partial\rho}{\partial S}\right)^2_P < |\delta S|^2 > + \left(\frac{\partial\rho}{\partial P}\right)^2_S < |\delta P|^2 >\right] \tag{1.5}$$

The correlation function $< |\delta\rho|^2 >$ in eq. (1.3) can be obtained by solving the hydrodynamic equations, which are expressed locally by the conservation equations for the number density $\rho(\mathbf{r},t)$, the momentum density $\mathbf{g}(\mathbf{r},t)$ and the energy density $e(\mathbf{r},t)$[12,13]:

$$\frac{\partial\rho}{\partial t} + \rho_o \nabla\cdot\mathbf{u} = 0 \tag{1.6a}$$

$$\rho_o \frac{\partial\mathbf{u}}{\partial t} + \nabla P - \eta_l \nabla(\nabla\cdot\mathbf{u}) = 0 \tag{1.6b}$$

$$\rho_o T_o \frac{\partial S}{\partial t} - \lambda\nabla^2 T = 0 \tag{1.6c}$$

Where u is the velocity of the fluid, λ is the thermal conductivity, and the subscript o denotes equilibrium quantities. The correlation function $< \delta\rho^*(\mathbf{q},0)\delta\rho(\mathbf{q},i\omega) >$ is then obtained by solving those equations and by Fourier transformation. For most pure fluids, the damping of sound waves is small compared with the sound velocity, which means the width of the Brillouin peaks, Γq^2, is much smaller than the Brillouin frequency shift, $\Gamma q^2 << \omega$. Then the calculated spectrum can be simplified into a sum of Lorentzian line shapes.[1,12] The *Rayleigh line* is centered at the incident light frequency and is broadened by the lifetime of the entropy waves, $[\rho C_P/\lambda]q^2$, where C_P is the specific heat at constant pressure. The *Brillouin lines* are centered at the frequencies $\pm\omega$ and are broadened by the lifetime of sound waves, $1/\Gamma$, where $\Gamma = \frac{1}{2}[(\eta_v + \frac{4}{3}\eta_s)/\rho]\, q^2$.

In 1934, Landau and Placzek predicted[14] that the ratio of the intensity of Rayleigh peak to Brillouin doublets should be

$$\frac{I_c}{2I_B} = \frac{C_p}{C_v} - 1 \tag{1.7}$$

where C_p and C_v are the specific heats at constant pressure and constant volume. This can be simply derived from eq. (1.2) and (1.5) as follows. The evaluations of mean-square fluctuations of density and pressure give $< |\rho|^2 >= \frac{1}{V}\rho^2 k_B T\chi_T$, where χ_T is the isothermal compressibility, and $< |P|^2 >= \frac{1}{V\chi_S} k_B T$, where χ_S

is the adiabatic compressibility. Since pressure fluctuations are responsible for Brillouin doublets, and $\chi_S = \rho^{-1}(\frac{\partial \rho}{\partial P})_S$ by definition, then

$$\begin{aligned}\frac{I_c + 2I_B}{2I_B} &= \frac{<|\rho|^2>}{(\frac{\partial \rho}{\partial P})_S^2 <|P|^2>} \\ &= \frac{\frac{\rho^2}{V} k_B T \chi_T}{\frac{\rho^2}{V \chi_S} k_B T \chi_S^2} \\ &= \frac{\chi_T}{\chi_S} \\ &= \frac{C_P}{C_v} \end{aligned} \tag{1.8}$$

Experimental results on simple fluids have not only confirmed the Landau-Placzek prediction, but also demonstrated the possibility of the study of structure contributions to the sound propagation at high frequencies.[4,12] Cummins *et al* measured[4] the Laudau-Placzek ratio for 11 common liquids. They found that a modification of the Landau-Placzek equation is needed in some molecular fluids, such as carbon tetrachloride CCl_4, due to the effects of dispersion.

Figure 1.2 shows the Brillouin spectrum of CCl_4. One can compare the spectral distribution for CCl_4 with that of methanol shown in Fig. 1.1. In the CCl_4 spectrum, there is a continuous background, or Mountain peak, between the Rayleigh peak and Brillouin doublets. Carome *et al* measured[6] the sound velocity and its attenuation using both ultrasonic and light scattering techniques, and they found that both the sound velocity, v, and the damping of the sound, Δv, are frequency dependent. Mountain realized that the additional central peak was induced by the relaxation processes in the fluid, and formulated a rather general theory. In his model,[13] Mountain attributes the structural relaxation of the liquid to the elasticity of the system. He pointed out that in CCl_4 there is a weak coupling between the molecular internal degrees of freedom and the translational motion of the molecules. This coupling is reflected in the density fluctuations through the longitudinal viscosity, $\eta_l(\omega)$, which is a function of frequency. Mountain used a

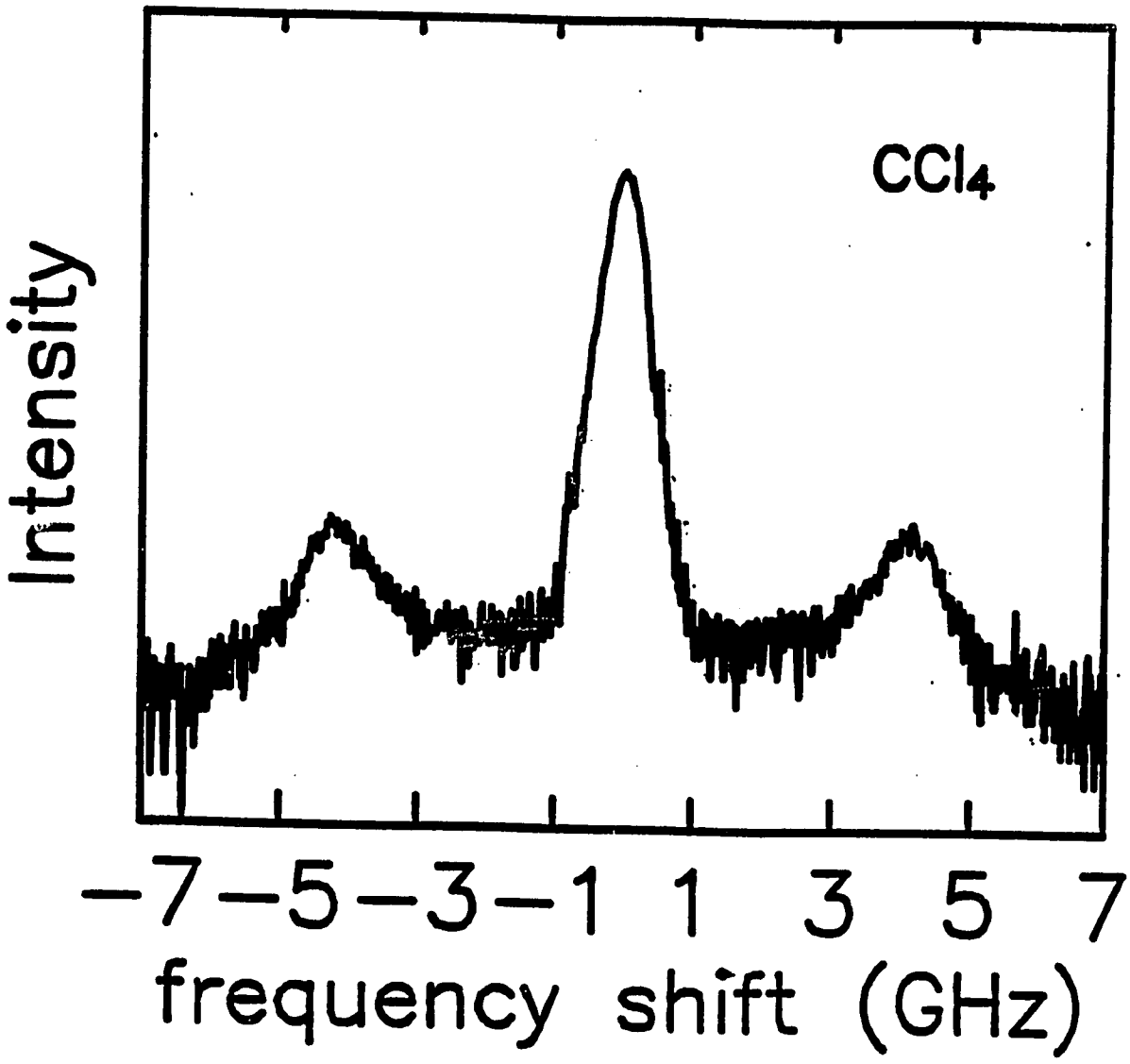

1.2 Brillouin spectrum of molecular liquid CCl_4 in 90°, with green light at 514.5Å.

generalized hydrodynamic theory, replacing the constant viscosities with frequency dependent quantities, $\eta_v(\omega\tau)$ and $\eta_s(\omega\tau)$, where the subscripts v and s denote the bulk and shear quantities respectively. The width of the additional central peak is found to be roughly τ^{-1}, where τ is the characteristic relaxation time in the molecular fluid. Mountain's formalism describes the Brillouin spectrum of CCl_4 very well. For CCl_4, τ is on the order of $10^{-11}sec$, as shown both by the spectral fitting by Gornall *et al*,[15] and by the frequency dispersion of the sound velocity measured by Carome *et al*[6]. In order to measure the contribution of structural relaxation to the elastic properties of the fluid, one must perform experiments on a time scale that is small compared to the structural relaxation time. For many molecular fluids, this relaxation time is longer than 10^{-12}sec, thus the ultrasonic and the light scattering measurements are ideally suited to study their elastic properties.

One of the most interesting aspects of the acoustic properties of complex fluids is the viscoelasticity due to the internal degrees of freedom which can dissipate energy. Complex fluids have large molecules which organize themselves on length scales of about 10Å to several microns. Thus there are many possible dissipation processes including vibrational, rotational, or configurational relaxations. The characteristic time, τ, for the dissipation process in complex fluid systems is often greater than 10^{-10}sec. When the structural relaxation time in the fluid is comparable to 10^{-10}sec, the fluid exhibits significant viscoelasticity in the hypersonic frequency range.[16,17] When a external perturbation with frequency $\omega^{-1} > \tau$ is applied to the system, the fluid responds viscously; but if $\omega^{-1} < \tau$, the fluid responds elastically, since it has insufficient time to relax. Therefore, the both the sound velocity and the attenuation can be measured as a function of frequency, and their dispersion in frequency gives the dynamical properties of the fundamental local structural rearrangements in the fluid. Even though there are a few publications

on the ultrasonic relaxation studies in microemulsion systems,[18,19] there are as yet few such investigations on complex fluids, such as microemulsions and colloidal systems.

We have studied the sound propagation in three different complex fluid systems. The first is made from the surfactant sodium di-2-ethylhexylsulfosuccinate (AOT). In micelles, the AOT surfactant molecules aggregate to form spherical droplets, which are dispersed in the continuous oil phase; in microemulsions, they stand at the interfaces of water and oil to form droplets with water cores which are dispersed in the oil. The second system consists of a quaternary component microemulsion with the surfactant polyoxyethylene-10-oleyl-ether (Brij-96), the co-surfactant butanol, and oil, and water which is the continuous phase in this system. The last system is polymethylmethacrylate (PMMA) spherical colloids which behave as a suspension of hard spheres. The similarity between these systems is that they are all composed of spherical particles dispersed in a fluid. However, the spheres for three systems have completely different characteristics. Their size can range from much smaller than the sound wavelength to comparable to the sound wavelength. Also the spheres are either aggregates of surfactant molecules, droplets of fluid coated with a shell of surfactant molecules, or solids. In addition, the interaction potentials are different. In the colloid system the interaction is very short ranged and repulsive, and is the hard sphere interaction. In the other two microemulsion systems, the interactions are either attractive or repulsive. The fundamental question one can ask is how is the sound propagation is modified by the spheres randomly suspended in the fluid, and how the results reflect the structural correlations of the spheres.

We have used both ultrasonic techniques and Brillouin scattering to measure the propagation of sound waves in AOT micelle and microemulsion systems. The sizes of the spherical droplets are $< 100\text{Å}$, which is much smaller than the sound

wavelength. The droplet phase is less compressible than the liquid phase. In addition, the interaction between the droplets is slightly attractive. We find a pronounced viscoelastic behavior in both the micelle and the microemulsion systems. The frequency dispersion of the sound velocity reflects a dynamic rigidity percolation, which results from the structural correlation of the droplets due to the attractive potential. The relaxation time, τ, which characterizes the interaction between droplets depends on the magnitude of the attractive potential. When the period of the sound wave, ω^{-1}, is comparable to or smaller than the relaxation time, the droplets form a connected network above a critical droplet concentration. Due to the rigidity of the spheres, this network can support shear. The shear modulus contributes to the longitudinal elastic modulus of the system when $\omega^{-1} < \tau$, and thus leads to a pronounced viscoelastic behavior in the system. The longitudinal elastic modulus, β, increases at high frequency, thus there is frequency dispersion in the velocity of sound. Since the droplets are very small compared with the sound wavelength λ_s, we use an effective medium theory to calculate the elastic modulus as a function of droplet volume fraction at each frequency. The results indicate that the shear modulus of the droplet phase is a function of frequency, and varies with a Debye relaxation form like the measured sound velocity. We also find that the relaxation time depends on the magnitude of the attractive interaction between the droplets, which can be varied by changing the droplet sizes or using different alkanes in the solvent. The relaxation time given from the Debye relaxation fit of the effective medium theory of the data is consistent with that obtained from fitting the Brillouin spectra using Mountain's formula.

A second microemulsion system that is studied using both ultrasonic techniques and Brillouin scattering is the four component system consisting of the surfactant Brij-96, the cosurfactant butanol, and oil, and water. In contrast to the AOT microemulsions, the interaction between the droplets is repulsive. In

AOT micelles and microemulsions, oil is the continuous phase. Thus the polar heads of the surfactant molecules are in the droplet cores while the long tails are penetrating in the oil phase. The overlapping of the AOT molecular tails between droplets leads to a short range, weak attractive interaction. However, in the Brij-96 quaternary microemulsions, water is a continuous phase. The surfactant molecular tails are packed inside the oil droplets, which are surrounded by the polar heads of the surfactant and cosurfactant molecules. Therefore, there is no attractive interaction between droplets and the repulsive interaction is dominant. The results indicate that the sound velocity is strongly affected by the interaction of the water and the alcohol. It has been found that in binary mixtures of water and alcohol, the sound velocity has a maximum at a critical alcohol concentration. The critical concentration depends on the solubility of the alcohol in water and on the temperature. The interpretation of this is due to the association complexes formed by water and alcohol molecules. Thus the rigidity is increased by the stiffness of the association complexes. A very similar velocity maximum is found in our microemulsion system, where the critical butanol concentration is determined by the solubility of butanol in water. In addition, we find that increasing the repulsive interaction between the droplets by adding charges in the microemulsion system has no obvious effect on the results. Unlike the AOT microemulsions where the attractive interaction between droplets leads to the observed viscoelastic behavior, this quaternary microemulsion shows that the enhanced repulsive interaction between droplets does not affect the structural correlation significantly, thus no different elastic behavior is found on the system. Due to the complexity of this four component microemulsion systems, a full understanding of the results still awaits more theoretical work.

The last system we have studied consists of suspensions of PMMA hard sphere colloids. The spheres are solid balls with a layer of adsorbed polymer with a

thickness of ~15nm. The diameters of the spheres are 370 or 680nm, including the polymer layers. We use dodecane and carbon disulphide as the suspending fluid allowing us to index-match the particles, eliminating multiple scattering. Since the size of the particles is comparable to the sound wavelength λ_s, we can investigate the sound propagation for a wide range of wave vectors q, where $qd < \pi$, $qd \simeq \pi$ and $qd > \pi$, corresponding to $\lambda > d$, $\lambda \sim d$ and $\lambda < d$, respectively. The results show a novel form of acoustic wave propagation. First of all, in the range of $qd < \pi$, when $\lambda_s > d$, the sound propagation can be described by effective medium theory, as expected. As q is increased and $qd \simeq \pi$, which means λ_s is comparable to the size of the spheres, an additional longitudinal acoustic mode appears. When $qd > \pi$, the two modes are clearly resolved in the Brillouin spectra. One of the modes has a velocity intermediate between that of the solid and fluid phases, and the other mode has a velocity slower than that of both the two pure phases. By varying the scattering angle, and therefore q, we measure the dispersion curves, ω as a function of q. The frequency of the fast mode increases with sphere concentration, while the frequency of the slow mode decreases with sphere concentration. The fast mode is a longitudinal acoustic mode that propagates through both the liquid and solid phases. The slow mode is interpreted as a coupled interface wave.

The final set of experiments to be discussed concerns measurements of the optical phonon relaxation using picosecond Raman scattering. The phonon life-time measured from the Raman linewidth is found to be on the order of 10^{-12}sec. However, the measurements are rather uncertain, since other factors can also affect the linewidth, such as defects in the lattice. In the time domain measurements, the decay of the intensity of anti-Stokes Raman peak as a function of time is measured. This allows direct investigations of the relaxation of the thermally excited phonon population. Using pump-probe time-resolved Raman scattering, we find that the thermally excited optical phonon population relaxation time in crystal

germanium is about 7 picoseconds at a temperature of 77K. The pulse duration is less than 3 picoseconds. We also measure the temperature dependence of the phonon relaxation time. We find a discrepancy in the temperature dependence of the measured relaxation times between our work and the linewidth measurements by Cardona *et al.*[20] The interpretation of this discrepancy is that the inverse of the linewidth is the sum of phonon lifetime and the pure dephasing contributions due to the scattering of the phonon by isotopic disorder. On the other hand, the phonon population lifetime from the time domain measurement reflects not only the decay of the optical phonon, but also the inverse processes which replenish the phonon population. The longer lifetime of the optical phonons is given by the time domain measurements.

The remainder of this thesis is organized as follows: in the next chapter, the details of the experimental techniques, both Brillouin scattering and ultrasonic techniques, will be given. The apparatus, the methods, and the experimental error sources are discussed. In chapter three, we discuss the study of dynamic rigidity percolation in AOT micelles in decane. In chapter four, we discuss further the sound propagation in AOT micelles and microemulsions as the interaction energy between the particles is varied. In chapter five, we report an unexpected result from another microemulsion system, made up of a water continuous phase so there is no attraction between the droplets. In chapter six, we discuss the novel acoustic propagation in hard sphere PMMA colloids, where we have found more than one longitudinal sound wave propagating through the disordered system. The last chapter is a study of optical phonon population relaxation in crystal germanium using picosecond Raman scattering techniques.

References

[1] B. J. Berne and R. Pecora. "Dynamic Light Scattering" John Wiley & Sons,Inc. New York, (1976)

[2] B. Chu. "Laser Light Scattering" **Ann. Rev. Phys. Chem.** 21, 1450 (1970)

[3] P. A. Fleury and J. P. Boon. "Laser Light Scattering In Fluid Systems" **Phys. Rev.** (1969)

[4] H. Z. Cummins and R. W. Gammon **J. Chem. Phys.** 44, 2785-2797 (1966)

[5] W. H. Nichola, C. R. Kunsitis-Swyt and S. P. Singal. **J. Chem. Phys.** 51, 5659-5662 (1969)

[6] E. F. Carome, W. H. Nichols, C. R. Kunsitis-Swyt and S. P. Singal. **J. Chem. Phys.** 49, 1013-1017 (1968)

[7] L. Ye. D. A. Weitz, P. Sheng, S Bhattacharya, J. H. Huang and M. J. Higgins. **Phys. Rev. Lett.** 63, 263 (1989)

[8] L. Ye. D. A. Weitz, P. Sheng, and J. H. Huang. "Dynamic Rigidity Percolation In AOT micelles and Microemulsions" **MRS Proceedings** (1990)

[9] D. A. Weitz, L. Ye, P. Sheng, J. H. Huang, D. J. Pine, J. Liu, P. M. Chaikin and P. N. Pusey. "Dynamics Of Concentrated Colloidal Suspensions" **MRS Proceedings** (1990)

[10] L. Brillouin. **Ann. Phys.** 17, 88 (1922)

[11] D. J. Coumou, E. L. Mackor and J. Hijmans. **Trans. Faraday Soc.** 60, 1539 (1964)

[12] P. A. Fleury and J. P. Boon. **Phys. Rev.** 186, 244-254 (1969)

[13] R. D. Mountain. **CRSS.** 1, 5 (1970)

[14] L. Landau and G. Placzek. **Z. Phys. Sowjetunion** 5, 172 (1934)

[15] W. S. Gornall, G.I.A. Stegeman, B. P. Stoicheff, R. H. Stolen and V. Volterra. **Phys. Rev. Lett.** 17, 297 (1966)

[16] C. J. Montrose, V. A. Solovyev and T. A. Litovitz. **J. Acou. Soc. Amer.** 43, 117-130 (1968)

[17] D. A. Pinnow, S. J. Candau, J. T. LaMacchia and T. A. Litovitz. **J. Acou. Soc. Amer.** 43, 131-142 (1968)

[18] S. Kato, D. Jobe, N. P. Rao, C. H. Ho and R. E. Verrall. **J. Phys. Chem.** 90, 4167-4174 (1986)

[19] N. P. Rao and R. E. Verrall. **J. Colloid and Interface Sci.** 122, 85-99 (1988)

[20] J. Menendez and M. Cardona. **Phys. Rev.** B29, 2051-2059 (1984)

Chapter 2

EXPERIMENTAL

In this chapter, the experimental details including instrumentation, measurement methods and error sources will be presented. There are three parts: the first describes the Brillouin scattering apparatus and its use for the measurement of sound velocity. The second part presents a technique for the measurement of sound velocity at much lower frequencies: ultrasonic time of flight. The last part describes the picosecond Raman scattering technique for measuring the optical phonon relaxation time. In each part an experimental error analysis is provided.

2.1 Brillouin Scattering

One way to measure the sound velocity is to scatter light from the thermally excited density fluctuations in the system; this is called Brillouin scattering, and is discussed in chapter 1. Our Brillouin scattering experiments are performed using either an Ar^+ laser at 5145 Å or an Kr^+ laser at 6471 Å . A schematic drawing of the apparatus is shown in Fig. 2.1. The laser beam is focused by a 100 mm focous lens to a spot of about 100 μm diameter in the sample cell. Light scattered through a particular angle is collected and collimated by a camera lens. The collimated beam then passes through a piezoelectrically driven, scanning, five-pass Fabry-Perot interferometer with stabilization controls. The signal from the Fabry-Perot is focused into a photomultiplier operating in the photon counting mode. The output is analyzed with a computer used as a multichannel analyzer to resolve the Brillouin spectrum. The various components of this experiment will now be discussed in detail.

The single-frequency laser power we use is typically 100 mW; we avoid higher incident power to prevent any thermal effects which could affect the spectra. For

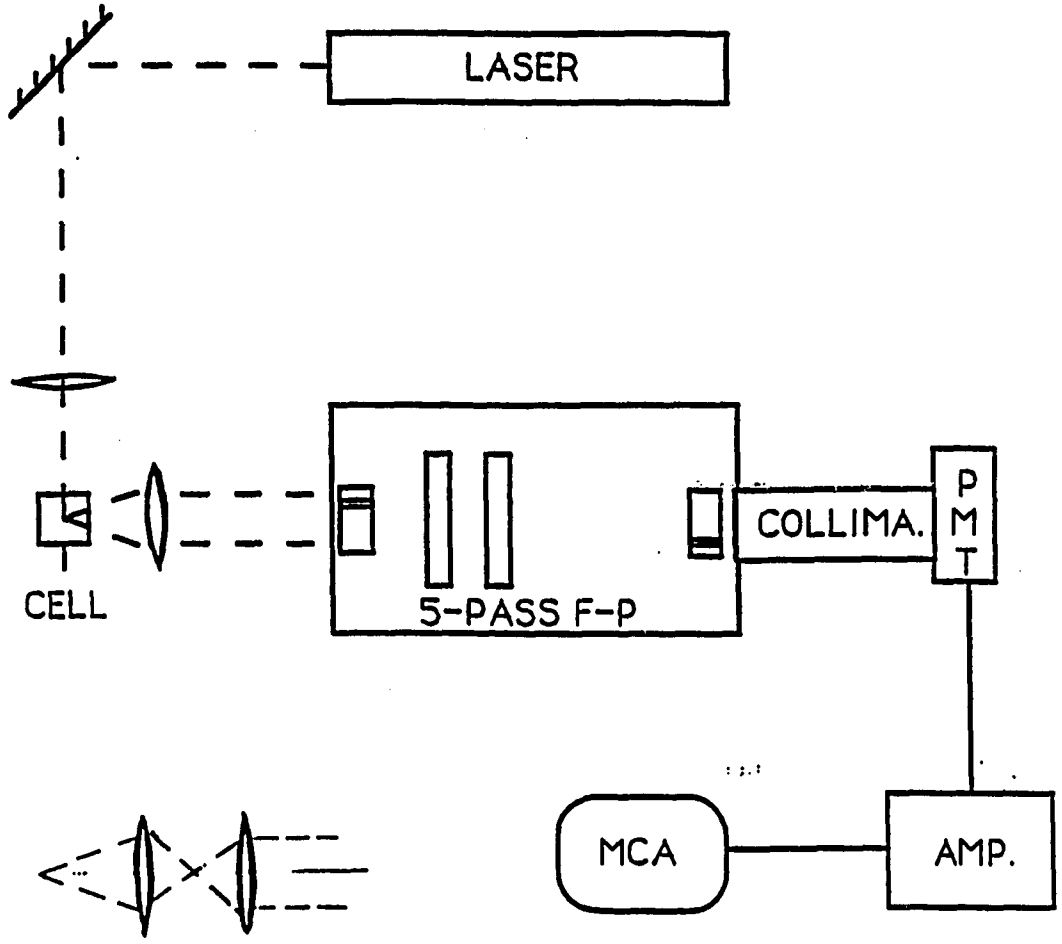

2.1 Schematic of the experimental system for Brillouin scattering with a Fabry-Perot interferometer in 5-pass operation.

example, in the PMMA colloids we observe strong self-focusing of green light when the incident power is larger than 100 mW. Scattering angles are between 15° and 175°, allowing us to vary the scattering wave vector, $q = \frac{4\pi n}{\lambda} \sin\theta/2$, from 0.003 cm^{-1} to 0.04 cm^{-1}.

The sample container is a 10x10 mm^2 square glass cuvette. The procedures of sample preparation will be discussed in the following chapters.

A Fabry-Perot interferometer consists of two plane mirrors held parallel to each other. One of the mirror is scanning to change the mirror spacing, d, and to sweep the Brillouin spectrum. The mirrors are wedge shaped (15 min) to avoid forming additional cavities between the outer uncoated surfaces. The inside faces of the mirrors are maintained parallel and have a high reflectivity to form the Fabry-Perot cavity. The outer surfaces have a small, but finite, reflectivity. The reflection of light from the uncoated surfaces can be detected when the scattered light is strong enough.[1] If the angle of the wedge of the mirror is Φ, a new beam appears due to the reflected light from the uncoated surfaces, making an angle of 2Φ with respect to the main beam from the Fabry-Perot cavity. This new beam adds to the symmetric Rayleigh peak in the Brillouin spectrum. It has weak intensity but contribute to only one side of the Rayleigh tail, giving rise to the appearance of a ghost image and making the Rayleigh peak appear asymmetric. This ghost pattern is a property of the Fabry-Perot interferometer, and the only way to eliminate it is to reduce the intensity of the unwanted scattered light from the line light source used in our experiments. When the scattered light from the line source is collimated, the light incident to the Fabry-Perot includes contributions collimated in different directions, causing the uncoated surfaces of the mirrors to produce a ghost image.

We have used two different optical configurations to collect the scattered light for different Rayleigh scattering intensities. The first is to use a single lens to

collect the scattered light, and is used in the microemulsion experiments. In the microemulsion experiments, the Rayleigh scattering is not enhanced too much by the static scattering from the droplets, because their size is < 100 Å. Thus, the scattered light is collected with a camera lens with focal length of 75 mm. The excited volume is at the focal plane of the lens, ensuring that the collected light is collimated into the Fabry-Perot.

The second configuration is to use a two-lens collecting system, which can eliminate the unwanted stray light from different directions. This is used in the PMMA colloid experiments, where the Rayleigh scattering is much more intense, due to imperfect index matching of the colloidal particles, whose size is comparable to the wavelength of the light. This can lead to a distortion of the Rayleigh peak in the spectra, due to a ghost effect which arises from spurious reflections from the uncoated surfaces of the Fabry-Perot mirrors.[1] These reflections result from light incident at off-normal angles. Therefore, we must use a better arrangement of the collection optics to eliminate the extra light, as shown in Fig. 2.1. The first lens has a focal length of 100 mm, and has a object length twice the image length, making an image of the excited volume onto the image plane, without magnifying it. An adjustable pinhole is placed at the image plane of the first lens. Typically, the pinhole size is about 150 μm. This pinhole selects the scattered light from a 150 μm spot of the excited volume, and eliminates the remainder of the light. The light which passes through the pinhole then acts as a point source allowing us to eliminate the unwanted scattered light from the line source. The second lens is focussed on the pinhole, and collimates the scattered beam into the Fabry-Perot as the lens in the first configuration. This modified configuration eliminates the ghost effect and results in high-quality spectra.

In our experiments, the scattered light is analyzed with a scanning Fabry-Perot interferometer driven by piezoelectric transducers from Burleigh. The mirror

set has a diameter of two inches and 88% reflectivity at the wavelength used. All the measurements reported here are using 5-pass operation. This is achieved by two corner cube retroreflectors on either side of the mirrors, which displace the reflected beams laterally and pass them through the mirror set 5 times. The aperture for 5 passes is 7mm in diameter.

The 5-pass operation offers high resolution and high contrast. The spectral resolution is defined by the ratio of the wavelength of the light, λ, to the minimum resolvable bandwidth of the instrument, λ_{BW}, which is measured from the full width at half maximum (FWHM) of the resolvable peak. For a Fabry-Perot interferometer, the *finesse* is the key measure to resolve closely spaced lines. The measured finesse in one pass is about 20, and in 5-pass operation is about 50, which means the peak resolution is about 2% of FSR. It is measured by the ratio of the free spectral range, FSR, to the FWHM of the Rayleigh peak, since the Rayleigh peak is narrower than the instrumental resolution. The free spectral range is the frequency difference between two Rayleigh peaks: FSR=$c/2d$, where c is the speed of light, and d is the mirror spacing of the interferometer. We use an extended light source from a white paper illuminated homogeneously by a defocused beam to obtain the instrument spectrum to measure the finesse.

Contrast is another important characteristic of a Fabry-Perot interferometer. It is the ratio of the maximum intensity of light transmitted to the minimum intensity of light transmitted, I_{max}/I_{min}, where I_{max} is the intensity of the Rayleigh peak, and I_{min} is the minimum intensity between the Rayleigh peaks. We measure, in one pass, the contrast is approximately 10^3, while in 5-pass it can be as high as 10^{10}. Both the measured finesse and contrast are lower than the theoretical expectations of 62 and 6×10^{11}, respectively. This may be due to the dust on the mirror surfaces, which produces extra scattering, reducing the finesse, and resulting in the lower transmission.

The sound velocity is determined from the measurement of the frequency shift of the peak of the Brillouin doublet, ω, and the scattering wave vector q: $v = \frac{\omega}{q}$. To calculate the wave vector q, we must know the index of refraction, n, and the scattering angle, θ. We measure the index of refraction n for each sample using a refractometer. The scattering angle is determined approximately from the geometry of the optics, and then is determined more precisely through a calibratation procedure using simple liquids with known sound velocities.

The most significant source of error is due to the uncertainty in the determination of the scattering angle, θ. An additional possible source of error arises in the determination of the FSR, which involves the precise knowledge of the spacing d. This latter error can be significant when d is small. To minimize our experimental error, we calibrate the system by measuring v from some simple liquids whose velocities are well known. These liquids include acetone, methanol and purified distilled water. The calibration procedure must determine both the plate spacing, d, and the scattering angle, θ. To determine d, we first measure the velocity of the calibration fluids with θ near 180°, where q is insensitive to θ. Once the FSR is determined, we then align the optics with the scattering angle we need, and measure the sound velocities from the three simple liquids again. Thus the scattering angle, θ, can be determined. The remaining uncertainties of both the FSR and the angle θ calibrated from this procedure are from the reading error.

The reading error arises from the uncertainty of the determination of peak positions in the spectra of the multichannel analyzer. For a typical Brillouin spectrum, the velocity of sound is obtained from

$$\begin{aligned} v &= \frac{\omega}{q} \\ &= \left(\frac{2\pi}{q}\right)\left(\frac{c}{2d}\right)\frac{N_B}{N_F} \end{aligned} \tag{2.1}$$

where N is the channel number, and the subscripts B and F refer to the Brillouin

peaks and the FSR, respectively. Roughly there are 600 channels in FSR, and 200 in the Brillouin shift. The uncertainty in the determination of the peak position is no more than 6 channels. This leads to a reading error for the FSR of $\pm\frac{6}{600} = \pm\ 0.01$, and for the Brillouin shifts of $\pm\frac{6}{200} = \pm\ 0.03$. Thus, the reading error for determining FSR in frequency is ~ 0.035. In the θ calibration, the error for determining q is ~ 0.05 by suming three errors above. Therefore, the systematic error in determining v can be as high as $\simeq 0.07$. However, the relative error for measurements of v as a function of ϕ is substantially less because all the calibration remains unchanged. It is only 0.01 due to the uncertainty of determining the Brillouin peak position.

The damping of sound Δv is measured from the full width at half maximum, Δ_{meas}, of the Brillouin peak after accounting for the system resolution, Δ_{sys}. The simplest way to deconvolute the system resolution is to use the approximate relation $\Delta_{meas}{}^2 = \Delta_{sys}{}^2 + \Delta_{real}{}^2$, which assumes that both the Brillouin peak and the system resolution function are Gaussian. When the width is significantly broader than the system resolution, this approximation gives reliable results. By contrast, when the measured width is comparable to the resolution, the results are less reliable.

We have also carried out more precise fitting of the spectral forms for some experiments, where theory is available. We convolute the theoretical spectrum with the instrumental response to calculate the spectral distribution

$$I_{obs}(\omega) = \int_{-\infty}^{\infty} I_{ins}(\omega') f(\omega - \omega') d\omega' \tag{2.2}$$

and fit to the data. Here, $I_{obs}(\omega)$ is the measured spectrum, $f(\omega)$ is the theoretical form, and

$$I_{ins}(\omega) = \left(\frac{1}{1 + \frac{FSR}{\pi\delta\omega} \sin \frac{\pi\omega}{FSR}} \right)^p \tag{2.2a}$$

is the instrumental function.[2] The instrumental response is obtained experimentally by using an extended source obtained from scattering from a piece of paper. We fit the measured response to eq. (2.2a) to obtain both the width of the Raleigh peak, $\delta\omega$, and the number of passes, p. While we should ideally have $p = 5$, we typically obtain better fits using $p \simeq 3.8$. In addition, our measured finesse is typically $\simeq 50$, which is less than the theoretical reflectivity finesse of 62. The discrepancy is due to other effects which degrade the finesse, including the mirror flatness and the pinhole size.

2.2 Ultrasonic Measurements

Another way to measure the sound velocity is to use an ultrasonic technique, in which the sound waves are excited externally in the MHz range. We use ultrasonic techniques to extend the measurement of the sound propagation in micelle and microemulsion systems to a lower frequency range. In these measurements, the sound velocity, v, is determined by the measurement of the time, t, for the sound wave to travel through a cell of length, L. The time measurements can be done either by measuring the time period between two echoes or by using a delay line technique.

The apparatus for our ultrasonic time of flight experiments is shown in Fig. 2.2. A continuous wave signal with a frequency f is obtained from a frequency synthesizer. It is divided into two parts by a power divider. One part is fed into a gate amplifier and forms a pulse of about .03 μsec long, which is used to drive the transducer to generate sound waves in the fluid of the cell. The sample cell is about 10 mm in length. Transducers are mounted on either side of the cell, one used as the oscillator and the other as the receiver. The time of flight of the sound can be measured directly using the receiver to determine the period, t_o, between the echoes of this pulse, which is reflected from two transducers and travels back

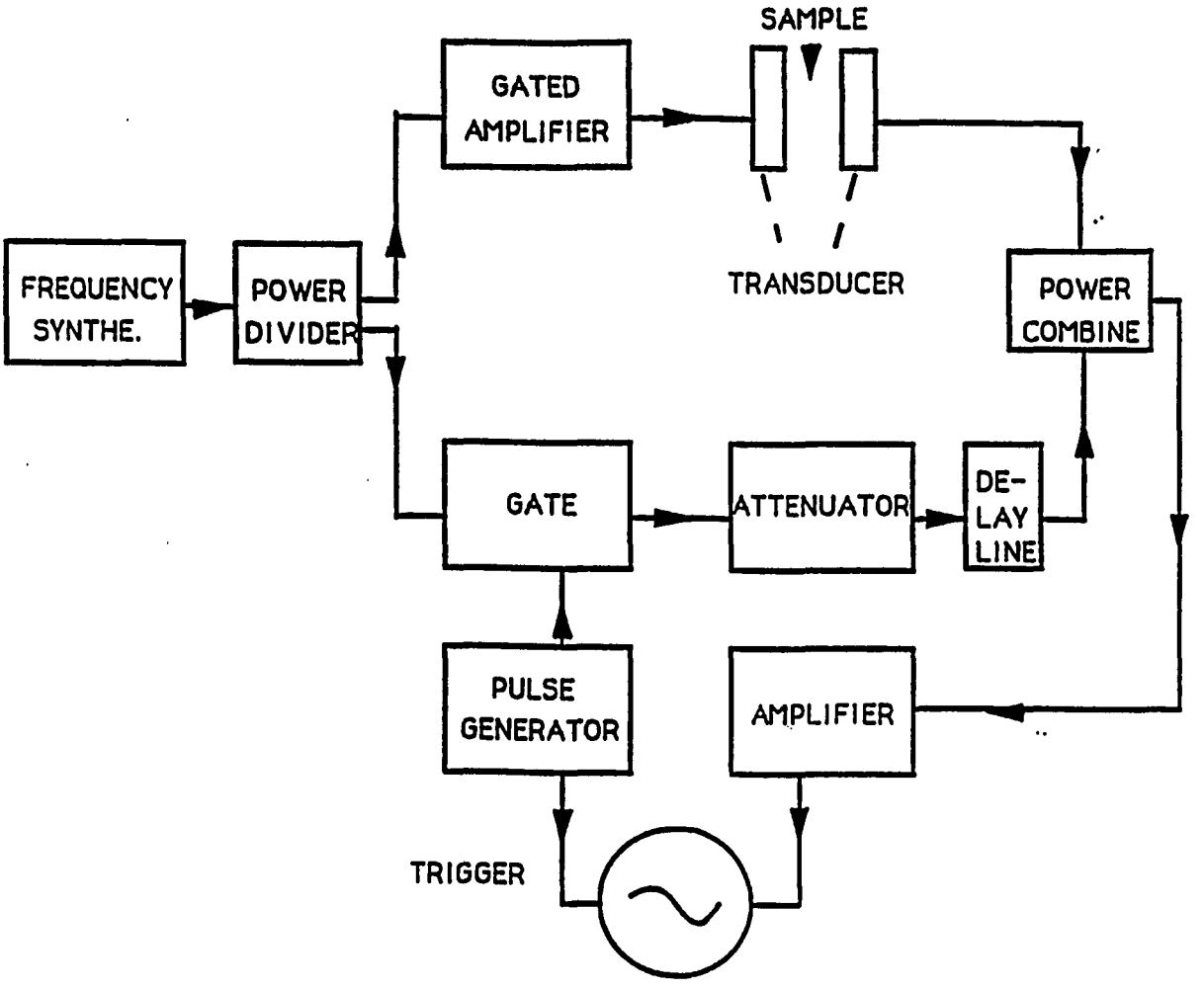

2.2 Block diagram of the equipment used for a time-of-flight technique for the ultrasonic measurements.

and forth across the cell. Alternatively, we can use a delay line technique. The second part of the cw wave is fed into another gate amplifier to form a second pulse. This pulse is sent down to delay lines and is combined with the signal from the receiver. It will has a phase shift compared the first pulse. By adjusting the delay line to match the phase of two pulses, and measuring the time difference required for matching, the transit time, Δt, can be determined.

We first use the echo measurement to determine t_o for the solvent. Then we vary the concentration of micelle or microemulsion droplets in steps of about 0.025, and measure the change in the transit time, Δt, using the delay line. The Δt can be measured with an accuracy as high as 10^{-3}. Then v is calculated from

$$v(\phi) = \frac{L}{t_o + \Delta t} \tag{2.3}$$

To measure the dispersion in the velocity, we use 2, 3, 10 and 15 MHz transducers. Data at 6 MHz is obtained using the third overtone of the 2 MHz transducer. We also tried to measure the signal at 45 MHz using the third overtone of the 15 MHz transducer, but the damping of the sound is too strong to measure the signal for $\phi > 0.3$ with our cell.

The length of the sample cell, L, is roughly measured using a ruler. In order to eliminate the error from the determination of L, we first calibrate the system by measuring v for simple liquids, such as acetone, methanal and purified distilled water where the velocity of sound is well known. The experimental error, therefore, arises from the measurement of t_o, and is typically $\delta t_o \simeq \pm\frac{.2\mu sec}{25\mu sec} \simeq 0.01$. Here .2 μsec is the accuracy of the measurement of t_o, and 25μsec is a typical value of t_o for fluids.

The damping of sound is measured by the decay in the amplitude of the first or second echo, $A(\phi) = A_0 e^{-\alpha(\phi)L}$, where α is the attenuation coefficient of sound, and A_0 is the amplitude of the initial phase. We also calibrate A_0 using simple

liquids. Due to the uncertainty in the amplitude measurement the reliabilities of α are reduced.

2.3 Picosecond Raman Scattering Measurements

Raman scattering results from the scattering of light by internal vibrations of molecules or optic phonons in crystals. We use an excite-and-probe scheme[3] of picosecond Raman scattering to study the optical phonon relaxation in crystal germanium, and to measure the thermal excited optical phonon relaxation time, τ_c. A laser pulse is split into two beams, one is time delayed relative to the other; the first beam on the sample generates the nonthermal equilibrium optical phonons, while the second beam probes the decay of those phonons by measuring the anti-Stokes Raman scattering as a function of delay time.

The apparatus used for the time-resolved picosecond Raman scattering experiment is shown in Fig 2.3. A mode-locked Kr^+ laser produces pulses of $\sim$ 150 ps in duration at 40 MHz repetition rate, and synchronously pumps a cavity-dumped dye laser using rhodamine 6G as the lasing medium. A photodiode is used to monitor the pulses from the Kr^+ laser. The output pulse from the dye laser has a photon energy of E=2.08 eV with the repetition rate changing from 0.8 to 40 MHz. These pulses are monitored by an autocorrelator using a potassium diphosphate (KDP) crystal in a background free second harmonic generation arrangement.[4] Typically, the autocorrelation traces indicate that the pulse has a half-width at half maximum of 2.3 ps. The laser output is then split into two beams of equal intensity, one of which is delayed using a computer controlled translation stage. The beams have the same polarization and are focused onto the $< 111 >$ surface of Ge with a spot diameter of 15 μm. The overlap and the focus of the beams is confirmed using a pinhole. The total back-scattered light is collected and dispersed in a Spex Triplemate monochromator. A photomultiplier is used in the photon

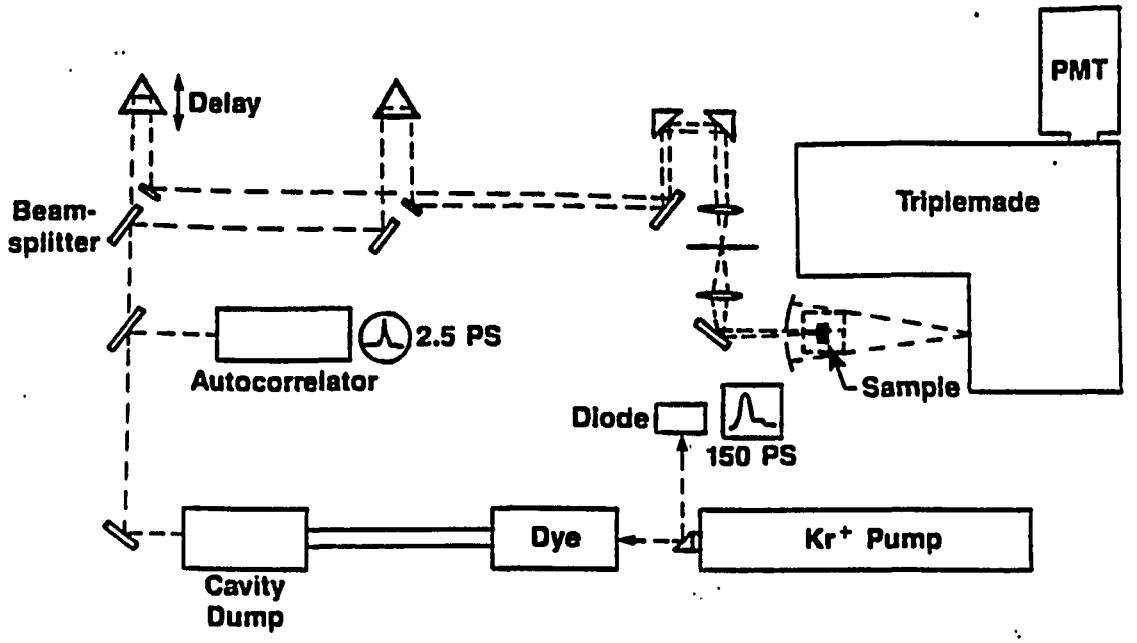

2.3 Experimental arrangement for time-resolved Raman scattering measurements.

counting mode to record the anti-Stokes Raman intensity as the delay between the pulses is varied. In addition, an optical multichannel analyzer is used to determine the Raman spectrum which is identical to that observed in cw Raman scattering within the 5 cm^{-1} resolution of the spectrometer.

The low temperature data are obtained when the sample is in contact with the cold finger of a Dewar with liquid nitrogen as the coolant. The sample is mounted on a copper block to insure good thermal contact. The temperature is monitored using a silicon sensor attached to the copper block. The temperature dependence of the phonon population relaxation as a function of delay time are measured while the Dewar slowly warms up, as the liquid nitrogen evaporates. It takes about 5 hours for the system to warm up from 77° to room temperature, and a typical measurement takes only about 15 min. Therefore, the measurement results are still reliable within the temperature uncertainty of a few degrees.

The relaxation time of the optical phonon population, τ, is obtained from the fitting of the measured exponential decay of the anti-Stokes Raman intensity as a function of pulse delay, $I_{mea}(\tau_D)$. The convolution of the excitation profile, I_{ex}, with the phonon density, $N(\tau)$, is used for the fitting, which is given by

$$I_{mea}(\tau_D) = const. \int_{-\infty}^{\infty} I_{ex}(t')\ N(\frac{t_D - t'}{\tau})\ dt' \qquad (2.4)$$

Where t_D repres$I_{mea}(\tau_D) = const. \int_{-\infty}^{\infty} I_{ex}(t')\ N(\frac{t_D - t'}{\tau})\ dt'$g parameter. The major experimental error arises from the instability of the pulse profile. The uncertainty of the pulse duration is $\simeq \pm .5$ ps obtained by measuring the autocorrelation traces from the oscillograph. Therefore, this leads to an uncertainty of $\tau = \pm 1$ ps.

References

[1] G. Hernandez. in **Fabry-Perot Interferometers** of *Cambridge Studies in Modern Optics* 3 (Cambridge Univ. Press, N.Y.) (1986)

[2] **Optics** ed. by E. Hecht and A. Zajac (*Addison – Wesley Pub. Co.* (1979) p.307

[3] D. Von der Linde, J. Kuhl and H. Klingenberg. **Phys. Rev. Lett.** 44, 1505-1508 (1980)

[4] E. P. Ippen and C. V. Shank. in **Ultrashort Light Pulses** of **Topics in Applied Physics** edited by S. L. Shapiro 18 (Springer, Berlin) (1970)

Chapter 3

DYNAMIC RIGIDITY PERCOLATION IN INVERTED MICELLES

The elastic behavior of inhomogeneous materials provides an informative probe of their physical properties and structure. For materials comprised of random dispersions of small particles, the elastic properties are critically dependent on the connectivity, providing a sensitive measure of the nature of the bonds and the spatial correlations between the constituent particles. Similarly, the viscoelastic properties of a complex fluid can also provide new insights into the spatial correlations and interactions of its components. In this case, however, the dynamics of the fluid add new richness to the behavior.

In this chapter, we discuss the unusual viscoelastic properties of inverted micelles, or very small spherical aggregates of surfactant suspended in an oil.[1–8] In these experiments, the surfactant is sodium di-2-ethylhexylsulfosuccinate (AOT) and oil is decane. We have measured the velocity of sound as a function of droplet volume fraction at different frequencies using both ultrasonic and Brillouin scattering techniques. The sound velocity is found to exhibit pronounced dependencies on both the frequency and droplet volume fraction. The frequency dependence reflects the dynamics of the interactions between the micelles. At low frequency, they behave as isolated spheres, while at high frequencies they behave as an instantaneous connected network. The rigidity of this network exhibits power-law scaling with volume fraction, consistent with rigidity percolation. This chapter will primarily discuss the physics of the dynamic rigidity percolation in AOT/decane inverted micelles.

In the next chapter, we discuss additional experiments that probe the elastic properties of related systems. These include the effect of changing the solvent in

micelle systems, or varying the size of droplets in microemulsion systems. The results indicate that there is a contribution of the networks of droplets to the elastic constant of the system, its magnitude and frequency dependence are strongly affected by the interaction between the droplets. The viscoelastic properties of different AOT micelle and microemulsion systems, the effective medium theory used to interpret volume fraction dependence of the sound velocity, and the fitting of the Brillouin spectra, will be discussed in detail in the next chapter.

In the inverted micelle systems, the surfactant head groups form a close packed, central core, with the tail groups oriented outward. The volume fraction of the micelles, ϕ, can be varied, while their radius, a, remains fixed. There is a weak, short-range attractive interaction[5,6] between the micelles, and the characteristic time scale of this interaction, τ_c, determines their behavior. On time scales long compared to τ_c, their diffusive motion ensures that the micelles are dynamically dispersed in the surrounding oil. By contrast, on time scales short compared to τ_c, the micelles form instantaneous, random cluster, which, at sufficiently high ϕ, form a connected network. These time-dependent correlations result in a surprising viscoelastic behavior in this relatively simple fluid. We account for the ϕ dependence of the viscoelastic properties by means of a static effective medium approximation for an elastic composite. We account for the frequency dependence of the viscoelastic properties through the parameters describing the micelle phase. The variation of these parameters also reflects the frequency dependence of the correlations between the micelles. At high frequencies the micelle phase exhibits a solidlike behavior which supports shear at $\phi \geq 0.2$. This high-frequency rigidity of the surfactant micelle phase exhibits power-law scaling with ϕ. We interpret this as dynamic rigidity percolation.

The inverted micelles investigated consist of spherical aggregates of AOT suspended in decane. By varying the contrast of the oil, small-angle neutron

scattering[7,8] was used to determine that $a \simeq 15.1$ Å, corresponding to aggregates comprised of 22 AOT molecules. This size remains constant as ϕ is varied.[1,3,5] We study the elastic properties by measuring both the speed and the damping of the longitudinal sound wave in the fluid. To establish the frequency dependence, we use both ultrasonic and Brillouin scattering measurements. For the lower frequency, time-of-flight ultrasonic measurements were performed between 2 and 45 MHz, using an interferometric technique to measure the velocity and the decay of the echo train to measure the damping. For the higher frequency, Brillouin scattering was performed at several scattering angles, using a five-pass Fabry-Perot interferometer with both 6471 Å Kr^+ and 5145 Å Ar^+ laser excitation. The speed of sound was determined from the peak positions of the Brillouin doublet; the damping was determined from the full width at half maximum.

The ϕ dependence of the speed of sound in the solution, v, is shown in Fig. 3.1 for several different frequencies. For $\phi \leq 0.2$, there is only a slight dependence on volume fraction and no discernible frequency dependence. By contrast, for $\phi > 0.2$, the speed of sound increases. Furthermore, there is a pronounced frequency dependence, with a significantly larger increase in v at higher frequency. To further investigate this dependence, the variation of v on frequency, f, is shown in the lower part of Fig. 3.2 for fixed volume fraction for several values of ϕ. The magnitude of the dispersion increases with increasing volume fraction. However, for all values of ϕ, the dispersion occurs in the same frequency range, around 10^8Hz. Furthermore, the data have reached their asymptotic limits at both the lowest and highest frequencies measured.

The initial decrease in v reflects the increased density of the mixture as the volume fraction of surfactant is increased. By contrast, the increase in v for $\phi \geq 0.2$ indicates an increase in the rigidity of the oil-surfactant mixture. Alternatively, the adiabatic compressibility of the mixture is decreasing, implying that the surfactant

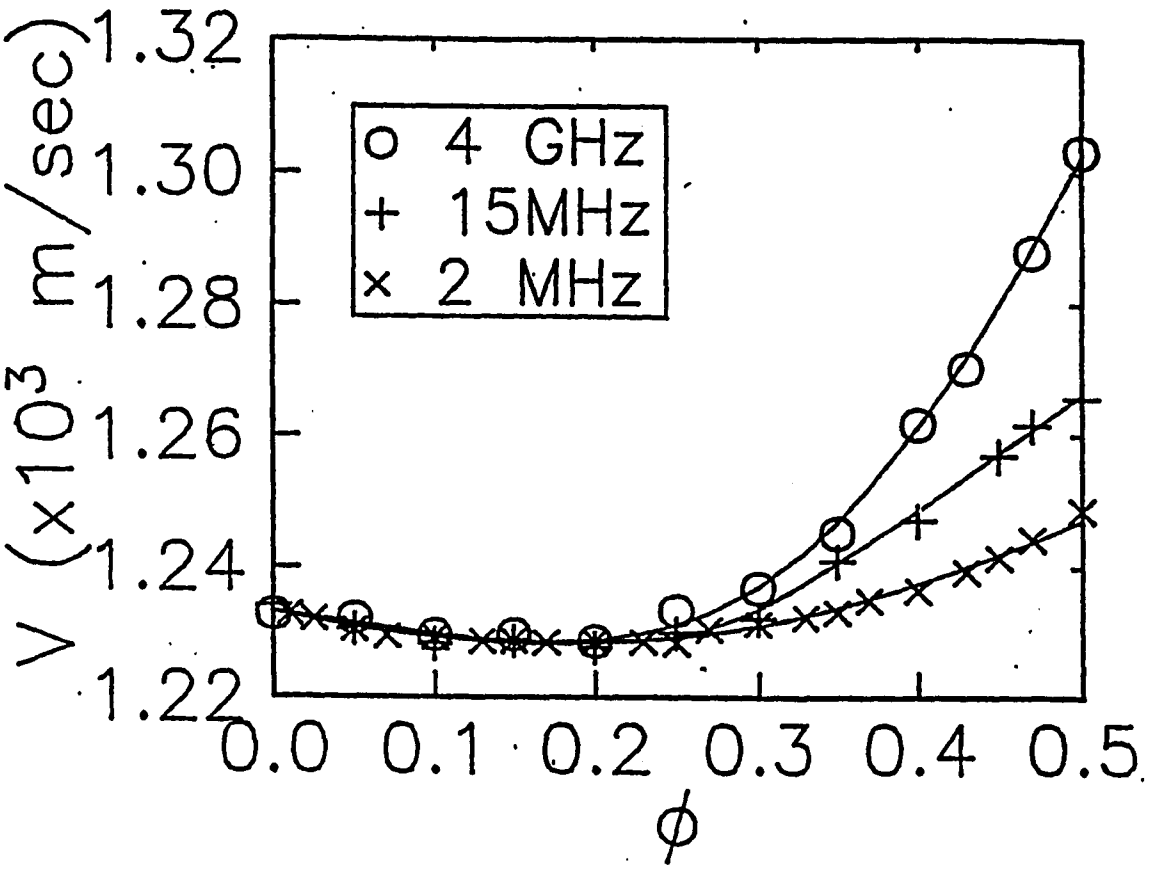

3.1 Sound velocity as a function of volume fraction for several different frequencies. The sound lines through the data are fits by the effective-medium theory, using isolated spheres for the surfactant phases for the lowest frequency and a random, connected network for the higher frequencies.

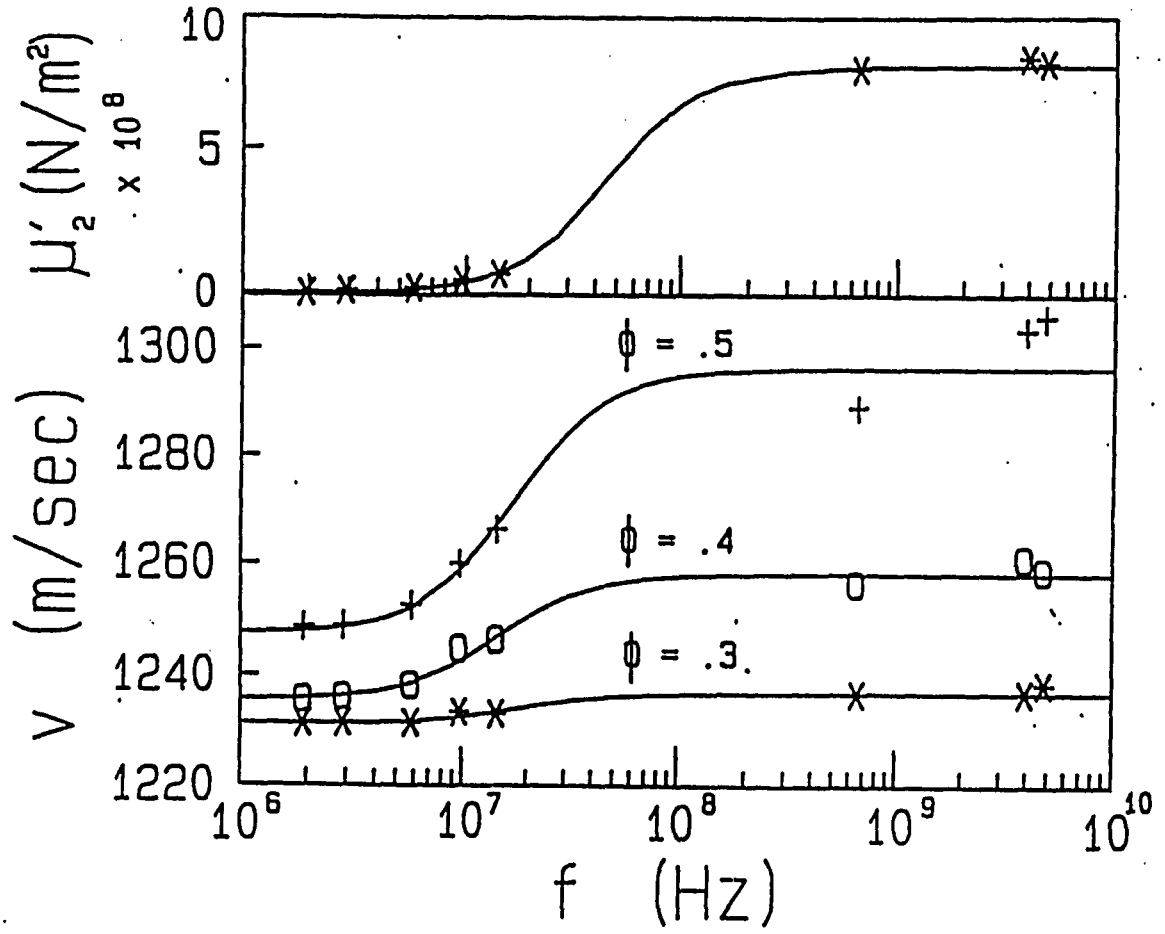

3.2 Frequency dispersion of the sound velocity for several volumn fractions and the real part of the shear modulus for the surfactant phases, μ_2', obtained from the effective- medium approximation. The solid lines represent the form of a single-relaxation-time Debye model.

is less compressible than the oil. The remarkable feature is the pronounced frequency dependence of the increase in v. This implies that rigidity of the surfactant micelle phase increases at higher frequency.

To account for the observed frequency dependence, we must consider the contribution of the surfactant micelle phase to the behavior of the mixture. We propose that it depends on the time scale of the measurement compared to the time scale of the dynamics of the micelles. This time scale arises from the short-range attractive interaction between the micelles[6]. Physically, this attraction may be due to the entanglement of the tails of the neighboring spheres[5], which can interpenetrate by about 3 Å. At sufficiently high frequency, the time scale of the measurement will be faster than the dynamics of this interaction and the micelle phase can be viewed as an instantaneous, connected network. This network will support shear, increasing the total fluid rigidity and hence the speed of sound. By contrast, at low frequencies, the dynamics of the micelles lead to a relaxation of any shear stress, so that the network is dynamic and the micelles behave as isolated spheres. Thus at low frequencies, there is no increase in the rigidity due to a shear modulus of the micelles.

To quantify this hypothesis, we characterize the surfactant-oil mixture by its average complex elastic constant, $\beta = \beta' + \beta''$, which is the inverse of the adiabatic compressibility associated with the longitudinal compressional wave. The use of β has the advantage that it is directly related to experimentally measurable quantities. The speed of sound is obtained from the real part, $v = (\beta'/\rho)^{\frac{1}{2}}$, where the ρ is the average density. Similarly, the damping of the sound wave is determined from the imaginary part, with the attenuation length for an ultrasonic propagation given by $\alpha = f\beta''/4\pi v^3\rho$, and the width of the Brillouin peaks given by $\Delta v = f\beta''/4v^2\rho$. Since $\beta = \kappa + (4/3)\mu$, where κ and μ are the bulk and shear moduli, the data are also sensitive to the shear rigidity of the mixture, although

only the longitudinal sound propagation is measured.

The average elastic constant of the mixture contains a volume-weighted mix of the elastic constants of each of the constituent phases. Thus, we attribute both an elastic constant, β_i, and a shear modulus, μ_i, to each phase, the oil ($i = 1$) and the surfactant micelles ($i = 2$). To describe the ϕ-dependent properties of the mixture at each frequency, we use a static-effective-medium approach. This should be appropriate since the sound wavelength is always much larger than the micelle size. The dynamics of the micelles, and the resultant frequency dependence of the behavior, must be accounted for by the frequency dependence of β_2 and μ_2, describing the properties of the micelle phase.

Both β_1 and μ_1 can be directly determined experimentally using the pure-oil phase. Measurement of the sound velocity and damping determines β_1' and β_1''. Furthermore, since a fluid cannot support a shear wave, $\mu_1' = 0$, while $\mu_1'' = 2\pi f\eta$, where η is the shear viscosity at $f = 0$, which is measured independently. We cannot, however, independently measure any of the constants for the second phase, as we cannot obtain a sample comprised of pure AOT micelles. Thus, there are four unknown, frequency-dependent parameters, the complex β_2 and μ_2, describing the AOT micelles. These are obtained for each frequency from a fit of the data for both the sound velocity and damping to the ϕ dependence of β predicted by the effective-medium model.

At low frequency, the dynamics of the micelles ensure that they may be regarded as noninteracting, isolated spheres, even at higher ϕ. Thus, we use an effective medium model that assumes a nonsymmetric description of the mixture,[9] treating the micelles as isolated spheres in the continuous oil phase. This results in the Wood's formula, $\beta^{-1} = \phi/\beta_2 + (1-\phi)/\beta_1$, which is accurate in the static limit.[10] The solid line through the data measured at 2 MHz reflects the good fit obtained.

We are unable to fit the higher-frequency data using this model. Instead, we must assume that the micelles phase is a connected, random network which behaves as a solid, supporting shear. We therefore use a symmetric description[9,11] of the structure for the two components, assuming that both the oil and the surfactant micelles form bicontinuous, intermixture phases. The symmetric description requires the role of the inclusion phase to be reversed as ϕ increases, and thus results in a percolation threshold. However, both components are assumed to be space filling. Since spheres cannot fill space, we have multiplied the effective-medium volume fraction by .64, corresponding to the volume fraction for random close packing of spheres.[12] To obtain agreement with data requires the use of a nonzero value for μ_2 in the fit, in accord with our physical picture. The solid lines through the data at 15 MHz and 4 GHz in Fig. 3.1 are examples of the excellent fits obtained.

The viscoelastic behavior of the mixture is reflected by the frequency dependence of β_2 and μ_2. Indeed, the symmetric model used in fitting the high-frequency data reduces exactly to the Wood's formula when $\mu_2 = 0$. The frequency dependence of the value of μ_2 obtained from the fits to the effective-medium theories is shown in the upper part of Fig. 3.2. It has roughly the same form of dispersion as the velocities, with a limiting value of 8×10^8 N/m^2 at the Brillouin frequencies. In addition, the bulk modulus of the micelle phase, κ_2', also exhibits a frequency dispersion, but it *decreases* as f increases, from 1.6×10^9 N/m^2 at 2 MHz to 8×10^8 N/m^2 at 5 GHz. Physically, this may reflect the different properties of the micelle phase due to the time dependence of their correlations. Thus, at low frequencies, κ_2' reflects a change in volume of the isolated micelles themselves. By contrast, at high frequencies, κ_2' reflects a change in volume of the random network of micelles, which can be accomplished by changing their relative positions. This requires a smaller force than changing the volume of the micelles themselves,

resulting in a reduction of κ_2'. This behavior is also reflects in a decrease in κ' at high frequencies for large ϕ. While this is highly unusual, this does not imply a violation of Le Chatelier's principle[13] because v still increases with frequency due to the contribution of the shear modulus, μ_2'. The small values of $\mu_2' \simeq \kappa_2' \simeq 10^9$ N/m^2 imply that the micelle network is relatively soft but nonetheless solidlike.

For $\phi \leq 0.4$, the behavior of v is reasonably well described by a single-frequency Debye relaxation model, $v = v_o + \Delta v(\omega\tau_c)^2/[1 + (\omega\tau_c)^2]$, where v_o is the low-frequency velocity, Δv is the total velocity dispersion, and τ_c is the characteristic relaxation time. The behavior of μ_2' also follows a similar form. This behavior is shown by the solid lines through the data in Fig. 3.2. At higher volume fractions, the velocity dispersion is no longer well described using only one relaxation time. Nevertheless, the characteristic range of relaxation times for all the data is $\tau_c \simeq 10^{-8}$ sec. Within our picture, τ_c reflects the dynamics of the micelles, and corresponds to their characteristic interaction time. We can test this hypothesis by using oils of different carbon chain lengths, which changes[6] the interaction energy, E_a, and thus τ_c. Replacing the decane with hexane decreases E_a, and we observe no dispersion in v, even at $\phi = 0.5$. This corresponds to a decrease in τ_c below our accessible range. By contrast, replacing decane with hexadecane increases E_a. In this case, we observe an immediate rise in v at the lowest accessible frequencies for $\phi = 0.5$, corresponding to an increase in τ_c. We note that the changes in τ_c are much greater than the changes in the viscosity of the oils, implying that the dynamics reflect the interaction time, rather than merely a Brownian diffusion time.

The dynamics of the inverted micelles lead to the unique behavior of this complex fluid. At low frequencies their dynamics ensure that the micelles behave as independent, isolated spheres even at high ϕ. By contrast, at higher frequencies, this is an ideal system to use to measure the elastic properties of random

inhomogeneous mixtures. The fact that they are a fluid ensures a truly random dispersion of spheres. The fact that we can measure the speed of sound at both low and high frequencies ensures that we can distinguish the additional contribution of the rigidity of the micelle network. The difference between the high- and low-frequency modulii, $\Delta\beta$, is, to lowest order, linear in the change in μ_2', and thus reflects the rigidity of the micelle network. We are able to discern a change in v only at volume fractions above $\phi \simeq 0.16$. Thus we plot $\Delta\beta$ as a function of $\phi - \phi_c$, on a logarithmic plot in Fig. 3.3. The resolution of the Brillouin peaks precludes measurements closer to ϕ_c. Nevertheless, we observe a clear power-law behavior, with a rigidity exponent of $\tau \simeq 2.5$. This scaling extends over a rather large range in $\phi - \phi_c$, and is strongly suggestive of the behavior of a random percolating network. We emphasize that this observation is based solely on the experimental data, independent of any model. However, this is a dynamic rather than a static measurement, which limits the spatial extent of the sensitivity to the rigidity to roughly the wavelength of the sound, which is nonetheless at least $100a$ at the highest frequency. Finally, this rigidity transition occurs only for the surfactant micelle phase, which forms the random connected network. The surrounding oil phase ensures that the mixture maintains a finite bulk modulus at all ø and does not exhibit a percolation threshold.

There are relative few results available for elasticity percolation of random networks in three dimensions with which these data can be compared. No calculations for random, multiply connected three-dimensional networks exist. It is found that the electrical conductivity[14] scales with an exponent $t \simeq 2$ in three dimensions, with $\sigma = (\phi - \phi_c)^t$. The elasticity exponent is expected to be the same as the conductivity exponent[15] provided only central forces exist between the constituent particle in the network.[16] By contrast, noncentral forces, or bond bending, break the similarity between conductivity and elasticity, leading to an

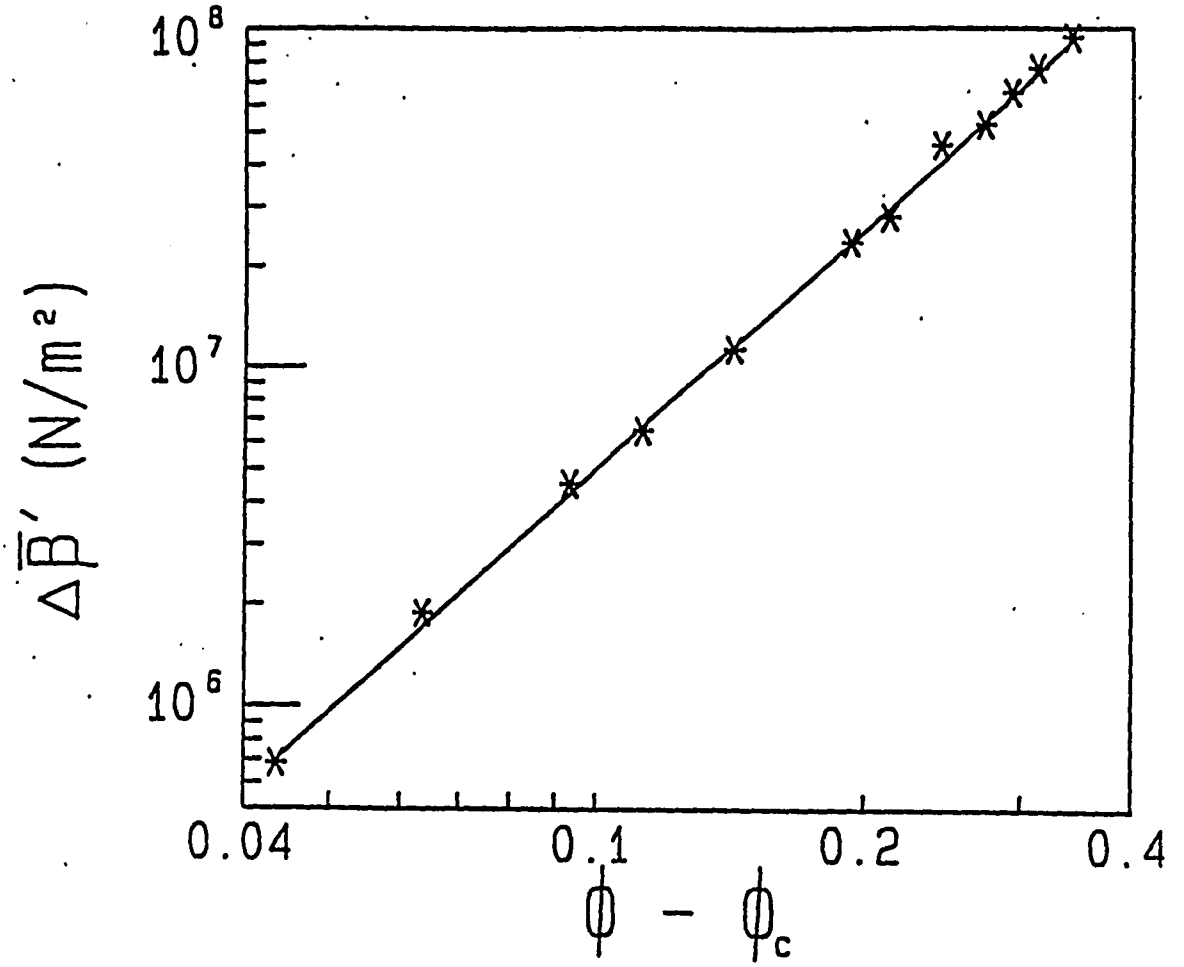

3.3 Critical behavior of the shear modulus contribution of the surfactant phase at high frequencies, when it forms a random connected network. The exponent is $\tau \approx 0.16$.

increase in the elasticity exponent.[17] For single connected networks,[18] the exponent is predicted to be about 3.5. Experimentally, measurements on beams of sintered metal[19] yielded $\tau \simeq 3.8$ with $t \simeq 2.2$, over an equally large range in $\phi - \phi_c$. The behavior of the shear rigidity of the network of surfactant micelles is considerably different. This may reflect the different nature of the micelle interactions, which might change τ. Finally, the value of ϕ_c found here is consistent with that found from simulations of interacting spheres.[20] It can be expected to change as E_a is varied, modifying τ_c. These inverted micelles allow the investigation of this important issue.

We conclude by emphasizing that the results presented here demonstrate that the elastic properties of complex fluids are both rich and varied, and provide new insights into their dynamics and interactions.

References

[1] P. Eckwell, l. Mandell and K. Fontell. **J. Colloid Interface Sci.** 33, 215 (1970)

[2] Y. C. Jean and H. J. Aacke. **J. Am. Chem. Soc.** 100, 6320 (1978)

[3] M. Zulauf and H. F. Eicke. **J. Phys. Chem.** 83, 480 (1979)

[4] T. Assih, F. Larche and P. Delord. **J. Colloid Interface Sci.** 89, 35 (1982) **J. Chem. Phys.** 44, 2785-2797 (1966)

[5] J. S. Huang, S. A. Safran, M. W. Kim, G. S. Grest, M. Kotlarchyk and N. Quirke. **Phys. Rev. Lett.** 53, 592 (1984)

[6] J. S. Huang. **J. Chem. Phys.** 82, 480 (1985)

[7] M. Kotlarchyk, J. S. Huang and S. H. Chen. **J. Chem. Phys.** 89, 4382 (1985)

[8] J. S. Huang, X. L. Wu and J. Sung **J. Colloid Interface Sci.** to be published.

[9] P. Sheng. in **Homogenization and Effective Modulii of Materials and Media** ed. J.L. Ericksen, D. Kinderleher, R. Kohn and J.L. Lions (*Springer – Verlag, N.Y.*) p.196 (1983)

[10] Z. Hashin. **J. Appl. Mech.** 29, 143 (1962)

[11] J. G. Berrymen. **J. Acoust. Soc. Am.** 68, 1809 (1980)

[12] R. Zallen. **The Physics of Amorphous Solids** (*Wiley, N.Y.*) p.46 (1983)

[13] L. D. Laudau and E. M. Lifshitz. **Fluid MechanicsJ. Acou. Soc. Amer.** 43, 117-130 (1968)

[14] D. Stauffer. **Introduction to Percolation Theory.** (Taylor and Francis, London, p. 52,. (1985).

[15] P.G. de Gennes. **J. Phys. Lett.** 37, L1. (1976).

[16] S. Alexander, **J. Phys.** (Paris) 45. 1939 (1984).

[17] S. Fend, P. Sen, B. I. Halperin and C.J. Lobb. **Phys. Rev.** B 30 5386 (1984).

[18] Y. Kantor and I. Webman. **Phys. Rev. Lett.** 52, 1891 (1984).

[19] D. Deptuck, J.P. Harrison and P. Zawadzki. **Phys. Rev. Lett.** 54. 913 (1985).

[20] S. A. Safran, I. Webman and G.S. Grest. **Phys. Rev. A.** 32. 506 (1985).

Chapter 4

SOUND PROPAGATION IN AOT MICELLES AND MICROEMULSIONS

4.1 Introduction

In the last chapter, we discussed the dynamic rigidity percolation in AOT/ decane inverted micelle systems. In this chapter, we further discuss the viscoelastic behavior in AOT micelle and microemulsion systems, which is studied using both Brillouin scattering and ultrasonic techniques. Here, we vary the size, the concentration and the interaction potential of droplets to determine the consequences on the sound propagation and elastic properties of the system. We find that by replacing the oil solvent in the micelles and microemulsions, or by varying the size of droplets in the microemulsions, the frequency dependence of the viscoelastic behavior is changed, due to the variation of interaction energy. Therefore, in this chapter, we present all the experimental results of the sound propagation in both AOT micelles and microemulsions. We also discuss in detail the effective medium theory which is used to account for the ϕ-dependence of the sound velocity at different frequencies. In addition, we discuss a theoretical model proposed by Mountain, that is used to calculate our measured Brillouin spectral distributions. A self-consistent picture of the viscoelastic behavior of these suspensions is developed accounting for all the observations. Finally, we show that, by turning the interaction energy, a dynamic rigidity behavior in AOT/water/hexane microemulsions is obtained, which is very similar to that reported in the previous chapter.

The AOT surfactant molecule has a hydrophilic head and a hydrocarbon hydrophobic tail.[1] Since the hydrophilic heads are water-like and the hydrophobic tails are oil-like, the surfactant molecules form an interface between water and oil, resulting in larger structures in the system at thermal equilibrium. In the systems

studied, all of the structures are spherical droplets.[2,3] The continuous phase is always an oil, hexane (C_6H_{14}), decane ($C_{10}H_{22}$) or hexadecane ($C_{16}H_{34}$). When there is no water in the solution, the hydrophilic heads of AOT molecules aggregate together to avoid the oil phase, while the hydrophobic tails dissolve in the oil. The resultant spherical structure contains 22 AOT molecules with a radius of 15 Å,[2] and is called an inverted micelle. When water is added to the system, the heads of the surfactant molecules associate with the water molecules resulting in droplets with water cores. As more water is added, the droplets are further swollen and their radius increases. The size of droplets is determined by the molar ratio of water to surfactant, $R = [H_2O]/[AOT]$.[3]

Both the micelle and the microemulsion systems are thermal equilibrium structures.[3] The fluctuations in droplet shape and size are small around room temperature. A key feature of these systems, which we exploit in all of our measurements, is the fact that the droplet size is insensitive to both the concentration of droplets and the equilibrium temperature. Therefore, by adding oil, we can dilute the droplet concentration or volume fraction, ϕ, without changing the size. However, since the micelles only form when the AOT concentration is above a critical value, $[AOT] = 0.225$ mM,[2,4] we use a 0.9 mM with a solution of AOT in oil to dilute and to change ϕ. This allows us to study the ϕ dependence of the velocity of sound.

There is a weak, short range, attractive interaction between the droplets.[5,6] Physically this is due to the overlapping of the short, branched, hydrophobic surfactant tails of droplets. The range of the overlapping is about 3 Å. The attractive interaction is an entropic effect. For the oil solvent molecules to fit in between surfactant tails, they must adopt certain configurations in their phase space, thereby decreasing their entropy. By contrast, the tails of surfactant molecules in a neighboring droplet are already optimally oriented by the droplet structure and are able

to interpenetrate without suffering much decrease in entropy. Thus, the total free energy of the system is lower when two droplets interpenetrate than when solvent oil molecules fit in between the tail groups of the droplets. This results in a net attractive interaction. The strength of this attractive interaction increases as the length of the solvent oil molecule increases, because the entropic cost for oil molecules to fit in between surfactant tails also increases. In addition, for microemulsions, as the droplet size increases, the area of overlapping surfactant tails also increases, leading to a larger interaction energy. This interaction energy also determines the characteristic time scale of the interaction, τ_c. Therefore, we can vary τ_c by using different oils or by changing the droplet size.

For the micelle system consisting of AOT in decane, we observe dispersion in the sound velocity as the volume fraction of micelles, ϕ, is varied. At high ϕ, we observe additional dispersion in the sound velocity as the frequency is varied. The physical picture for the additional dispersion of sound velocity is the following:[7] the observed frequency dependence of v indicates the existence of a relaxation process in the system with a characteristic relaxation time, τ_c. For sound frequencies sufficiently high that the period of the wave is less than τ_c, the modulus of the system reflects the contribution of both the continuous fluid, as well as the instantaneous configuration of the micelles. Because of the attractive interaction, the micelles can form extended clusters, which, at sufficiently high ϕ, can span the whole system. Furthermore, because the tail groups of the micelles overlap, those micelle networks can support shear. This shear modulus increases the total longitudinal modulus of the system, thereby increasing the sound velocity. At lower frequencies, when the period of the wave is greater than τ_c, the micelles adopt many different configurations in a single period, thereby relaxing any shear. The absence of any shear modulus results in a smaller total longitudinal modulus and a slower sound velocity. This accounts for the additional frequency dispersion

in the sound velocity. At all frequencies, the ϕ-dependence of the sound velocity reflects the change in both the average density, ρ, and average modulus, β, of the mixture. With increasing concentration of surfactant molecules, both ρ and β increase, since the surfactant molecules have a higher density and a higher elastic modulus than the oil solvent.

In order to test how the characteristic time, τ_c, changes when we vary the interaction energy between droplets, we study the frequency dependence of the sound velocity using different solvents with the micelles. In all cases, we find a ϕ-dependent velocity; however, the frequency dependence is very different for the various systems. For the AOT/hexane micelles, the interaction is weak and no frequency dispersion of the sound velocity from 2 MHz up to 5 GHz. By contrast, with hexadecane as the solvent, the interaction is much stronger and there is considerable frequency dispersion in the sound velocity.

For microemulsion systems, the interaction energy still is large due to the increased area of contact between droplets. However, the water core reduces the inherent rigidity of the droplets themselves. These two effects compete, accounting for the behavior observed in these systems. If the droplet size is small enough, so that the attractive interaction energy is larger, yet the inherent rigidity of the droplets has not substantially decreased, we find a similar dispersion in the velocity with both ϕ and f as is found for the micelles. By contrast, as more water is added to increase the droplet size, the inherent rigidity of the droplet is decreased, and the extended networks can no longer support shear at any frequency. Thus no additional frequency dispersion of the velocity is observed for the larger sized droplets.

We use an effective medium theory[8] to describe our systems, since the size of droplets is much smaller than the wavelength of sound. The calculations of the elastic modulus as a function of volume fraction are carried out using two

models. One model assumes that the droplets are independent and do not support shear. This model is used to account for the sound propagation at low frequencies. The second model assumes that the droplet phase and the solvent phase form similar, interpenetrating morphologies. Thus, it includes the contribution of a shear modulus to the elastic modulus in the calculations. We find that only the second model with a shear modulus can fit the ϕ-dependence of the velocity at higher frequencies. Therefore, the theory suggests that the shear modulus from the instantaneous random network is responsible for the observed viscoelastic behavior.

The solid-like elastic behavior at high frequencies is a function of droplet volume fraction. For the surfactant phase to support shear, the molecules must span the whole system. This only occurs above some critical volume fraction, ϕ_c. Thus, the increase in the elastic modulus due to the contribution of shear exhibits a critical behavior. Indeed, we observed a power-law scaling of the additional increase in the elastic modulus, $\Delta\beta$, with volume fraction above $\phi \sim 0.16$. The scaling exponent is $t \simeq 2.5$. Thus the surfactant phase exhibits a dynamic rigidity percolation.

4.2 Effective Medium Theory

Effective medium theory is used to calculate the characteristics for a inhomogeneous system as a function of volume fraction of the constituent phases. It can be used to evaluate the effective elastic moduli for multicomponent composites.[8] The basic assumption of this theory is that the length scale of probing waves is much larger than the size of inclusions, so that the medium appears homogeneous to the probing wave, and so that multiple scattering effects due to the inhomogeneity are negligible. For a two-phase mixture, where one phase is a continuum and the other consists of inclusions randomly embedded in the continuous matrix, an effective medium theory are used to evaluate the average elastic modulus, β.

It is derived from the consideration of an inclusion isolated in an infinite effective matrix, which includes the effects of other inclusions.[8,9] In our experiments, the length scale is greater than 2000 Å, and the size of droplets are smaller than 200 Å. Thus, we apply the effective medium theory to determine the ϕ-dependence of the sound velocity in micelles and microemulsions.

The measured sound velocity, v, and the damping of sound, Δv, can be related to the complex effective elastic modulus, $\beta = \beta' + i\beta''$, by

$$v = \sqrt{\frac{\beta'}{\rho}} \quad , \quad \Delta v = \sqrt{\frac{\beta''}{\rho}} \tag{4.1}$$

where the average density is given by

$$\rho = \phi\rho_d + (1-\phi)\rho_o \tag{4.2}$$

where ρ_d and ρ_o are the densities for the droplet phase and the oil phase, respectively. The imaginary β'' is related to measured quantities by $\beta'' = \alpha 4\pi v^3\rho/f$ in the ultrasonic measurements and $\beta'' = \delta\nu 4v^2\rho/f$ in the Brillouin scattering, where α is the measured damping of sound from the ultrasonic measurements and $\delta\nu$ is the half width at half maximum (HWHM) of the Brillouin peak. The effective medium theory is used to determine the effective elastic modulus, including both β', and β''.

In order to calculate the effective complex elastic modulus, β, the elastic properties for the two constituent phases must be known. In our systems, all the required parameters for the oil are known either from the literature[10] or from measurements, including sound velocity, viscosity and index of refraction. We define the elastic modulus and the shear modulus, μ, for oil phase by adding the subscript o, and for droplet phase by adding d. The elastic modulus of the oil, β_o, is determined from the measured sound velocity, v_o, and the density, ρ_o, which is given from the literature, $\beta_o' = v_o^2\rho_o$. The imaginary part of the elastic

modulus of the oil, β_o'', is determined from the measured damping of sound, Δv, $\beta_o'' = (\Delta v_o)^2 \rho_o$. The measured shear viscosity, η_o, is used to determine the imaginary shear modulus, $\mu_o'' = i\omega\eta_o$. Since a viscous liquid has no shear, we set $\mu_o' = 0$. By contrast, a pure phase of AOT configured as droplets does not exist, so most of the parameters describing the surfactant phase can not be determined experimentally. The only parameter that is known is the density, $\rho_d = 1.13\ \mathrm{g/cm^3}$. Thus, we have four unknown parameters describing the oil phase, which are used to fit the data. They are the complex elastic modulus, β_d, and the complex shear modulus, μ_d.

The effective medium theory is a static model by its nature. However, the viscoelastic behaviors measured in our systems are frequency dependent. Therefore, we use the static model to fit our data for each frequency separately. The parameters for each phase in the fits could be frequency dependent, which reflect the frequency dependent of the viscoelastic behavior.

The selection of different basic structural units of the composite in the mixture produce different physical characteristics,[8] because the microstructure of the grains and their topological arrangements have an important influence on the calculated effective physical quantities. In fact, we have used two models in order to fit our experimental results.

At low frequency, we use a model which treats the micelles as independent droplets. The effective elastic modulus, β, is calculated using the Wood's approximation, which weights the inverses of β_o and β_d with their volume fractions,

$$\frac{1}{\beta} = \frac{\phi}{\beta_d} + \frac{1-\phi}{\beta_o} \tag{4.3}$$

This simple model does not admit any shear in the system. We use it to fit the data measured at low frequencies, where the system can not support shear because the extended networks formed by the droplets relax in a time much shorter than

the period of the sound. At high frequency, a random network is formed by the surfactant phase, and we must account for the possibility that this network supports shear. Thus we use an equal bases model, which can account for the formation of extended clusters by the droplets, which can support shear. This model includes the complex shear modulii, μ_o and μ_d, in the expression of β,[7]

$$\frac{1}{\beta} = \frac{\phi}{\beta_d + 4/3(\mu - \mu_d)} + \frac{1-\phi}{\beta_o + 4/3(\mu - \mu_o)} \tag{4.4a}$$

$$\frac{1}{\mu + H} = \frac{\phi}{\mu_d + H} + \frac{1-\phi}{\mu_o + H} \tag{4.4b}$$

where

$$H = \mu \frac{9\beta - 4\mu}{6\beta + 4\mu} \tag{4.4c}$$

The model reduces to the simple model of Eq.4.3, if μ_d and μ_o are zero. However, we take the value of μ_d' to be nonzero, implying that the droplet network does support shear. These equations reflect the fact that the longitudinal elastic modulus is modified by the shear modulus, because the system reacts elastically in response to an applied strain rate.

To solve these equations, there are four fitting parameters, which are those describing the pure AOT droplet phase, β_d', β_d'', μ_d' and μ_d''. The effective elastic modulus, β, in eq.4.4 is calculated by recasting those equations into a polynomial equation in μ,

$$2\mu^4 + M_3\mu^3 + M_2\mu^2 + M_1\mu + M_0 = 0 \tag{4.4'}$$

where M_i (i=0,1,2,3) are coefficients determined by ϕ, β_o, μ_o and the fitting parameters β_d and μ_d. The roots of eq.4.4' are determined, and the proper root is chosen by ensuring that both μ' and μ'' are positive. We then calculate β from eq. (4.4a), and finally determine v and Δv from eq. (4.1).

We use a nonlinear least squares routine to find the optimal values of the fitting parameters to compare with the volume fraction dependent data, $v(\phi)$ and

$\Delta v(\phi)$. Since the measurements of the sound velocity are much more reliable than those of the sound damping, we give a larger weight, by a factor of 5, to $v(\phi)$ than $\Delta v(\phi)$. We find that the fitting procedure is robust, and is relatively insensitive to the choice of initial values for the fitting parameters. Finally, since the effective medium theory assumes that both components in the system are space filling, while hard spheres cannot fill space, we have multiplied ϕ by .64, corresponding to the volume fraction for random close packing of spheres.[10]

The fitting parameters of β_d and μ_d in micelles represent the elastic constants of AOT micelles configured as networks of droplets. For the microemulsions, the parameters β_d and μ_d describe the behavior of the droplet phase, which is comprised of both water cores and the surfactant shells that separate the water from the oil. The additional rigidity must arise from the surfactant shells. Thus, it is interesting to know the elastic behavior for the pure AOT configured as the shells of the droplets, and to understand the contribution of this behavior to the β_d and the μ_d.

We use a coated sphere model to determine the contribution of the shells. This assumes the dispersed inclusions do not touch to each other; instead they are taken as coated grains dispersed in the matrix material. Thus the basic unit is a coated grain, or a water droplet coated by a surfactant layer. Using the subscript A to characterize the AOT surfactant shell, and W to characterize the water core, the calculations of β_d and μ_d from the coated sphere model are given by

$$\beta_d = \frac{\beta_A[4(\mu_A - \mu_W) + 3\beta_W]}{[4(\mu_A - \mu_W) + 3\beta_W](1-\phi) + 3\phi\beta_A} - \frac{4}{3}(\mu_A - \mu_d) \qquad (4.5a)$$

$$C1(\mu_A - \mu_d)^2 + C2(\mu_A - \mu_d) + C3 = 0 \qquad (4.5b)$$

Where the coefficients C1, C2 and C3 are coefficients determined by elastic properties of AOT shells and water cores, β_A, μ_A, β_W and μ_W, as well as the volume fraction, ϕ, of water in AOT. In fact, β_d and μ_d are determined from the sym-

metric model, then β_A and μ_A are fitting parameters in eq.(4.5). The elastic properties of water are known from either the literature[10] or our measurements. From the sound velocity measurements, $\beta_W{}' = v_W{}^2\rho_W$, and $\beta_W{}'' = (\Delta v_W)^2\rho_W$. Since water has no shear, we set $\mu_W{}' = 0$; also $\mu_W{}'' = i\omega\eta_W$, where $\eta_W = 1$ cp. We find that the elastic modulus for the AOT shells is $\sim 2 \times 10^9$ N/m^2, while the shear modulus is $\sim 9 \times 10^8$ N/m^2. Thus, the rigidity of the droplets is due to the contribution of the AOT shells since the water cores have no shear modulus and have a larger compressibility.

4.3 Experiment

The micelle and microemulsion systems are composed of spherical droplets dispersed in the continuous phase consisting of an alkane. We use AOT surfactant from Fluka without further purification, while the solvents, including decane, hexane, hexadecane are all Gold label. The droplet volume fraction is determined by the composition of each component. Each material is added by weight and then converted to volume fraction using the bulk densities with the assumption that there is no penetration of the oil within surfactant tails. In fact, there is some penetration of the oil into surfactant tails, which makes the actual values of ϕ less well defined due to the uncertainty of the *real* volume for a droplet.

In the micelles, 22 AOT molecules aggregate to form each spherical droplet.[2] In the microemulsions, the number of AOT molecules in each droplet varies with the size of the droplet and the amount of water added. For example, there are about 500 AOT molecules in each droplet when the radius is 50 Å.[3] The sizes of microemulsions we have studied are 25 Å, 45 Å and 75 Å in radius, which correspond to [H_2O]/[AOT] of 8, 25 and 41, respectively.

The determination of the speed of sound by Brillouin scattering experiments requires a knowledge of the scattering wave vector, $q = \frac{4\pi n}{\lambda}\sin(\theta/2)$, where θ is

the scattering angle, and n is the index of refraction of the system. The index of refraction is measured by a refractometer for each diluted sample at a uncertainty of ± 0.001. The measurement result of the ϕ-dependence of n for AOT micelles in decane is shown in Fig. 4.1. We find that the variation of n with ϕ is linear, and that the experimental data can be fit using a formula, $n(\phi) = (1-\phi)n_o + \phi n_d$, where n_o=1.4113 is the measured index of refraction for pure oil solvent, and $n_d = 1.448$ is the fitting parameter for pure AOT micelles phase. We also find that this value of n_d can fit the rest of results of n(ϕ) for all other samples. This indicates that the optical quantities in this two-phases system can be perfectly described by effective medium theory.

We have used both Brillouin scattering and ultrasonic techniques to measure the sound velocity from the micelle and microemulsion systems. Brillouin scattering allows us to measure sound velocities in the frequency range of 10^9 Hz, while ultrasonic techniques probe the velocities in the frequency range of 10^6 Hz. If the system has relaxation processes for which τ^{-1} is of order of MHz-GHz, we then can investigate this relaxation phenomenon by performing these experiments. On the other hand, if τ_c^{-1} is not in the frequency range measured, there is no frequency dispersion observed in the sound velocity.

4.4 Results and Discussion

In the last chapter, a detailed discussion of the sound propagation of AOT micelles in decane was presented, as well as the physical picture of dynamic rigidity percolation in the system.[7] In this section, those results will be extended by changing the chain length of the hydrocarbon solvent, or by adding water to form microemulsions. We will show that the variation of the interactions between the droplets due to the use of different solvents or variation in the size of the droplets results in different frequency dependencies of the speed of sound, and thus different

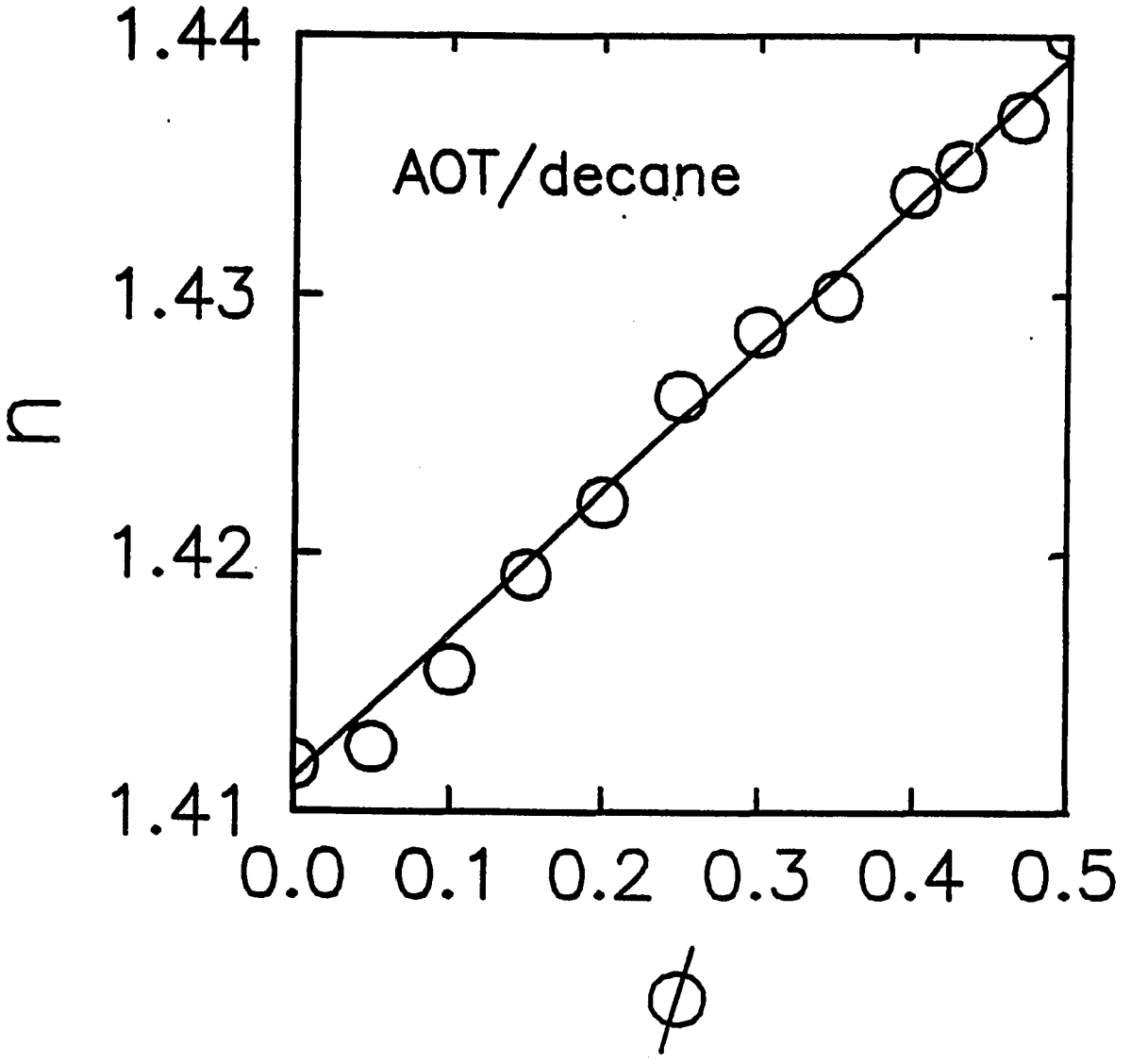

4.1 Index of refraction of the AOT/decane micelle and AOT/decane/water microemulsion systems as a function of droplet volume fraction. The solid line is a fit using $n = (1-\phi)n_o + \phi n_d$ with $n_d = 1.448$, and $n_o = 1.4113$.

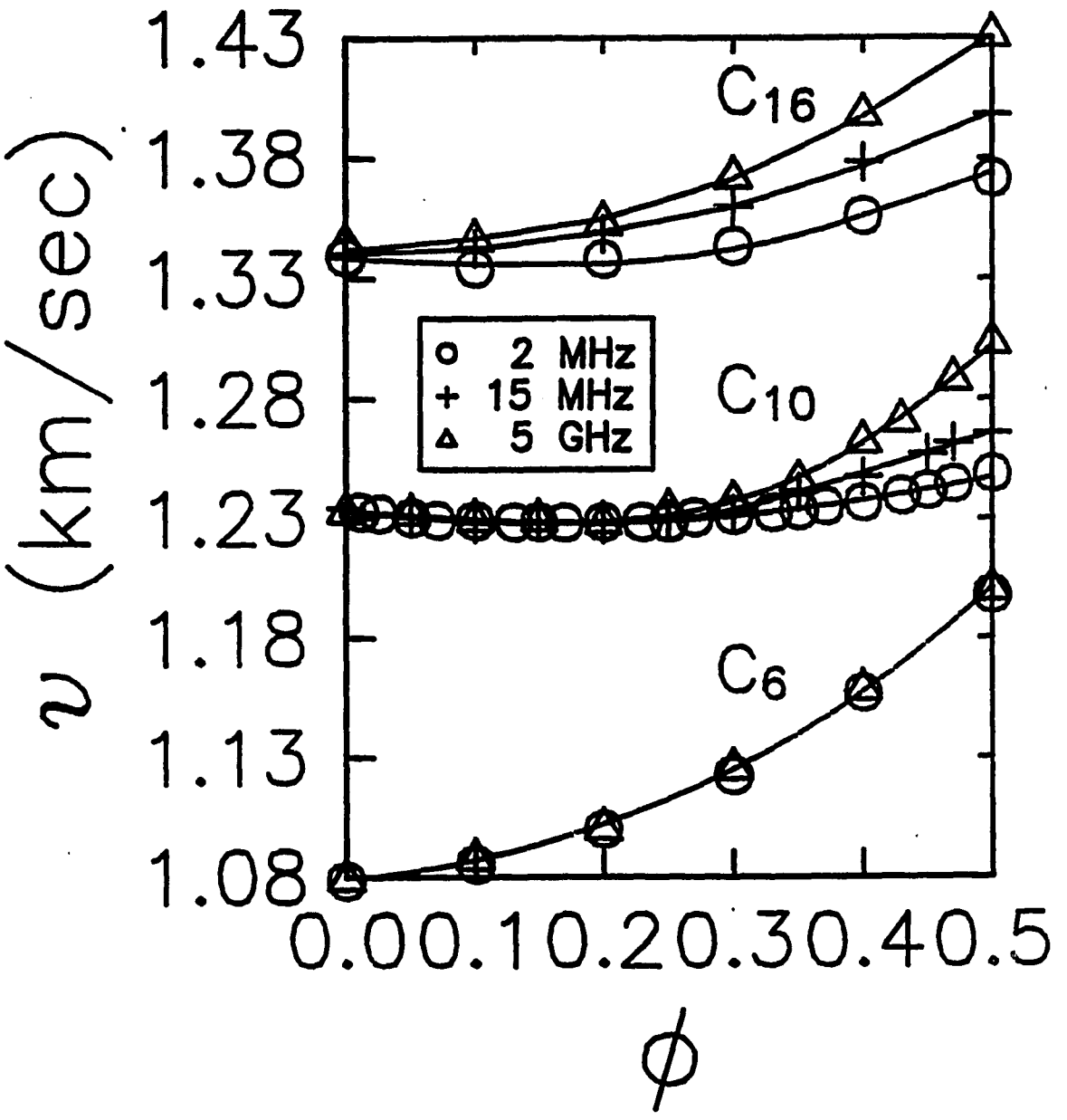

4.2 Velocity of sound in AOT inverted micelles as a function of volume fraction for several different solvents, hexane (C_6), decane (C_{10}) and hexadecane (C_{16}). Ultrasonic measurements were used to obtain the 2 MHz and 15 MHz data; Brillouin scattering was used to obtain the high frequency data. The solid lines are the fits with the effective medium theory.

viscoelastic behavior. We develop a self-consistent picture to account for all the observations and describe the dynamics of the AOT/water/oil mixture.

In inverted micelles, the solid core formed by the close packed head groups of AOT molecules is less compressible, or more rigid than the suspending fluid. Thus, with increasing volume fraction of micelles, the sound velocity increases due to the inherent rigidity of the micelles themselves. We illustrate this behavior in Fig.4.2, which shows the ϕ-dependence of v measured for micelles in different solvents, hexane (C_6H_{14}), decane ($C_{10}H_{22}$) and hexadecane ($C_{16}H_{34}$), and at different frequencies, obtained from both ultrasonic measurements (MHz) and Brillouin scattering (GHz). These measurements allow us to probe the effects of the different interaction energies between the droplets on the frequency dependence of the elastic properties.

There are several things one can learn from Fig.4.2. The average sound velocity changes with solvent, increasing as the alkane number in the solvent increases. The amount of dispersion in frequency also changes substantially as the chain length of the solution is increased. For hexane, there is no frequency dispersion of the sound velocity at all within the frequency range we measured. The solid line through the hexane data is the fit using Eq.4.3, the simple model which does not include any shear modulus. From the fit, we obtain the elastic constants of the droplets, $\beta'_d \simeq 9 \times 10^8$ N/m^2 and $\beta''_d \simeq 4 \times 10^6$ N/m^2. The absence of a shear modulus implies that the relaxation time is very fast due to the smaller interaction energy between droplets. Therefore, the critical frequency, f_c, for the system is too large to be seen in our frequency range.

As we increase the alkane number of the solvent by using decane, the data exhibit a pronounced frequency dispersion for $\phi \geq 0.16$. The larger interaction energy between droplets in this system leads to the longer relaxation time τ_c. For the low frequency measurements, with $\omega < 1/\tau_c$, we use the isolated droplet model

to describe the ϕ-dependence of the velocity. The results are shown by the solid line through the 2 MHz data. The use of this model to fit the data indicates that there is no contribution from shear at low frequencies. By contrast, if we apply the same model to the higher frequency data, we are unable to fit the data. Instead, we must use the symmetric model which accounts for the contribution of a shear modulus of the surfactant phase to the system. The solid lines through the 15 Mhz and 4 GHz data in Fig.4.2 are the results of the fit using the symmetric model. The fit gives $\mu' \sim 10^8$ N/m^2 at 5 GHz. The fitting parameters of β_d are $\beta'_d \simeq 1.62 \times 10^9$ N/m^2 at 2 MHz increasing to $\simeq 1.98 \times 10^9$ N/m^2 at 5 GHz, and $\beta''_d \simeq 6. \times 10^6$ N/m^2 at 2 MHz increasing to $\simeq 7. \times 10^7$ N/m^2 at 5 GHz. In addition, the frequency dependence of the shear modulus, μ'_d, has a Debye relaxation form, which was shown in Fig.3.2. Finally, the imaginary part of μ_d varies from 10^5 to 10^7 N/m^2 within the measured frequency range. The increase of β_d as frequency indicates that the stiffness in the droplet phase increases due to the formation of random networks, which contribute an additional shear modulus, μ_d.

When we further increase the alkane number of the solvent using hexadecane, a larger velocity dispersion in frequency is seen in Fig.4.2. In this case, however, the dispersion exists for all volume fractions. Indeed, even the hexadecane itself (ϕ=0) exhibits a slight frequency dispersion. To fit these data, we must use the symmetric model at all frequencies. We find that μ_d increases from $\simeq 2 \times 10^8$ N/m^2 at 2 MHz to 2.2×10^8 N/m^2 at 5 GHz, which means that the aggregation of droplets starts at the lowest frequencies that we measured. The fitting parameter, β_d, increases from 1.97×10^9 to 2.02×10^9 N/m^2 as the frequency increases from 2 MHz to 5 GHz, and the imaginary part of the shear modulus, μ''_d, increases from 1×10^6 N/m^2 to 3×10^6 N/m^2 from 2 MHz to 5 GHZ.

The data for all solvents exhibit a velocity dispersion in volume fraction, ϕ,

which reflects the fact that the droplet phase is more rigid than the solvent phase. By contrast, the average density increases as the AOT concentration is increased, which would tend to decrease the sound velocity. Thus the consequences of the density are not as important as those of the modulus in determining the sound velocity.

The observed variation of the frequency dependencies of the sound velocity on different oil solvents reveals a fact that the viscoelastic behavior of the micelles is directly related to the characteristic of the oil used. However, it is not simply the viscosity of the oil, as might be expected since the Brownian diffusion coefficient is inversely proportional to the viscosity. The viscosity for hexane, decane and hexadecane are 0.7, 1.3 and 3.1 cp, respectively;[11] while the frequency, f_c, shifts from micelles in decane to hexane by an order of magnitude, and from decane to hexadecane by even more than a order of magnitude. The experimental results indicate that the dynamics reflect the microstructural interaction time, rather than merely a Brownian diffusion time.

Another way to vary the interaction energy, and hence τ_c, is to change the size of droplets by swelling them with water to form microemulsions. This increases the radius of curvature, and thereby increases the area of overlapping tails for two interacting droplets, leading to an increase in the interaction energy. To study these effects, we show in Fig.4.3, the results of v as a function of ϕ for microemulsions in decane with three different sizes, 25 Å, 45 Å, and 75 Å in radius. They are obtained at 5 GHz using Brillouin scattering. The velocities for three systems increase with ϕ. The lines through the data represent the results of fits using effective medium theory. For the two microemulsions with smaller sizes, the fits must use the symmetric model, which includes the shear modulus due to networks formed by the microemulsion phase. The values of μ_d' from fits are $\sim 1.5 \times 10^8$ and 1.0×10^8 N/m^2 for the 25 and 45 Å radius samples, respectively.

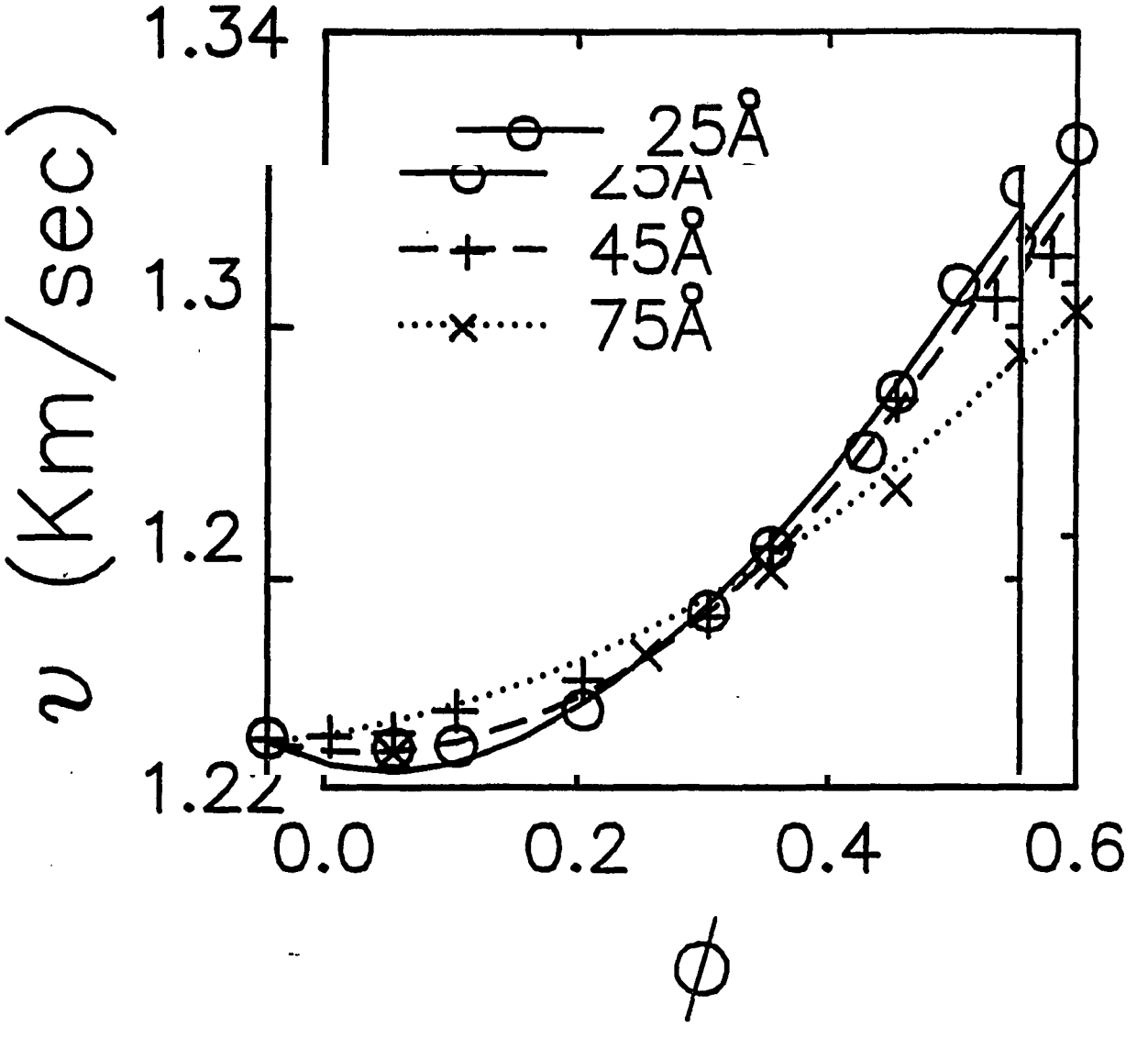

4.3 The velocity of sound for AOT/decane/water microemulsions of different sizes as a function of volume fraction. The solid lines represent fits to the effective medium theory.

By contrast, for microemulsions with 75 Å radius, the fit requires the simple model without shear. These results suggest that the interaction between microemulsions due to the entanglement of tails again leads to the formation of networks at high frequencies. For microemulsions with small size, the shear modulus results an increase of the longitudinal elastic modulus, β. However, as the microemulsion droplets grow in diameter, the increasing volume of water as compared to surfactants reduces the intrinsic rigidity of droplets themselves. Thus the shear modulus decreases as the droplet size grows.

We also investigate the frequency dispersion of the sound velocity in microemulsions by measuring the dependence of v on ϕ using ultrasonics from 2 MHz to 30 MHz. Virtually no additional frequency dispersion is observed for any of these microemulsion samples, which suggests that the increased contact area, resulting from the larger radius of curvature of microemulsions, causes the interaction energy to increase. Thus τ_c is increased, so that $f >> \tau_c^{-1}$ for all the frequencies used.

To confirm this picture, we can exploit the behavior observed for the micelles, and change the interaction energy by varying the chain length of the hydrocarbon solvent. In order to bring the frequency dispersion into an experimentally accessible region, we must decrease the interaction energy between droplets, which requires the use of a solvent with a shorter chain length. Thus we repeat the measurements for the 25 Å radius microemulsions using hexane as the solvent. As expected, considerable additional frequency dispersion is indeed observed. This is illustrated in Fig.4.4, where we show the sound velocity as a function of droplet volume fraction ϕ measured in three different frequencies. The data in MHz regime are measured using ultrasonic techniques, and the data in GHz regime are using Brillouin scattering. A similar frequency dispersion with velocity, as seen in the micelles in decane, also appears here. The effective medium theory fit to the 2

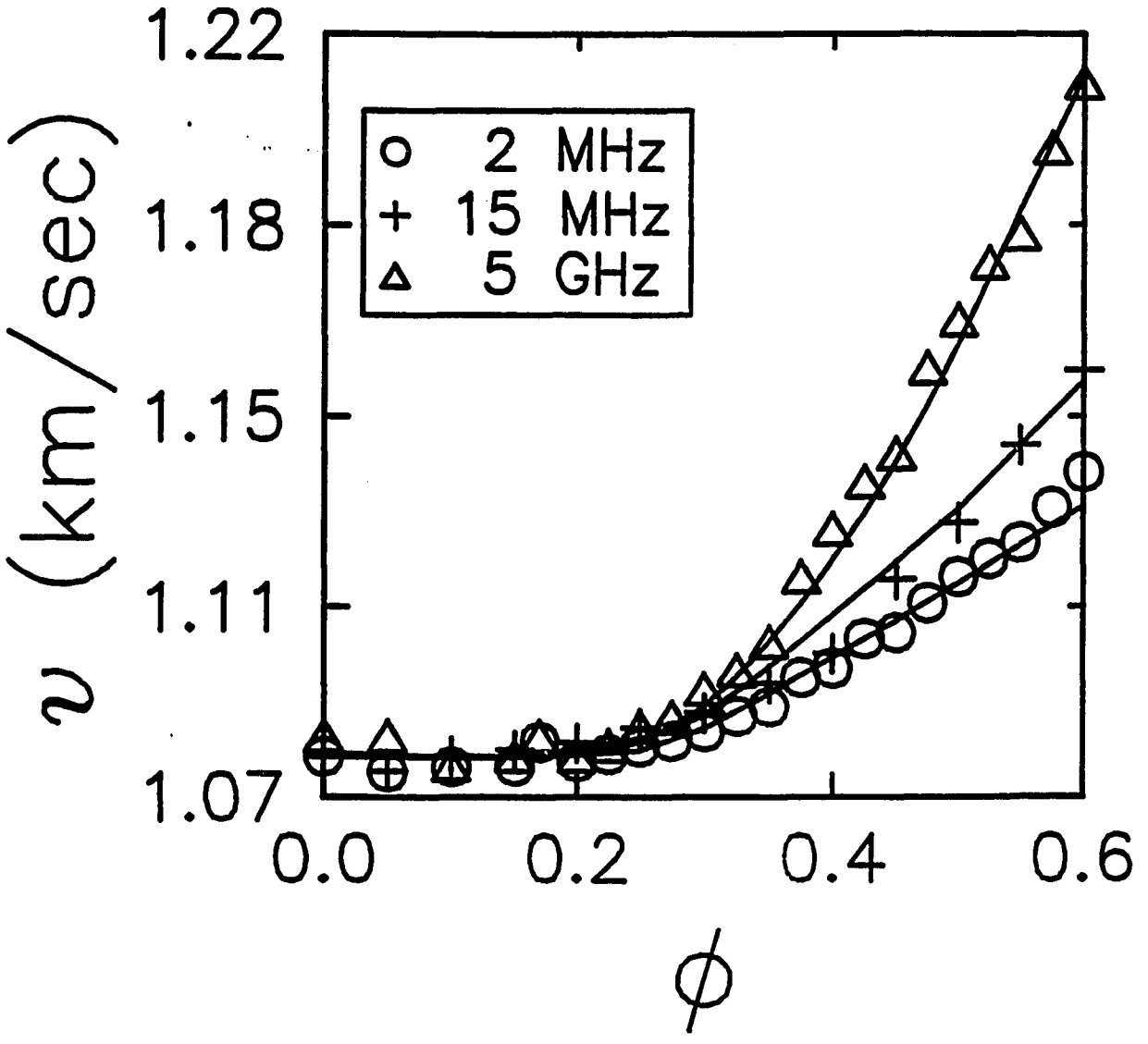

4.4 Velocity of sound in AOT/hexadecane/water microemulsions as a function of volume fraction for different frequencies. The droplet sizes are 25 Å in radius. The solid lines represent fits to effective medium theory.

MHz data results in a shear modulus near zero for the microemulsion phase. By contrast, the fits to the data at highest frequency yield a shear modulus, $\mu_d \simeq 1.8\times10^8$ N/m^2. In fig.4.5 we plot the velocity as a function of frequency for several different volume fractions. The behavior is again similar to that observed in Fig. 3.2 for the AOT micelles in decane: an additional increase in v as the frequency increases, with the asymptotic values approached at both high and low frequencies. Furthermore, the increase in v is larger for higher droplet volume fractions. The solid line are fits to a Debye model with a single relaxation time, $\tau_c \sim 10^{-8}$ sec. These results confirm the physical picture of a transition of the surfactant phase from a viscous liquid behavior to a elastic behavior at high frequency, due to the short-lived random networks formed by droplets.

Since the behavior of 25 Å radius microemulsion in hexane is very similar to that seen for micelles in decane, we can also look for a scaling behavior indicative of dynamic rigidity percolation. Thus in Fig. 4.6, we plot the increase in β' between low and high frequencies, $\Delta\beta'$, as a function of $\phi-\phi_c$ on a logarithmic scale. The scaling behavior is again observed. The solid line is a fit to $\Delta\beta' \sim (\phi-\phi_c)^\tau$, where we obtain $\phi_c \simeq .15$ and $\tau \approx 2.5$. Both parameters are in excellent accord with the scaling behavior of the micelle data shown in Fig.3.3. Thus we successfully observe a dynamic rigidity percolation for the microemulsion system as well, provided we adjust the solvent to bring τ_c into a measurable range.

4.5 Spectral Fitting

The Brillouin spectral distribution is derived from thermodynamics and hydrodynamics, since the density fluctuations, which scatter the light, involve collective motions of large numbers of molecules. For simple liquids, the spectrum is a sum of Lorentzian peaks as is discussed in chapter 1. However, for molecular fluids, an additional prominent continuous background is found between the Rayleigh and

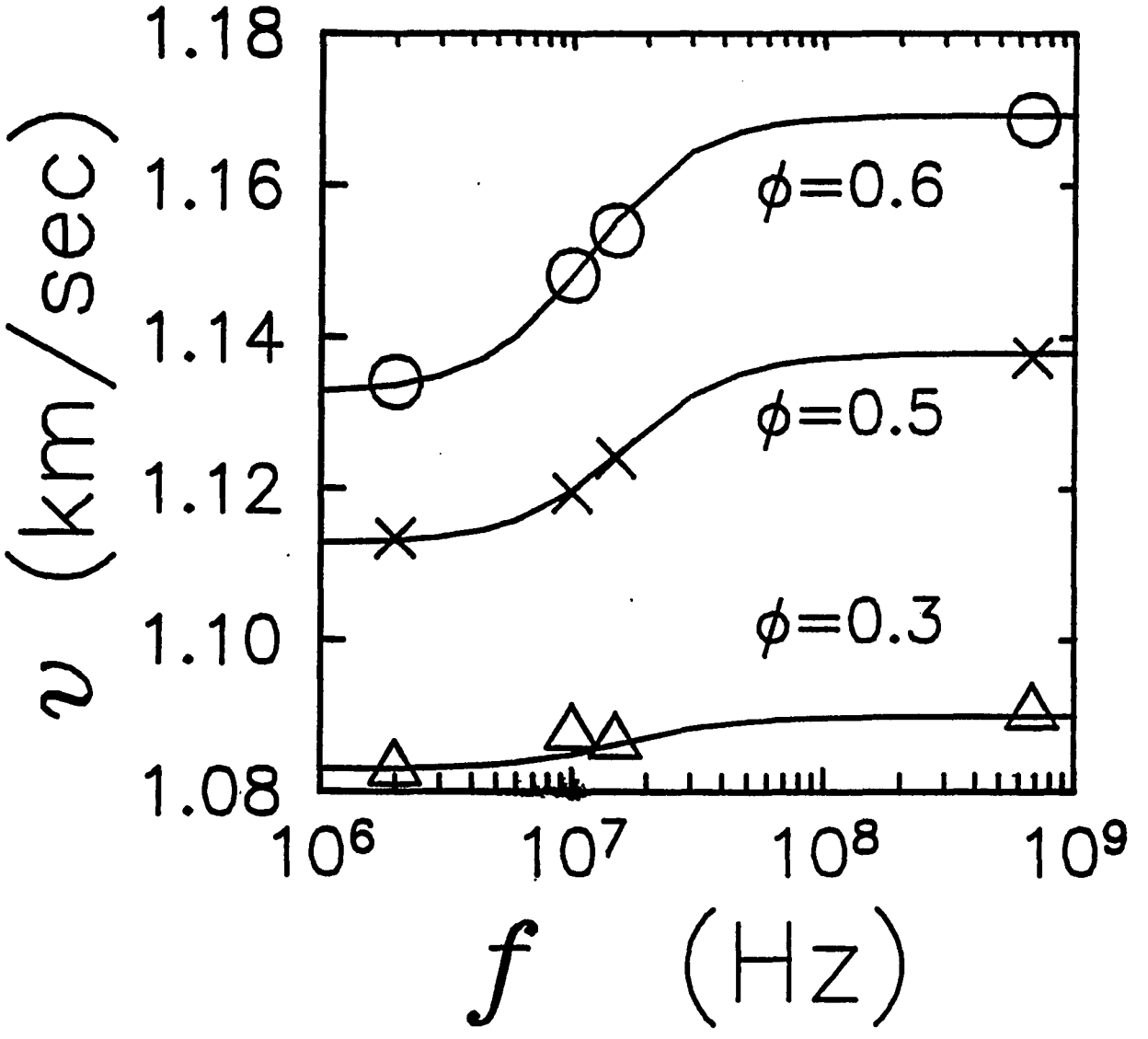

4.5 Frequency dispersion of sound velocity at three volume fractions: $\phi = 0.3$, 0.5 and 0.6. The solid lines are single Debye relaxation with $\tau \simeq 1 \times 10^{-8} sec.$ The additional increase of v at high frequency is a function of ϕ, which implies an increase in the elastic modulus due to the micelle networks.

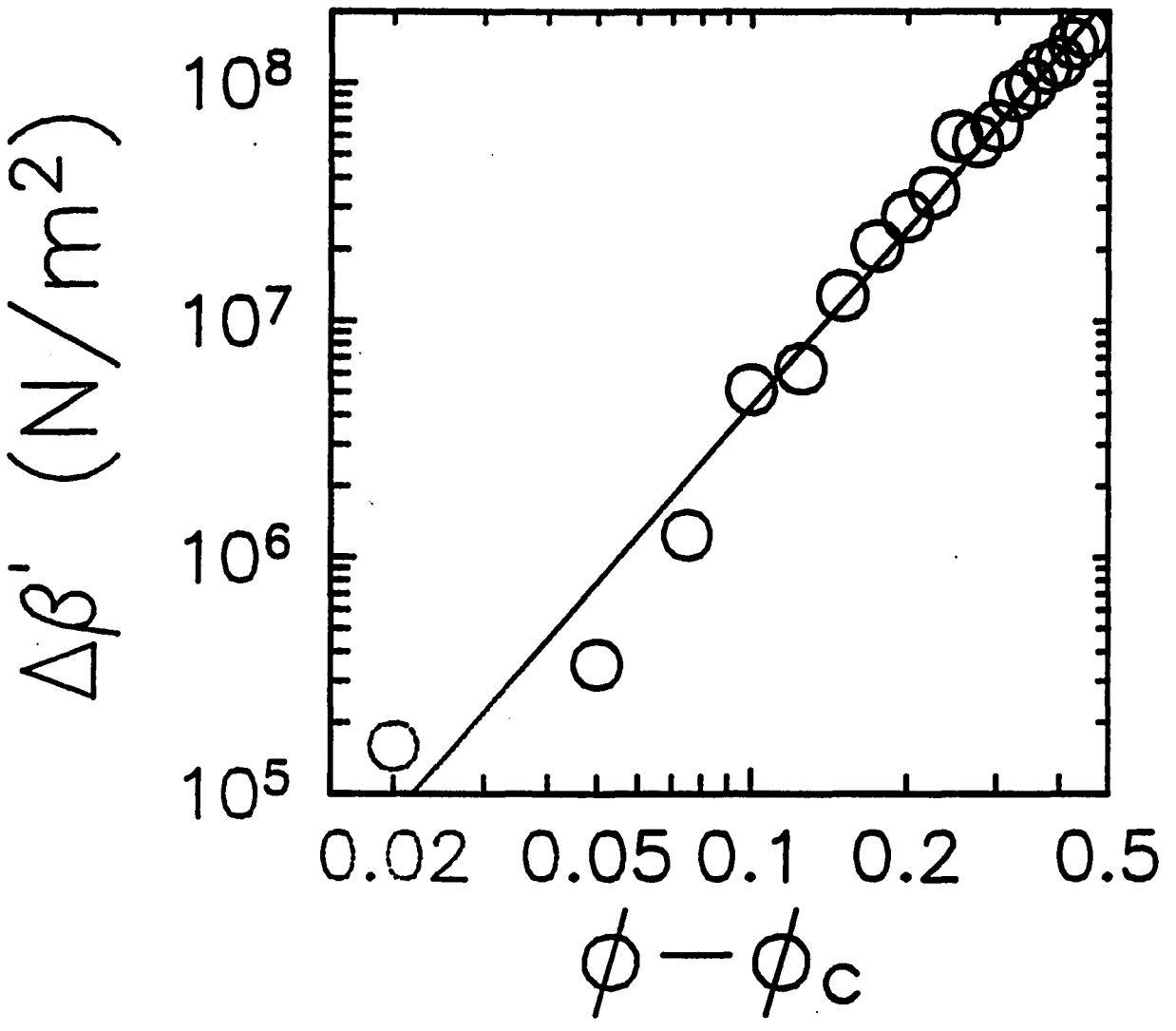

4.6 An additional elastic modulus, $\Delta\beta$, at high frequencies as a function of the volume fraction of droplets, which shows the critical behavior of the shear modulus contribution at high frequencies in microemulsions in hexane. The solid lines are calculations of $(\phi - \phi_c)^t$ with $t \simeq 2.5$, and $\phi_c = 0.15$.

the Brillouin doublet.[13] A typical spectrum is shown in Fig.1.2 for CCl_4. The interpretation is that the molecular internal degree of freedoms couples to the translational motion, and thus contribute to the scattered light.[14] Therefore, the Rayleigh and Brillouin peaks are no longer Lorentzian in shape. Furthermore, the theory must account for the dynamics of the molecular relaxation, and the additional intensity in the spectra between the Rayleigh and Brillouin peaks.

The Brillouin spectra of micelles and microemulsions in our experiments also show significant intensity in the region between the Rayleigh and Brillouin peaks. We might expect the relaxation of the extended networks to produce this broad background in a analogous to the molecular relaxation of simpler molecules. To test this hypothesis, we have employed Mountain's formula[15] to compare to our measured spectra. Excellent results are obtained, both for the shape of spectra and for the fitting parameters which describe the dynamics of structural relaxation process.

In 1966, Mountain developed a generalized hydrodynamic theory[14] to describe the Brillouin spectra of viscous fluids, in which the structural relaxation plays a important role. He proposed a molecular relaxation model by modifying shear and bulk viscosities with additional relaxation mechanisms, and deduced a frequency dependent bulk viscosity, $\eta_V(\omega)$, given by[15,16]

$$\eta_V(\omega) = \eta_V + \frac{(v_\infty^2 - v^2(\omega))\tau}{1 + i\omega\tau} \tag{4.6}$$

where η_V is the center-of-mass part of the bulk viscosity at constant volume, V, and is frequency independent; τ is the relaxation time, and v_∞ is the sound velocity in the high frequency limit. The frequency dependence of $\eta_V(\omega)$ is such that for ω small compared to the relaxation rate $1/\tau$, $\eta(\omega) \to \eta_V + [v_\infty^2 - v^2(\omega)]\tau$; for frequencies large compared with $1/\tau$, $\eta_V(\omega) \to \eta_V$. Thus, $\eta_V(\omega)$ describes the dynamics of the molecular relaxation process in the viscosity. Based on the classical

hydrodynamics which yields the Brillouin spectra for simple fluids, Mountain then applied the new concept to calculate the spectra for viscous fluids. The intensity distribution, for constant q, is given by [15,16]

$$I(\omega) = const.\frac{N_1(\omega)D_1(\omega) + N_2(\omega)D_2(\omega)}{D_1{}^2(\omega) + D_2{}^2(\omega)} \tag{4.7}$$

where

$$N_1(\omega) = -\omega^2 + \gamma D_T D_V q^4 + v^2 q^2(1 - 1/\gamma) + (\gamma D_T b'_1 q^4 + b'_1 \omega^2 q^2 \tau)/(1 + \omega^2\tau^2) \tag{4.7a}$$

$$N_2(\omega) = \omega[\gamma D_T q^2 + D_V q^2 + (b'_1 q^2 + \gamma D_T b'_1 \tau q^4)/(1+\omega^2\tau^2)] \tag{4.7b}$$

$$D_1(\omega) = -\omega^2(\gamma D_T q^2 + D_V q^2) + v^2 q^4 D_T + (\gamma D_T b'_1 \omega^2 q^4 \tau - b'_1 \omega^2 q^2)/(1 + \omega^2\tau^2) \tag{4.7c}$$

$$D_2(\omega) = \omega[-\omega^2 + v_2 q^2 + \gamma D_T D_V q^4 + (b'_1 q^2 \omega^2 \tau + \gamma D_T b'_1 q^4)/(1+\omega^2\tau^2)] \tag{4.7d}$$

and where

$$b'_1 = \frac{(v_\infty{}^2 - v^2)\tau}{\rho}$$

In these equations, D_T is the thermal diffusivity, $D_V = \eta_l/\rho$, is the longitudinal kinematic viscosity, and γ is the Landau-Placzek ratio.

The exact expression for the Brillouin spectrum with the structural relaxation involved in Eq. 4.7 is simplified under the condition of small viscosity, such that $D_V q^2 << \omega(q)$, where $\omega(q)$ is the frequency of the Brillouin shift. Then the spectrum is comprised of three Lorentzian peaks: the first is the Rayleigh peak, the second is the pair of Brillouin peaks, while the third is a broad Mountain peak centered at zero frequency.[17] The width of the Rayleigh peak depends on the thermal diffusivity, $D_T = \frac{\lambda}{\rho C_P}$, where λ is the thermal conductivity, and C_P is the specific head at constant pressure. The Brillouin doublet has a frequency shift $|\omega| = vq$, and the width depends on the longitudinal viscosity, η_l. The width of the Mountain peak depends on the structural relaxation time, τ^{-1}.

We have convoluted these equations with the instrumental response function in Eq. 2.1a to calculate the spectra observed. In our calculations, those known constants are: the average density ρ, and the average sound velocity v measured from experiments. The velocity v is measured from the frequency shift of the Brillouin peaks. In fact, we have also tried to fit the spectra using v as a fitting parameter. We find that the influence of the Mountain peak on the position of the Brillouin peaks does not result a significant difference between the measured v and the fitting parameter of v. The Mountain peak is sensitive to both the relaxation time, τ, and the ratio of v/v_∞. If both v and v_∞ are used as fitting parameters, unreliable values are obtained for these parametrs as well as τ. To avoid this, we fix the value of v using the maximum of the Brillouin peaks. Thus the fitting parameters are: D_T, D_V, γ, τ, v_∞ and the intensity normalization constant.

The fits to the spectra using Eq. 4.7 for micelles in hexane, decane, and hexadecane are shown in Fig.4.7, for ϕ=0.5, and measured at $\theta = 90°$. There is an additional continuous background, between the Rayleigh peak and Brillouin peaks, when compared with the spectrum for simple liquid shown in Fig.1.1 of chapter 1. This additional central peak is due to the coupling between the translational and the structural rearrangement motion associated with the relaxation behavior of the dynamic viscosity.

We find that the shape of the spectrum is sensitive to each of fitting parameters, but their effects can be distinguished. The width of the Reyleigh peak is determined by $D_T q^2$; since the measured width is close to the limit of the resolution of the interferometer, we are unable to precisely determine the value of D_T. It is on the order of 10^{-3} cm^2/sec, which is the same order of magnitude as D_T determined for decane or CCl_4.

The width of the Brillouin peak is determined by $D_v q^2$. For simple liquids, the width of the Brillouin peak is expected to increase with increasing viscosity

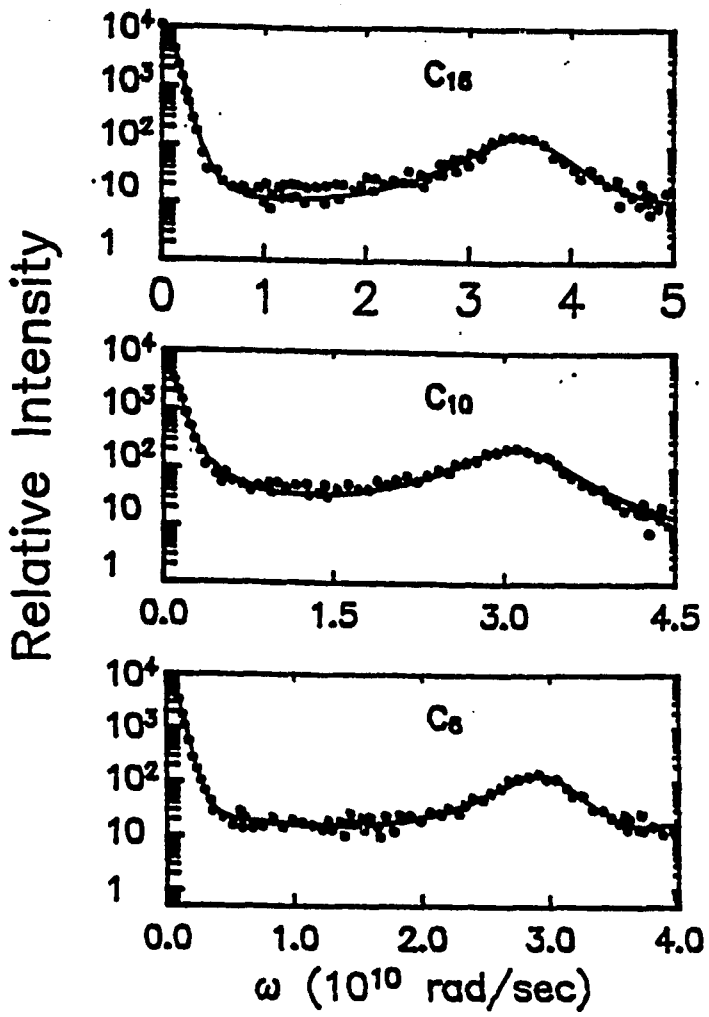

4.7 Brillouin spectra of AOT micelles for several different solvents, hexane (C_6), decane (C_{10}) and hexadecane (C_{16}) at ø=0.5. The solid lines are the theoretical spectra calculated from Eq. (4.7). The scattering angle is 90°.

since $D_V = \eta_l/\rho$. However, for viscoelastic fluids, both the shear and the bulk viscosities are frequency dependent, $\eta \sim \frac{\tau}{1+\omega^2\tau^2}$,[18] where ω is the frequency shift of Brillouin peaks. The width of the Brillouin peaks will reflect the structural relaxations in the fluid. When $\omega\tau < 1$, the width of the Brillouin peak is proportional to τ since $\eta \sim \tau$; while when $\omega\tau > 1$, the width of the Brillouin peak is proportional to $\frac{1}{\omega^2\tau}$, which means the width becomes narrower as τ is larger in this regime. For micelles in decane, we have measured both the static shear viscosity, using a viscosimeter, and the width of the Brillouin peak. From the static measurements, we find that η_s increases from .78 cp for pure decane up to 17.6 cp for micelles at ϕ=0.5; while from the Brillouin scattering, the D_V increases by less than an order of magnitude from low to high volume fraction: $D_V \simeq 2.3 \times 10^{-2}$ cm^2/sec for decane while $D_V \sim 1.1 \times 10^{-1}$ cm^2/sec at $\phi = 0.5$. For decane, the structural relaxation time is $\sim 1 \times 10^{-10}$ sec from our spectral fitting, which means the measured width is $\propto \tau$ even at $\omega = 4$ GHz. However, for the micelles in decane at ϕ=0.5, $\tau \sim 10^{-8}$ sec. Therefore, at GHz frequency regime where $\omega\tau > 1$, the width of the Brillouin peak is on the same order as the width of decane at GHz frequency regime.

The prominent background induced by the relaxation mechanism in the spectrum depends on the relaxation time, τ, and the velocity ratio, v/v_∞. For micelles in decane and microemulsions in hexane, where continuous backgrounds are observed, the values of τ obtained from fits are $\tau_{C_{10}} \simeq 1.4 \times 10^{-8}$ sec and $\tau_{C_6} \simeq 2.4 \times 10^{-8}$ sec. These are in excellent agreement with the values of τ obtained from the measured frequency dispersion of the velocity fit to a single relaxation time Debye behavior. In addition, the values of v_∞ obtained from the spectral fitting of the two systems are also consistent with those obtained from measured frequency dispersions: the fits to the spectra give $v_\infty \simeq 1309$ m/sec for micelles in decane at $\phi = 0.5$, and $v_\infty \simeq 1140$ m/sec for the 25 Å radius mi-

croemulsions in hexane with $\phi = 0.5$. The values are in excellent agreement with the values of 1298 m/sec in Fig.3.2 for the micelles and of 1138 m/sec in Fig.4.5 for the microemulsions. When $\omega\tau > 1$, the Mountain Peak becomes very narrow and can not be distinguished from the Rayleigh peak. Thus for micelles in hexadecane, where $\tau > 10^{-7}$ sec compared with micelles in decane, we do not see a Mountain peak. In addition, for 75 Å radius microemulsions in decane, when the swollen water cores reduce the rigidity of the droplet phase, there is no contribution of the microemulsion structures, and the spectra are again similar to those of simple fluids where we do not see a Mountain peak.

The Landau-Placzek ratio, $\gamma - 1$, is the intensity ratio of the Rayleigh peak to the Brillouin doublet, as explained and derived in chapter 1. As a fitting parameter, we find $\gamma \simeq 1.2$ for decane, consisted with $\gamma = 1.219$ measured for n-hexadecane by Patterson et al.[19] We find that γ increases up to 1.8 at high ϕ in micelle systems. However, the values of γ obtained from the fits to the spectra of microemulsion systems, at larger droplet sizes and higher ϕ, are as large as 10. This is due to a strong Rayleigh scattering in the system. Similar behavior has been found in polymer fluids[20], where the intensity ratio of the central peak to the Brillouin doublet is often much greater than unity.

We also attempted to apply a binary mixture model to fit our spectra. The binary mixture model accounts for additional concentration fluctuations which contribute to the density fluctuations. Thus the central component consists of a superposition of two peaks, one resulting from entropic fluctuations, and the other from concentration fluctuations. We find that this model can not adequately describe our results. The calculated Rayleigh peak from the model is too broad to fit our spectrum, which implies that concentration fluctuations do not play an important role in these microemulsion systems.

In summary, the spectral fitting using Mountain's relaxation model is very

successful. The coupling between the translation and structural rearrangement motions leads to a new nonpropagating mode, with a width on the order of $1/\tau$.[13,15] For the micelle and microemulsion systems, the parameter τ reflects the dynamic structure relaxation in the system. In addition, the relaxation time, τ, and high frequency sound velocity, v_∞, from the spectral fitting are consistent with those given by the Debye relaxation model fit to the measured frequency dispersion of the sound velocity. Finally, the computed curves are in good agreement with most of the measured spectra.

4.6 Relaxation of Surfactant Molecules

In this section we discuss an additional dramatic frequency dispersion of the sound velocity found in all the micelle and microemulsion systems. Near the backward scattering configurations, we find that the sound velocity increases rapidly within a very short frequency range, regardless of solvents and droplet sizes. We interpret this behavior as a further relaxation process of the surfactant tails themselves.

The experimental results are shown in Fig.4.8, where we plot the dependence of v on frequency for micelles and for three sizes of microemulsions, with radii 25 Å, 45 Å and 75 Å, all at ϕ=0.5 and all in decane. The data are obtained by varying the scattering angle from 30° to nearly 180°, using an Ar^+ laser at 5145 Å, except for the last data point for each system, which is obtained with the 4880 Å blue line at nearly 180o. The velocity, v, for each system, increases dramatically, by as much as 5%, when the frequency varies from 5GHz to 8 GHz. Furthermore, this additional frequency dispersion of v is observed in all AOT micelle and microemulsion systems, regardless of the size of the droplets or the solvent used. These results imply a further relaxation process, which results the increase in the stiffness of the mixture at higher frequency.

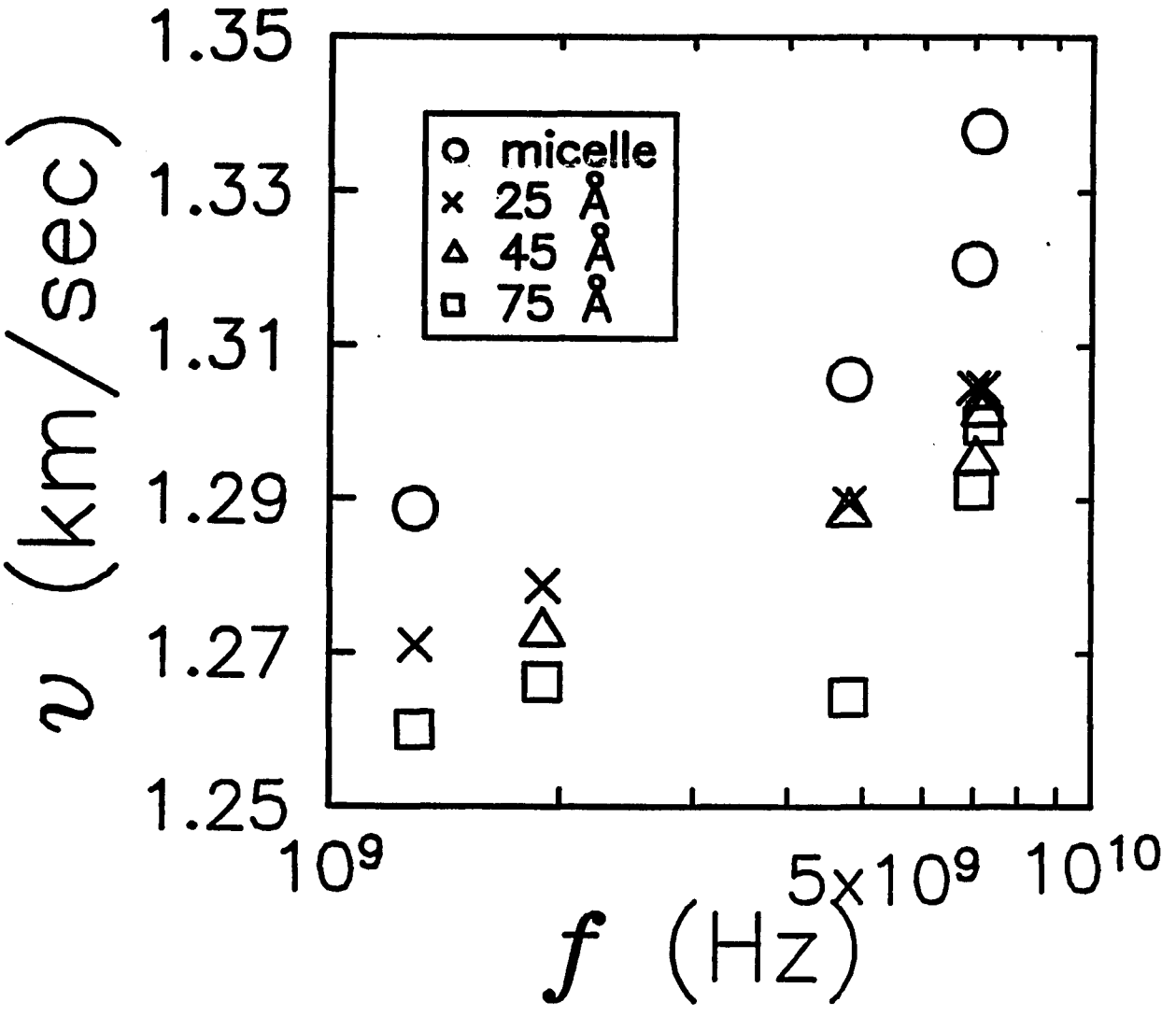

4.8 Additional frequency dispersion of sound velocity for AOT micelle and microemulsions in decane at $\phi = 0.5$, indicating a relaxation of the tails of the AOT molecules themselves.

We interpret this behavior as arising from the additional relaxation of the surfactant tails, since it is independent of the solvent and the droplet size. Thus, there is an additional characteristic time, τ_{ac}, corresponding to some form of motion of the tails. The inverse of the relaxation time is slightly above 5 GHz. When the period of sound wave is shorter than τ_{ac} at higher frequency, there is no enough time for this tail motion to relax, and the system appears stiffer, increasing the velocity of sound. This additional molecular internal degree of freedom may also contribute to the stiffness of the extended networks formed by the droplets. To examine this possibility, in Fig.4.9, we plot the increase in the elastic modulus from 1 GHz, which is the plateau of the single Debye relaxation, as a function of $\phi - \phi_c$ for the micelles in decane. Unlike the previous dispersion observed at lower frequencies, we are unable to reach the asymptotic value of v at the highest frequencies. Thus we chose the value measured at the highest angle we can achieve. In Fig.4.9, we again find that the data exhibits a power-law scaling. As before, the data are well described by $\Delta\beta' \sim (\phi - \phi_c)^\tau$, with $\phi_c \sim 0.16$ and $\tau \sim 2.5$, in excellent agreement with the previous value. This implies that the additional rigidity contributed by the "frozen" surfactant at high frequency also contributes to percolating networks. At higher ϕ, there are more AOT molecules in the system to contribute to the enhancement of the elastic modulus, making it a function of droplet volume fraction.

The experimental results of the frequency dependence of elastic behaviors reveal a fact that these micelles and microemulsions phases involve more than one structural relaxation processes. These relaxations contribute in different time scales, and thus these systems exhibit a rich viscoelastic behavior.

4.7 Conclusion

In summary, we have measured the frequency dependence of the sound velocity

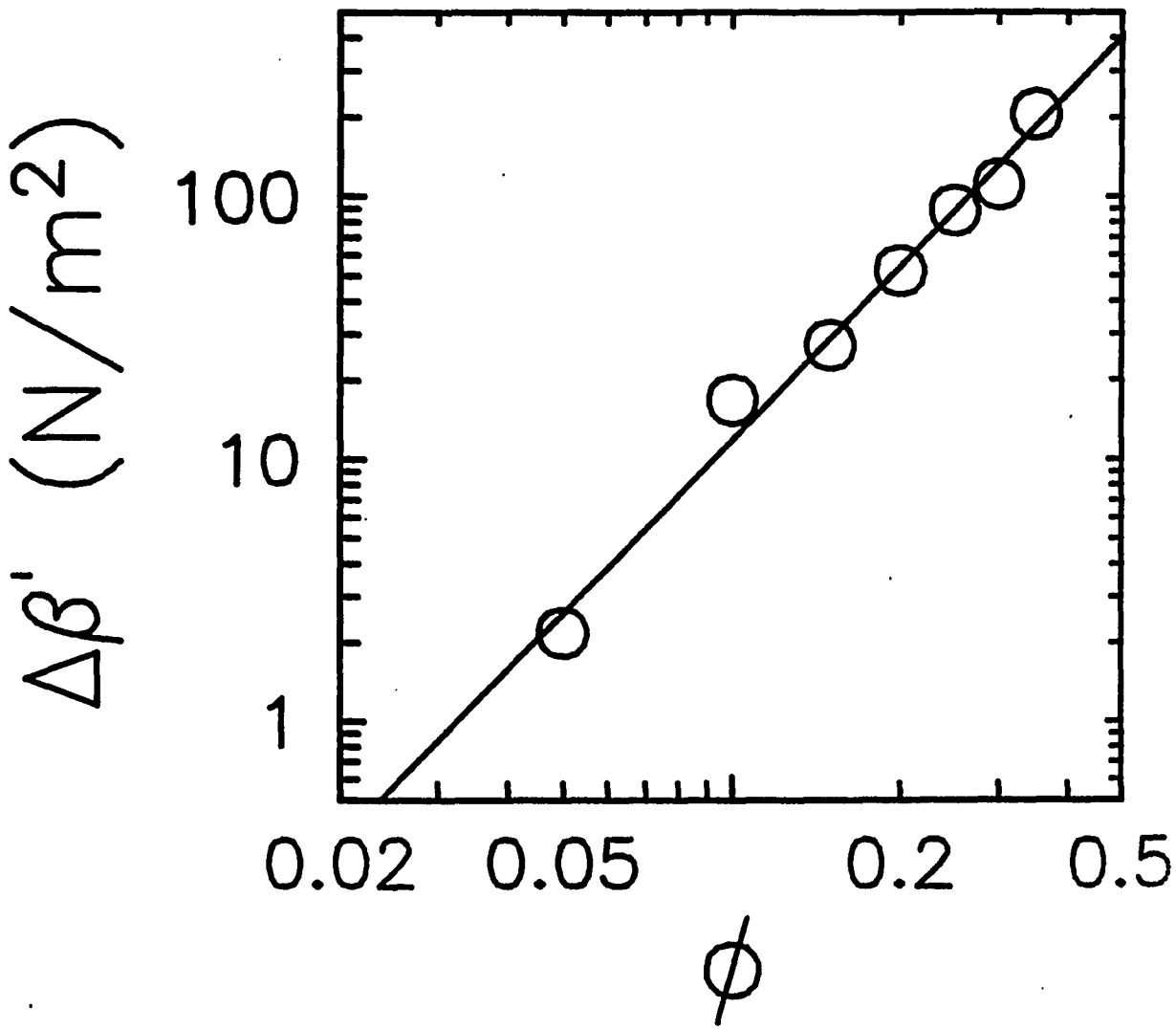

4.9 Additional elastic modulus due to the relaxation of the tails of AOT surfactant molecules in the system, as a function of volume fraction, demonstrating a further enhancement of the dynamic rigidity. The solid lines are calculations of $(\phi - \phi_c)^t$ with $t \simeq 2.5$, and $\phi_c = 0.16$.

in micelle and microemulsion systems at varying droplet concentrations. The velocity dispersion arises from the formation of short lived, long range structures due to the weak attractive interaction between droplets. The frequency dispersion is well described by a Debye relaxation model with a single relaxation time, with $\tau \sim 10^{-8}$ sec. The relaxation time varies with the interaction energy, which can be changed by using different solvents and by changing the sizes of the droplets. The larger the alkane number of the solvent, or the larger the size of the droplet, the larger the interaction energy, and hence the longer the relaxation time.

In addition, the observed increase in the elastic modulus at high frequency has a power-law scaling with the droplet volume fraction, which suggests a dynamic rigidity percolation. The scaling exponent is $t \simeq 2.5$, and the volume fraction threshold is $\phi \sim 0.16$ for both the micelle and the microemulsion systems. The same scaling behavior in both systems provides a consistent picture of the dynamics in each system.

The effective medium approach to the sound velocity as a function of droplet volume fraction enables us to determine the contribution of the shear modulus of the droplet networks to the total elastic modulus. In addition, the frequency dependence of the shear modulus for rigid droplet phase given by the fitting shows a Debye relaxation form, which behaves the same as the measured sound velocity. Therefore, effective medium theory provides a self-consistent picture on the description of the structural dynamics of the micelle and microemulsion systems.

Finally, the fits of the spectra using Mountain's formula is successful for both the micelles and the microemulsions. The contribution of the dynamics of the structural rearrangements to the observed intensity distribution is very well described in terms of the dynamics of frequency dependent viscosities. Both the relaxation time, τ, and the high frequency limit of v, v_∞, are given by the fitting

process and are consistent with those given by the Debye relaxation model.

Therefore, we conclude that the study of sound propagation in AOT micelles and microemulsions provides a fundamental understanding of the viscoelastic behavior in complex fluids. When the length scale of microstructures is small compared with that of probing waves, an effective medium approach can be used to describe the effective elastic modulus; the frequency dependence of the sound velocity indicates a dynamic relaxation, accounting for the dynamics of microstructural rearrangements, as well as the compressibility of each phase in the system.

References

[1] **Surfactants in Solution** ed. by K. Mittal and B. Lindman. *Plenum, N.Y.* (1984)

[2] M. Kotlarchyk and J. S. Huang. **J. Phys. Chem.** 89, 1985 (1985)

[3] M. Kotlarchyk, S. H. Chen and J. S. Huang. **J. Phys. Chem.** 86, 3273 (1982)

[4] T. Assin, F. Larche and P. Delord. **J. Colloid Interfaces Sci.** 89, 35 (1982)

[5] J. S. Huang. **J. Chem. Phys.** 82, 480 (1985)

[6] J. S. Huang, M. Kotlarchyk and N. Quirke. **Phys. Rev. Lett.** 53, 592 (1984)

[7] L. Ye. D. A. Weitz, P. Sheng, S Bhattacharya, J. H. Huang and M. J. Higgins. **Phys. Rev. Lett.** 63, 263 (1989)

[8] P. Sheng. in **Homogenization and Effective Modulii of Materials and Media** ed. J.L. Ericksen, D. Kinderleher, R. Kohn and J.L. Lions (*Springer – Verlag, N.Y.*) p.196 (1983)

[9] G. T. Kuster and M. N. Toksoz **Geophysics.** 39, 587-618 (1974)

[10] R. Zallen **The Physics of Amorphous Solids** (Wiley, N.Y.) (1983) p. 49

[11] **Handbook of Chem. and Phys.** 66, ed. by R. C. Weast, (CRC *Press*) (1985-1986)

[12] L. Ye. D. A. Weitz, P. Sheng, and J. H. Huang. "Dynamic Rigidity Percolation In AOT micelles and Microemulsions" **MRS Proceedings** (1990)

[13] E. F. Carome, W. H. Nichols, C. R. Kunsitis-Swyt and S. P. Singal. **J. Chem. Phys.** 49, 1013-1017 (1968)

[14] R. D. Mountain. **J. Chem. Phys.** 44, 832-833 (1966)

[15] R. D. Mountain. **CRSS.** 1, 5 (1970)

[16] B. J. Berne and R. Pecora. "Dynamic Light Scattering" John Wiley & Sons,Inc. New York, (1976) p. 247

[17] W. H. Nichols and E. F. Carome. **J. Chem. Phys.** 49, 1000 (1968)

[18] P. J. Carroll and G. D. Patterson. **J. Chem. Phys.** 81, 1666 (1984)

[19] G. D. Patterson and C. P. Lindey. **J. Appl. Phys.** 49, 5039 (1978)

[20] G. D. Patterson **Methods of Experimental Phys.** *Academic Press*, (1980) p.170

Chapter 5

SOUND PROPAGATION IN A QUATERNARY MICROEMULSION

5.1 Introduction

We have demonstrated in the foregoing chapters that sound wave propagation in complex fluids is strongly modified by the dispersed phase and its properties, including the size, and rigidity of the droplets and the interaction between them. Given a complex fluid system with a known thermodynamic structure, we can study its dynamics by probing the sound wave propagation as a function of frequency and droplet volume fraction. For AOT micelles and microemulsions, we found a pronounced viscoelastic behavior. This behavior is a result of dynamic rigidity percolation of droplets due to the formation of extended networks caused by the weak attractive interaction. Also, when we change the interaction energy by varying the solvent or the size of droplets, there is a corresponding change in the characteristic relaxation time. Therefore, measurements performed on time scales characterizing the lifetime of clusters in the complex fluid allow us to probe the contribution of these structures to the elastic behavior of the system. In this chapter, we continue the investigation of the modification of sound waves in another microemulsion system formed with the surfactant polyoxyethylene-10-oleyl-ether (Brij-96): Brij-96/butanol/hexadecane in D_2O or H_2O. In this system, the repulsive interaction between droplets is dominant.

This four-component microemulsion system[1] consists of oil droplets in a continuous aqueous phase. The Brij molecules are the surfactant while the alcohol is a cosurfactant, which makes the interface more flexible. The cosurfactant is also needed to solubilize appreciable amounts of the surfactant component in the oil. The droplet phase has a weight fraction of Brij-96, butanol and hexadecane of .591,

.309 and .100, respectively. All components are mixed initially to form a homogeneous, clear solution, and then diluted with water to the desired volume fraction of dispersed phase, ϕ. This system is also thermodynamically stable like other common microemulsion systems.[1] From dynamic light scattering results and other experimental data,[1,2] it was found that when $\phi \leq 0.21$, the droplets are spherical with size $\simeq$ 50 Å in radius, while when $\phi > 0.21$, it is unclear whether or not the droplets are still spherical.

This system is a normal microemulsion, in which water is the continuous phase and the oil is inside the droplets. Thus the surfactant tails, as well as the cosurfactant tails, face inward, toward the droplet oil core; while the surfactant heads are on the interfaces facing toward the water. Consequently, the short range attractive interaction, induced by the overlapping of the surfactant molecular tails, can not exist here. Indeed, previous measurements[2] indicate that the dominant interaction between droplets in this four-component system is a repulsive Coulombic interaction. Thus, we do not expect the droplets in this system to form any extended network that support shear. Therefore, the behavior should be markedly different from that found in AOT systems.

We again use both ultrasonic and Brillouin scattering techniques to measure the sound velocity as a function of frequency and volume fraction of the dispersed phase in the system. In all frequency ranges, we find that the sound velocity increases quickly when $\phi < 0.15$, and then reaches a plateau. When H_2O is used as the continuous phase, we find that as ϕ increases further, v *decreases*. This behavior is markedly different from what we have found in the AOT microemulsions. However, this behavior is strikingly similar to that of a binary mixture of alcohol and water, where the sound velocity has a maximum at a critical alcohol concentration.[3,4] There is a strong interaction, in an aqueous solution of alcohol, between water and alcohol molecules within certain alcohol concentrations. This

leads to a reduction in the total compressibility of the mixture, and thus to an increase in the velocity of sound. The analogy between the behavior that we observe in the four component microemulsion system and that observed in a binary water-alcohol mixture is striking; it is the only reasonable explanation for the behavior that we observe. The consequences are that our measurements have important implications about the structure of the microemulsion system, and the arrangement of the constituent molecules, which are not obtained from other structural probe.

Since the experimental techniques have been discussed in the foregoing chapters, the experimental results will be presented in next section, including different modifications of the system by changing the core size of droplets, adding ionic charge to the system, and replacing the aqueous continuous phase with D_2O instead of H_2O. Due to the complicated nature of the structure in the system, we can only propose some qualitative interpretations for our observations without a detailed theory.

5.2 Results and Discussion

The behavior of the sound velocity as a function of droplet volume fraction in Brij-96/butanol/hexadecane in H_2O microemulsions is plotted in Fig.5.1. The low frequency data are measured using ultrasonic techniques, while the highest frequency data are measured with Brillouin scattering. The most unusual feature is the velocity dispersion in ϕ for each frequency: v increases quickly and reaches a maximum around $\phi = 0.2$, and then decreases as ϕ increases further. The maximum velocity for each frequency is higher than the velocity of three pure components; for butanol, $v = 1315$ m/sec, for H_2O, $v = 1483$ m/sec, and for hexadecane, $v = 1340$ m/sec. The observed behavior of the velocity is not caused solely by the variation of the average density, ρ, which decreases linearly as ϕ

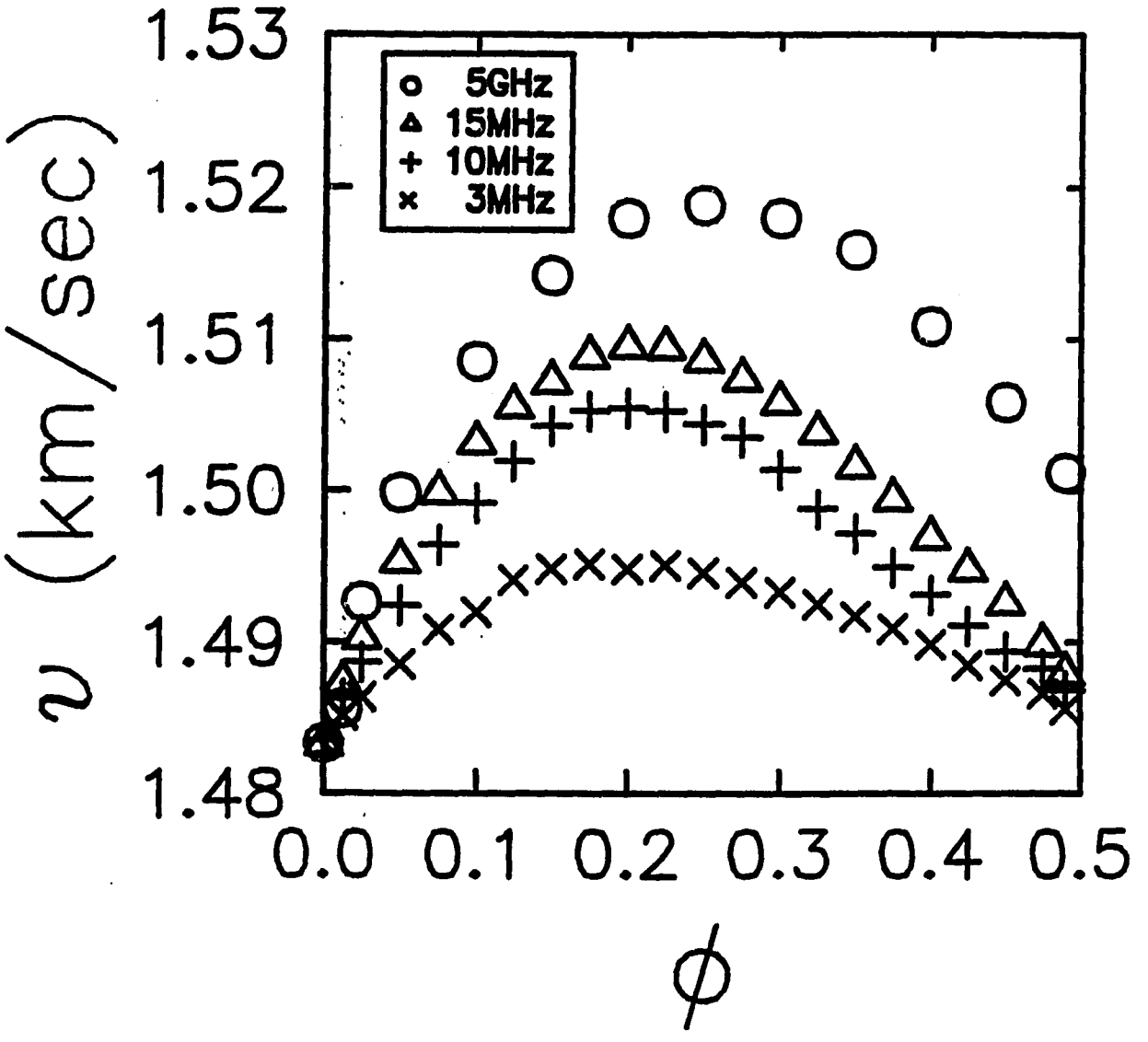

5.1 The velocity of sound in Brij-96/butanol/hexadecane/H_2O microemulsions as a function of volume fraction, measured at different frequencies. The MHz data are obtained using ultrasonic measurements, and the GHz data are measured using Brillouin scattering.

increases,[2] and thus would result in a linear increase of v with ϕ, rather than the behavior observed.

We find a strong analogy in the sound velocity dispersion in ϕ between our microemulsion system and a water-alcohol binary mixture. In Fig.5.2,[3] we show the dependencies of both v and β on the concentration of an aqueous solution of methyl alcohol, where β is the average elastic constant. This aqueous solution of alcohol exhibits an unusual behavior in which the sound velocity has a maximum which is larger than the velocity of any single phase in the system. This behavior is quite generally observed for water alcohol mixtures. It is believed that this behavior is due to the unique structural properties of water and the ability of the alcohol solute to promote such structural effects.[4] Each water molecule in the alcohol solution is hydrogen bonded to three or four neighbors, which tend to form a tetrahedral "iceberg" structure.[5] The alcohol molecules fill and promote these cage-like structures of water molecules. These structures induce an unusual behavior in the adiabatic compressibility, which is responsible for the observed behavior of the sound velocity.[4,5] The critical concentration of alcohol in water where the velocity maximum is defined depends on the solubility and temperature. Therefore, if the alcohol has a limited solubility in water at constant T, the enhanced elastic constant relaxes at higher ϕ, and v decreases.

To elucidate the contribution of a butanol-water interaction to the elastic behavior in our microemulsion system, we measure the sound velocity in a butanol-H_2O binary mixture. In Fig.5.3, we plot v as a function of butanol concentration in both the butanol-water binary and the microemulsion system. In the binary mixture, v increases linearly as the butanol concentration, ϕ, increases when $\phi \leq 0.05$; then v reaches a velocity maximum, $v = 1535$ m/sec at about $\phi \simeq 0.09$. The

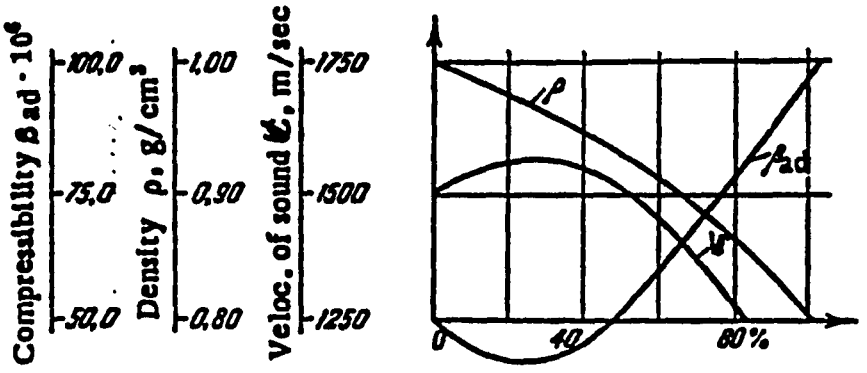

Fig. 2. Dependence of the velocity of sound and the elastic constants on the concentration of an aqueous solution of methyl alcohol.

5.2 Dependence of the velocity of sound and the elastic constants on the concentration of an aqueous solution of methyl alcohol.

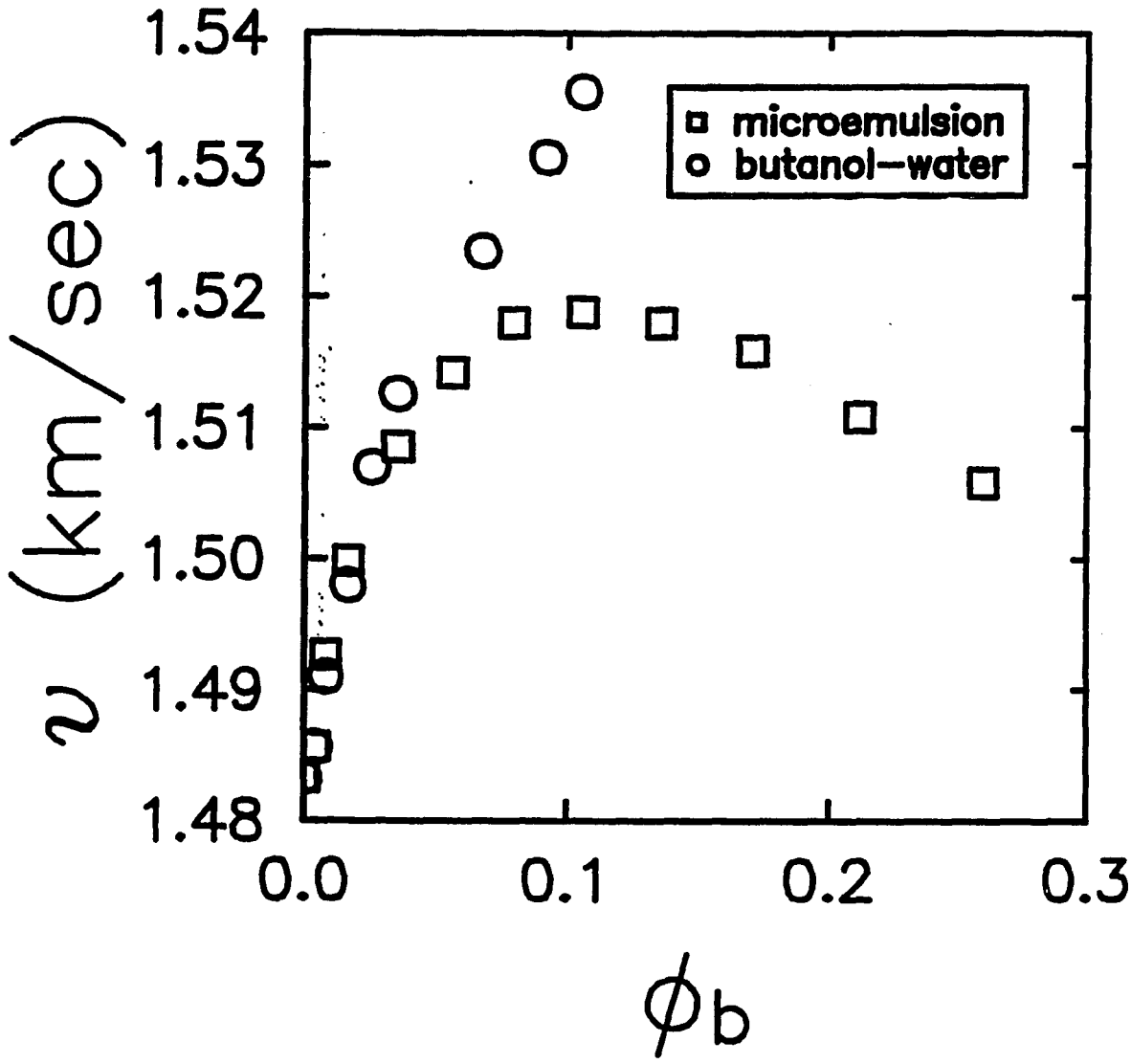

5.3 Dependencies of the velocity of sound on the concentration of butanol, ϕ_b, in both an aqueous solution of butanol and the four component microemulsion system. v_m is the velocity of sound for the microemulsion system, and v_{bw} is for the butanol-water binary mixture.

velocity maximum is larger than both the sound velocities of water, $v = 1483$ m/sec, and of butanol, $v = 1315$ m/sec. We find that the maximum solubility of butanol in H_2O is about 0.09. As more butanol is added to the mixture, a phase separation occurs. In the microemulsion system, on the other hand, v increases linearly at $\phi \leq 0.05$, and then increases slowly to reach a maximum at $\phi \simeq 0.09$, $v = 1520$ m/sec. As ϕ continues to increase, v is decreased. The similar velocity maximum observed in the microemulsion system suggests that the interaction between butanol and water molecules is strong when the butanol concentration is low, which reduces the compressibility of the solution due to the structural effect of water-butanol complexes. The maximum solubility of the butanol in water results the minimum compressibility of the solution, and thus causes the maximum velocity measured. However, due to the higher compressibility of the droplet phase, the velocity decreases as ϕ increases after the maximum solubility of butanol in water. Finally, the question remains unclear that where the alcohol molecules stay at in the microemulsion system. According to the previous investigations,[1,2] at low concentration of dispersed phase, the butanol molecules basically participate the formation of droplets, which means they are on the interfaces between oil and water. It is also possible that some of the butanol molecules displace to the continuous phase, and associate with water molecules directly, especially at higher ϕ. Nevertheless, we believe that the observed anomalous behavior of the sound velocity in this microemulsion system is due to the association of alcohol-water molecules, which increase the stiffness of the droplet phase, as is seen in water-alcohol binary mixture.

The measurements of the sound velocity in different frequencies in alcohol-water binary mixture, using either ultrasonic techniques or the light scattering, indicate that there is a frequency dispersion of the sound velocity due to the structural relaxation of the system.[4,6] The general interpretation for the frequency

dispersion of v is that the clusters formed, due to the alcohol/water interaction, have a characteristic relaxation time, and the dynamics of this structural relaxation leads to the frequency dependence of the observed elastic behavior of the system. We also find a similar frequency dependence of the sound velocity in our microemulsion system. As shown in Fig.5.1, there is a velocity dispersion in the measured frequency regime of MHz-GHz using ultrasonic and Brillouin scattering techniques. One of the obvious features there is that the velocity maximum moves from $\phi \sim 0.2$ at low frequency to $\phi \sim 0.25$ at high frequency. However, since the system has a complicated structure, there might be more than one relaxation processes, such as the droplet vibration, or the droplet-droplet interaction. Thus it is hard to conclude from these data which relaxation process is responsible for the observed frequency dispersion in v.

The measurement results from both the butanol-water binary and the quaternary microemulsion systems strongly suggest that the molecular interaction of butanol and H_2O plays an important role in the elastic behavior of the system. Since D_2O molecule has a stronger hydrogen bonding than H_2O molecule, as well as different density and elasticity, the replacement of H_2O with D_2O in the microemulsion may results different elastic behavior, allowing us to study the contribution of the hydrogen bonding to the structural correlation of the system. Thus we perform the same measurements using the same dispersed phase while replacing H_2O to D_2O. We find that the two systems have very different behavior. The behavior of the sound velocity as a function of ϕ at different frequencies for the microemulsion in D_2O is shown in Fig.5.4. When $\phi < 0.2$, there is a similar initial increase of v, then v reaches a maximum for each frequency. The velocity maximum is higher than the velocities for D_2O, $v = 1380$ m/sec, and for both the butanol and the hexadecane as well. When ϕ increases further, the velocity remains constant. In addition, the frequency dependence of v occurs mainly at

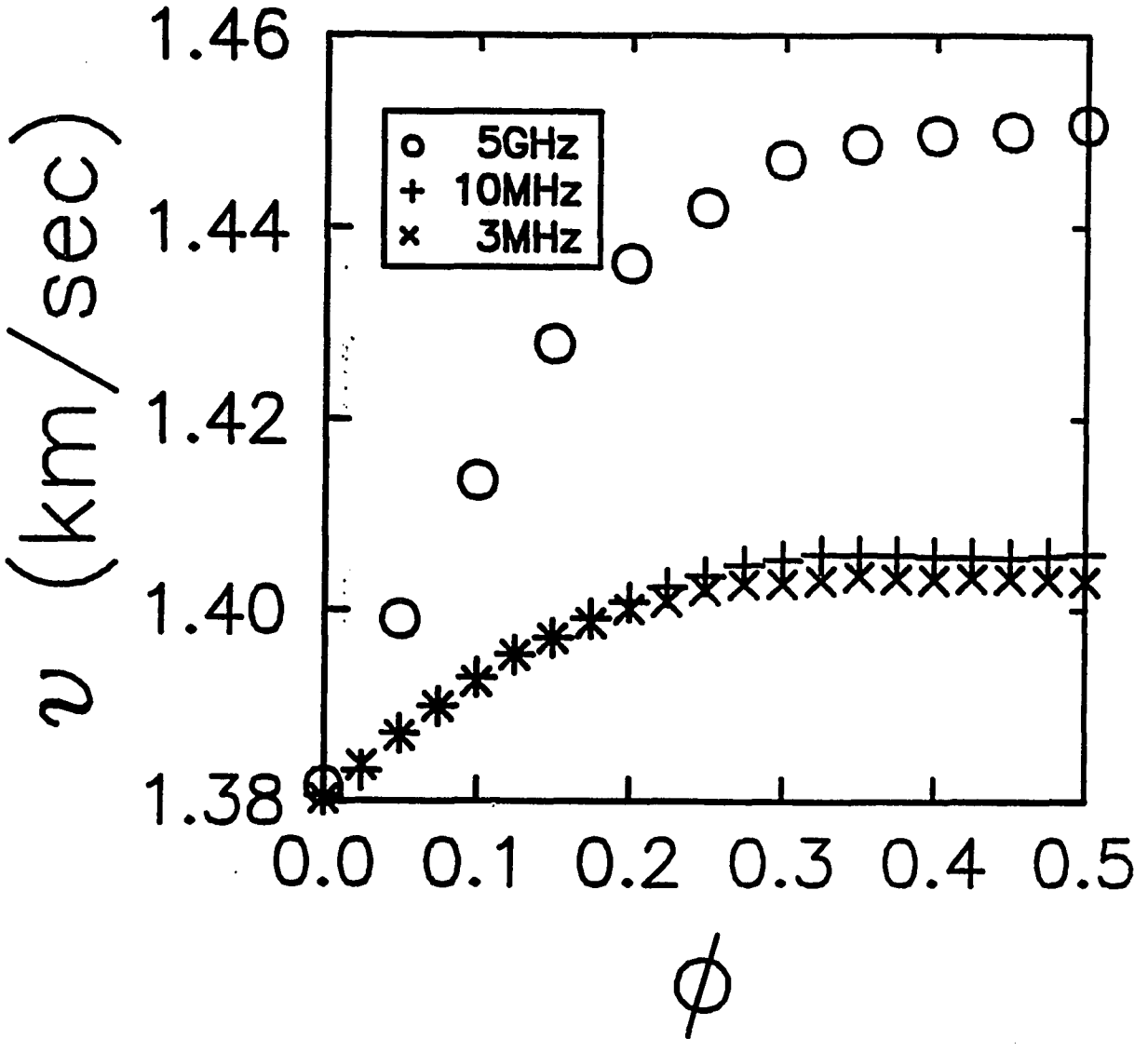

5.4 The velocity of sound in Brij-96/butanol/hexadecane/D_2O microemulsions as a function of volume fraction for different frequencies. Ultrasonic measurements were used to obtain the MHz data; Brillouin scattering was used to obtain the high frequency data.

high frequency, which means the relaxation frequency shifts to a higher frequency compared with microemulsion in H_2O. Also the volume fraction where the velocity reaches its plateau level moves to ~ 0.3 at high frequency. Therefore, there is a similar anomalous structural contribution to the elastic behavior due to the water-alcohol interaction in this microemulsion system. However, due to the different H-bonding of H_2O and D_2O to the butanol, the elastic behaviors are different. In addition, the different frequency dependencies in two systems reflect the different associations between butanol molecules and the two types of water molecules.

The measurements of the sound propagation in microemulsion in both H_2O and D_2O indicate that the strong interaction between alcohol and water molecules leads to the observed elastic behavior at low ϕ. It is still not clear how the droplet-droplet interaction influences the sound propagation. In order to investigate the modification of sound velocity by the interaction between droplet-droplet, we introduced a small fraction of the charges to the system in order to enhance the repulsive interaction between droplets.

We add some salt, sodium dodecyl($NaC_{12}SO_4$), in a mole ratio of surfactant to salt of 50:1 or 15:1, to the Brij-96/butanol/hexadecane/D_2O microemulsion system. The introduced ionic interaction only enhances the repulsive potential between droplets without affecting the structure of the dispersed phase.[7] The comparison of the behavior of the sound velocity as a function of ϕ, both with and without the ionic charge, is shown in Fig. 5.5. The 3 MHz data are obtained with ultrasonic measurements and the 5 GHz data are obtained with Brillouin scattering. The elastic behavior of the ionic microemulsion is exactly the same as the nonionic microemulsion, which is discussed in Fig.5.4. The results indicate that the charges do not affect the elastic behavior of the nonionic system, even though the ratio of surfactant to salt increases from 50:1 to 15:1. In AOT microemulsions, the attractive interaction between droplets leads to the observed viscoelastic

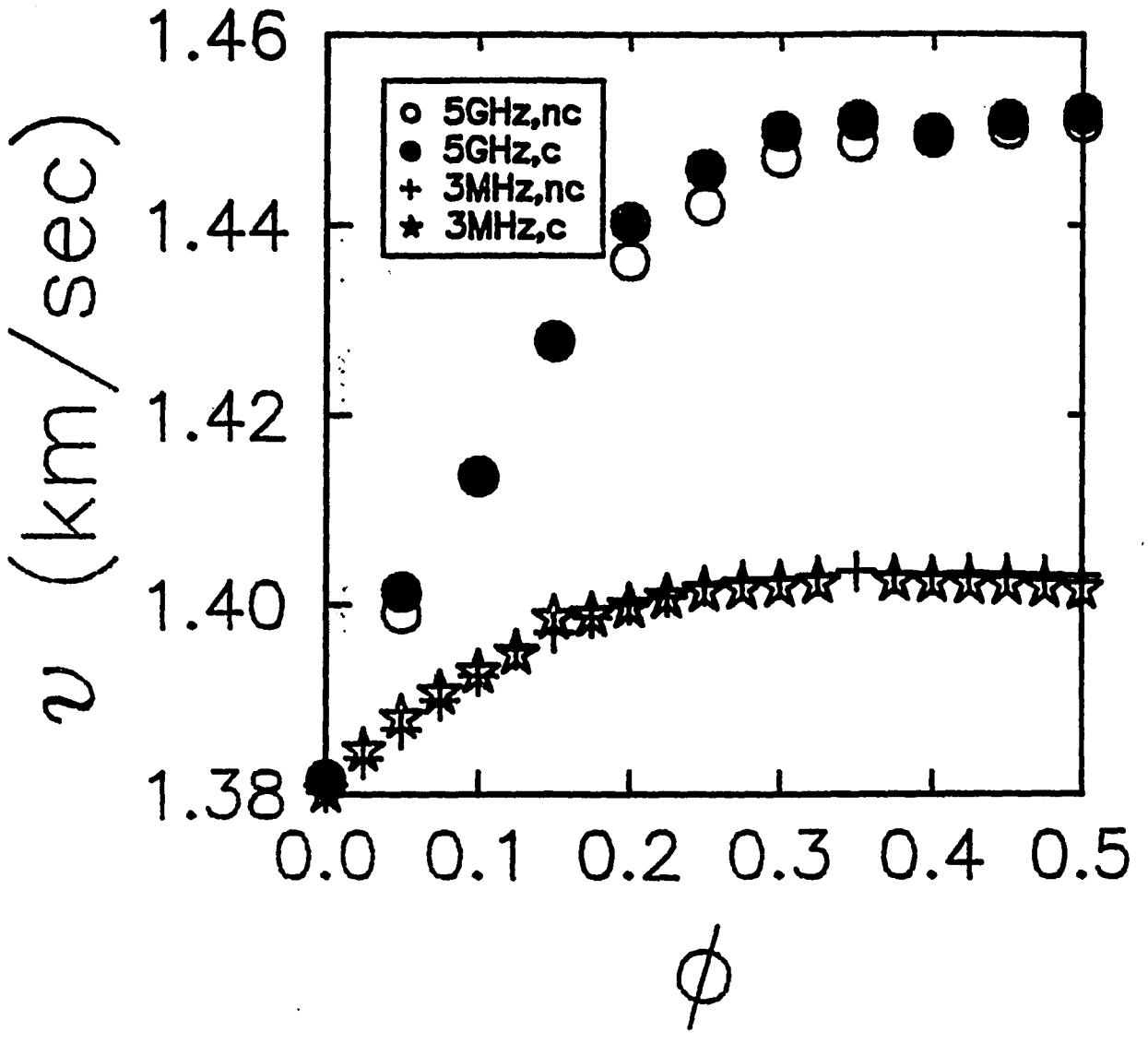

5.5 The velocity of sound in Brij-96/butanol/hexadecane/D_2O ionic microemulsions as a function of volume fraction for different frequencies, with the ratio of surfactant to salt ($NaC_{12}SO_4$) 15:1.

behavior due to the formed dynamic rigidity networks. The variation of the attractive interaction changes the characteristic relaxation time, and thus changes the viscoelastic behavior of the system. However, in this quaternary microemulsion, no rigidity network is formed due to the repulsive interaction. Therefore, the enhanced repulsive interaction between the droplets does not modify the sound propagation in the way that the attractive interaction does.

CONCLUSION

In summary, the study of sound propagation in the microemulsions of Brij-96/butanol/hexadecane in water indicates that the elastic behavior is strongly modified by association between the butanol and water molecules. This anomalous structural effect of alcohol in water is frequency dependent. By introducing a certain amount of charges in the system, the enhanced repulsive interactions between droplets can not affect this unusual structure effect. In addition, the replacement of the continuous phase, from H_2O to D_2O, in this microemulsion exhibits a different elastic behavior, since the hydrogen bonding, the compressibility and the density for the two aqueous phases are different.

Here we have once again demonstrated that the measurements of the sound propagation in complex fluids provide insight into the contribution of structural correlation to the elastic behavior of the system. The elastic behavior in these quaternary microemulsions is similar to that observed in a water-alcohol binary mixture, where the association complexes of alcohol and water molecules lead to a elastic constant maximum at certain alcohol concentration. A further theoretical investigation to the measurement results is needed in order to understand the physics of our observations in this quaternary microemulsion.

References

[1] D. B. Siano, J. Bock and P. Myer. **Colloids and Surfaces** 26, 171 (1987)

[2] D. B. Siano and J. Bock. **J. Colloid and Interface Sci.** 123, 224 (1988)

[3] **Ultrasonics and its Industrial Applications** ed. by O. I. Babikov. *Consultants Bureau, N.Y.* (1960) p. 20.

[4] G. D'Arrigo and A. Paparelli. **J. Chem. Phys.** 88, 405 (1987)

[5] R. J. Speedy. **J. Phys. Chem.** 88, 3364 (1984)

[6] T. M. Bender and R. Pecora. **J. Phys. Chem.** 90, 1700 (1986)

[7] D. B. Siano, P. Myer and J. Bock. **J. Colloid and Interface Sci.** 117, 534 (1987)

Chapter 6

PHONON DISPERSION IN SUSPENSIONS OF HARD SPHERE COLLOIDS

Abstract

We use Brillouin scattering to measure the dispersion of the propagating acoustic modes in a suspension of hard sphere colloids. We find two distinct longitudinal modes when the sound wavelength becomes comparable to the sphere diameter. The higher frequency mode has a velocity intermediate between those of the pure solid and the pure liquid phases, and its velocity increases with increasing volume fraction, ϕ. The lower frequency mode has a velocity less than the velocities in either the pure fluid or pure solid phases, and its velocity decreases with increasing ϕ. We interprt the higher frequency mode as a compressional wave which propagates through both the solid and the fluid, as expected for a composite medium. The lower frequency mode has not been observed before, and is interpreted as a surface acoustic mode, which prpagates between adjacent spheres through a decaying portion of the excitation in the fluid.

6.1 Introduction

The propagation of acoustic waves through a random, disordered material is one of the most fundamental properties that characterize the medium. This is particularly true of granular materials, where the structure and correlations between the grains can have a profound effect on the propagation of acoustic waves. One class of granular material whose acoustic properties have been widely studied is porous media, comprised of solid and fluid phases. Their acoustic properties are of immense practical importance because of their utility for seismic investigations and other non-intrusive probes; they are also of great fundamental interest because

of the rich variety of fascinating phenomena that have been observed. The complex interplay between the acoustic frequency, sound wavelength and characteristic size of the microstructure, as well as the presence of large interfacial areas and the frequency dependence of the viscous coupling between the solid and the liquid, lead to new mechanisms for the propagation of acoustic waves in these materials.

The structure and connectivity of the solid grains play a critical role in determining the propagation of acoustic waves through these media. One of the simplest and most fundamental structures consists of uniform solid spheres immersed in a fluid[1]. The characteristics of this system are highly controllable, as the grain size, solid volume fraction, acoustic wavelength and acoustic frequency can all be independently varied. An example of such a structure is a hard sphere colloid[2]. This consists of a dispersion of monodisperse, solid spheres immersed in a fluid, interacting solely by the hard sphere repulsion due to the fact that two solid spheres can not occupy the same volume. In this paper, we present the results of a study of the acoustic propagation through a hard sphere colloid[3]. We report Brillouin scattering measurements of the thermally excited, propagating acoustic modes, and present the dispersion curve for longitudinal phonons in a hard sphere colloid. The behavior observed is surprising and unexpected. Since the continuous phase is a fluid which can not support shear, there is no long range rigidity in this medium. Thus, in the limit of long wavelength, it can be rigorously shown that the medium can support only one propagating longitudinal acoustic wave[4]. This behavior is widely expected to persist to shorter wavelengths[1]. In this paper, we show that this is not the case. As the sound wavelength becomes comparable to the sphere diameter, a new and unexpected mode appears which exhibits unusual behavior. We suggest that this new excitation is a coupled interface mode.

The hard sphere colloids used here consist of monodisperse polymethylmethacrylate (PMMA) spheres, sterically stabilized by a thin layer of grafted polymer,

with a thickness of about 15 nm. The colloidal particles are immersed in an index-matching mixture of dodecane and carbon disulphide, eliminating multiple scattering, even at the highest volume fractions. This makes it possible to use light scattering techniques to study the structure and characteristics of these colloids, even though the particle size is comparable to the wavelength of light. These hard sphere colloids have been of great interest in their own right, as they exhibit a rich phase behavior that possesses strong analogies to that of a simple, hard sphere atomic system[2]. At low volume fractions, ϕ, the colloidal particles behave as a fluid, with short range correlations between the particles that are well characterized by a liquid like structure factor. For larger volume fractions, $\phi > 0.49$, the colloidal particles form either a colloidal glass or a colloidal crystal.

We use static light scattering to determine the structural correlations of the spheres by measuring the static structure factor, $S(q)$, where q is the scattering wavevector. We use Brillouin scattering to determine the frequency of the propagating sound modes by measuring the dynamic structure factor, $S(q,\omega)$. Brillouin scattering probes the thermally excited propagating longitudinal acoustic waves in the medium. A peak is observed in the Brillouin spectrum at a frequency corresponding to a propagating sound wave whose wavelength, λ, matches the inverse scattering wavevector. By varying q, we can vary the size of the acoustic wavelength relative to the sphere diameter, d, and we can measure the dispersion curves for the longitudinal phonons in the suspension of hard sphere colloids.

At small q, when $\lambda > d$, a single propagating sound mode is observed, and the ϕ-dependence of the sound velocity is well described by an effective medium picture. However, as λ becomes comparable to d, internal vibrational modes of the spheres can be excited, and there is a qualitative change in the sound propagation, when ϕ is greater than about 0.2. Two sound modes are observed. One mode has a velocity that is intermediate between that in the pure solid phase and the pure

fluid phase. Furthermore, the sound velocity of this mode increases with ϕ. The other mode has a velocity that is significantly lower than the slowest sound velocity of any constituent pure phase in the medium. Furthermore, this velocity decreases as ϕ increases. We suggest that this second mode reflects a surface or Stonely wave that is coupled between the adjacent spheres by the decaying longitudinal portion of the excitation in the fluid.

6.2 Experimental

The Brillouin scattering was performed using single-mode Ar^+ or Kr^+ lasers with wavelengths of 5145 Åor 6471 Årespectively. The spectra at a given q were found to be independent of the laser wavelength. The colloids exhibit rather strong self-focusing of the laser beam, which is considerably more pronounced in the green than in the red. Thus the power incident on the sample was kept below about 100 mW, focused to a beam of about 100 μm diameter. At all times, we ensured that the incident power was sufficiently low as to not affect the spectra. The scattered light was imaged onto a 150 μm diameter pinhole and then collimated into a Fabry-Perot interferometer. Despite the fact that the colloids were index matched, the elastically scattered light was still about four orders of magnitude more intense than the Brillouin peaks. Thus, to obtain sufficient rejection of the intense Raleigh peak, and to increase the resolution, the Fabry-Perot interferometer was operated in a five-pass configuration with a finesse of about 50.

We measure the velocity of the acoustic modes from the frequencies of the peaks in the Brillouin spectra, $v = \omega/q$. By varying the scattering angle, we can vary the scattering wavevector, q, enabling us to measure the dispersion relation for the longitudinal phonons. Our Brillouin measurements are made at scattering angles ranging from about 9° to 170°, corresponding to q varying from .003 to .04 nm^{-1}. Since we are interested in the properties of the acoustic propagation as

the sound wavelength changes with respect to the sphere size, the dimensionless parameter of interest is qd. We extend the accessible range of qd by using spheres of different sizes. The first sample consists of spheres which have diameters of 370 nm, including the grafted polymer layer. The core diameter, consisting of solid PMMA, is then 340 nm, allowing data to be obtained for qd ranging from about 1 to 14. These spheres are most convenient for studying the spectra around the peak in the static structure factor, which occurs near $qd \approx 2\pi$. The second sample consists of spheres which have diameters of 680 nm, with core diameters of 650 nm, allowing data to be obtained for qd ranging from about 2 to 25. Thus, these spheres are most convenient for studying the behavior as qd becomes much larger than 2π.

In addition to varying qd, we also obtain data for different values of the volume fraction of the solids, ϕ. This is determined from their phase behavior[2]. The samples are gently centrifuged until the colloids sediment at the bottom of the containers. We assume that the sediment is comprised of randomly close packed spheres, with $\phi_e = 0.64$, and use this as the highest volume fraction studied. For the other samples, the heights of the sediment and the supernatent are measured and the volume fraction of colloids in the total suspension is calculated. The samples are then well mixed again before the Brillouin experiments are performed. This method provides a measure of the effective hard sphere volume fraction which determines the phase behavior of the colloids and includes the contribution of the thin layer of stabilizing polymer coating each sphere. The colloids themselves form a disconnected system of solid spheres, even at the highest volume fractions. We calculate the volume fraction of the solid PMMA, or the core volume fraction, ϕ_c, from ϕ_e by assuming that the grafted layer of stabilizing polymer has a thickness of 15 nm. We estimate the total uncertainties in the values determined for ϕ_c to be about $\pm 5\%$, arising primarily from the errors introduced when measuring the

heights. Thus the uncertainty is substantially less for the sample with the highest volume fraction, $\phi_e = 0.64$, where the uncertatinty arises only in the knowledge of the precise thickness of the grafted polymer layer. Finally, we ensure that none of the samples are allowed to settle and form colloidal crystals, so that there is no long range order between the particles used to obtain the data reported in this manuscript.

6.3 Results

In the limit of very low scattering angles, when the wavelength of the sound is much larger than the sphere size, we expect to observe hydrodynamic behavior, with only a single propagating sound mode. The lowest value of qd that we can achieve is $qd \approx 1$, using the smaller spheres. Brillouin spectra for three different volume fractions, $\phi_c = 0.16$, 0.38, and 0.51, are shown in Fig.6.1. For the lowest volume fraction, $\phi_c = 0.16$, the Brillouin peak is almost unchanged in shape and position from that observed in the index matching fluid with no spheres present. However, the intensity of the Raleigh peak is increased by several orders of magnitude with the addition of the spheres, while the intensity of the Brillouin peak is virtually unchanged. As ϕ_c increases, the Brillouin peaks shift to larger frequencies and become broader. This behavior is expected, since the velocity of sound in the solid is roughly twice that in the fluid.

Since λ is substantially larger than d, the behavior can be well described using an effective medium model to account for the velocity of sound as a function of volume fraction. In Fig.6.2, we plot the sound velocity determined from the frequency of the Brillouin peak, $v = \omega/q$, as a function of core volume fraction, ϕ_c. We compare the data to a theoretical prediction based on an effective-medium theory appropriate for isolated spheres immersed in a fluid[5]. We take the average

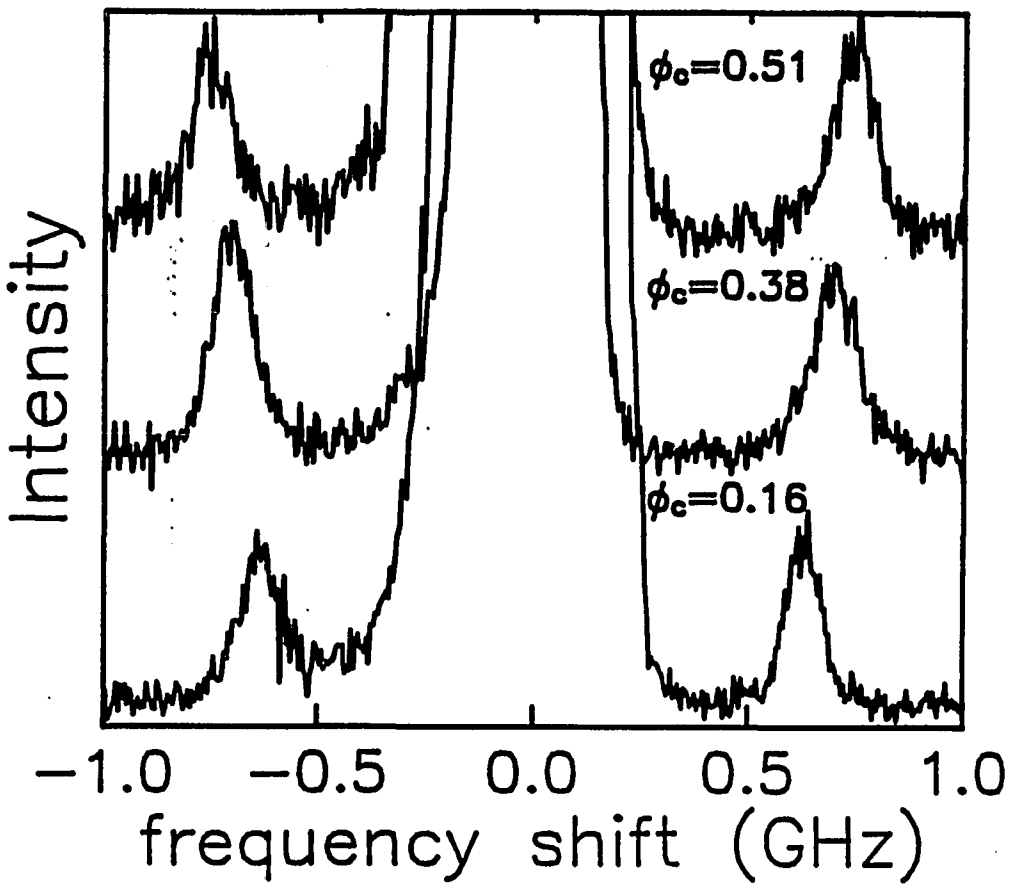

6.1 Brillouin spectra for three different volume fractions of 370 nm diameter PMMA spheres measured at a $q = 0.0034\ nm^{-1}$, corresponding to $qd = 1.1$, in the hydrodynamic regime for the propagation of acoustic waves.

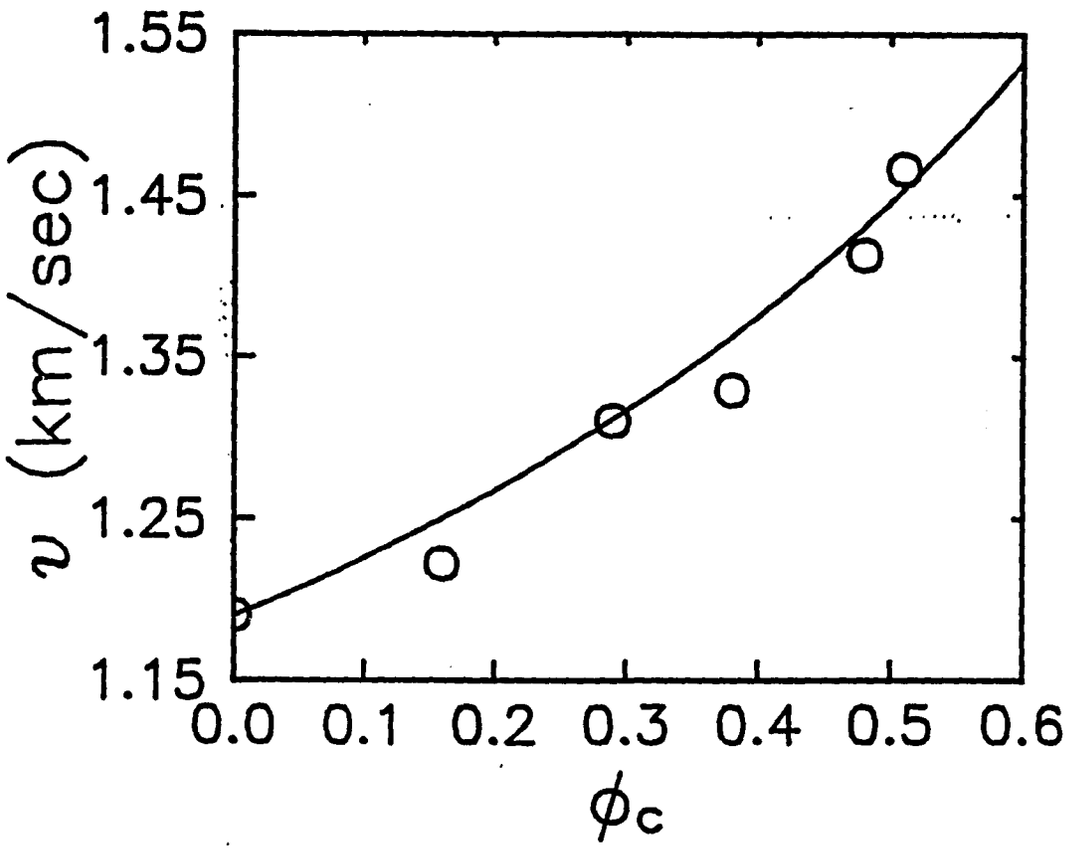

6.2 The volume fraction dependence of the sound velocity measured at small angle, $qd = 1.1$, in the hydrodynamic regime for the propagation of acoustic waves using the 370 nm diameter spheres. The solid line is the effective medium theory calculation using the measured values for the sound velocities in the pure phases. Much better agreement is obtained using the core volume fraction, ϕ_c, rather than the the effective volume fraction, ϕ_e.

velocity to be

$$v = \sqrt{\frac{\beta}{\rho}} \tag{6.1}$$

where the average elastic modulus is given by Wood's approximation,

$$\frac{1}{\beta} = \frac{\phi}{\beta_s} + \frac{1-\phi}{\beta_f} \tag{6.2}$$

and the average density is given by

$$\rho = \phi\rho_s + (1-\phi)\rho_f \tag{6.3}$$

where the subscripts s and f refer to the solid and fluid respectively. This approximation for the elastic modulus is rigorously correct in the limit of long sound wavelength[4], as is the case for these values of qd. All the parameters in these expressions are known. The elastic modulii of both the solid and the liquid phases are determined experimentally using Brillouin scattering from the pure materials. The density of the index-matching fluid is determined from the measured ratio of solvents used to index match the spheres, while for the PMMA, we use the bulk density. As shown by the solid line in Fig.6.2, the agreement with the data is very good, confirming the hydrodynamic nature of the acoustic behavior in this region. Furthermore, much better agreement is obtained using the core volume fraction, ϕ_c, than using the effective hard sphere volume fraction determined from the phase behavior. This confirms that the grafted polymer layer behaves more like the fluid rather than the solid for sound propagation. Thus we use the core volume fraction and the core radius to characterize the spheres for all our measurements.

As q increases, a qualitative change is observed in the Brillouin spectra. This change is initially observed when q approaches 0.009 nm^{-1}, which corresponds to qd approaching π. Here, the Brillouin peaks no longer increase in frequency as the volume fraction increases. Furthermore, a second Brillouin peak appears at higher frequencies for the two larger volume fractions, albeit at much lower intensity. As q

increases still further, these changes become more pronounced, as the two Brillouin modes are clearly resolved for the two larger volume fractions, and are of roughly equal intensities. This behavior is illustrated by the spectra for $\phi_c = 0.16$, 0.38 nad 0.51 for the smaller spheres, with $q \approx 0.026\ nm^{-1}$, corresponding to $qd \approx 2.8\pi$, shown in Fig.6.3. For the lowest volume fraction, $\phi_c = 0.16$, only one mode can be resolved, although its shape is perhaps slightly asymmetric, suggesting that the two modes may still exist, but their frequencies may not be sufficiently separated to clearly resolve the peaks. Both Brillouin peaks correspond to longitudinal modes as confirmed by the absence of any depolarized scattering.

To summarize the behavior of both Brillouin modes, we plot the dispersion relations for the smaller spheres in Fig.6.4, for three different volume fractions, $\phi_c = 0.16$, 0.38, 0.51, corresponding to effective hard sphere volume fractions of $\phi = 0.21$, 0.49, and 0.64. For comparison, we also show the linear dispersion curves for the longitudinal sound modes that would exist in the pure phases. The dashed line corresponds to the solid PMMA, while the solid line corresponds to the pure index-matching fluid. The values of the velocities used to plot these dispersion curves are obtained from experimental measurements made at very high qd using the larger spheres, as discussed later.

There are several remarkable features in the dispersion curves shown in Fig.6.4. At low q, only a single mode is observed for all ϕ, with linear dispersion as q goes to zero. The frequencies of this mode increase with increasing volume fraction of PMMA. However, as q increases further, all three dispersion curves begin to flatten and the frequency for the higher volume fractions actually drops below that of the lower volume fractions. For ϕ_c above 0.16, the second, higher frequency mode appears at $q \approx 0.009\ nm^{-1}$, corresponding to $qd \approx \pi$. This mode persists as q increases, and the splitting between the two modes increases with increasing volume fraction. At the lowest volume fraction, the measured frequency of the

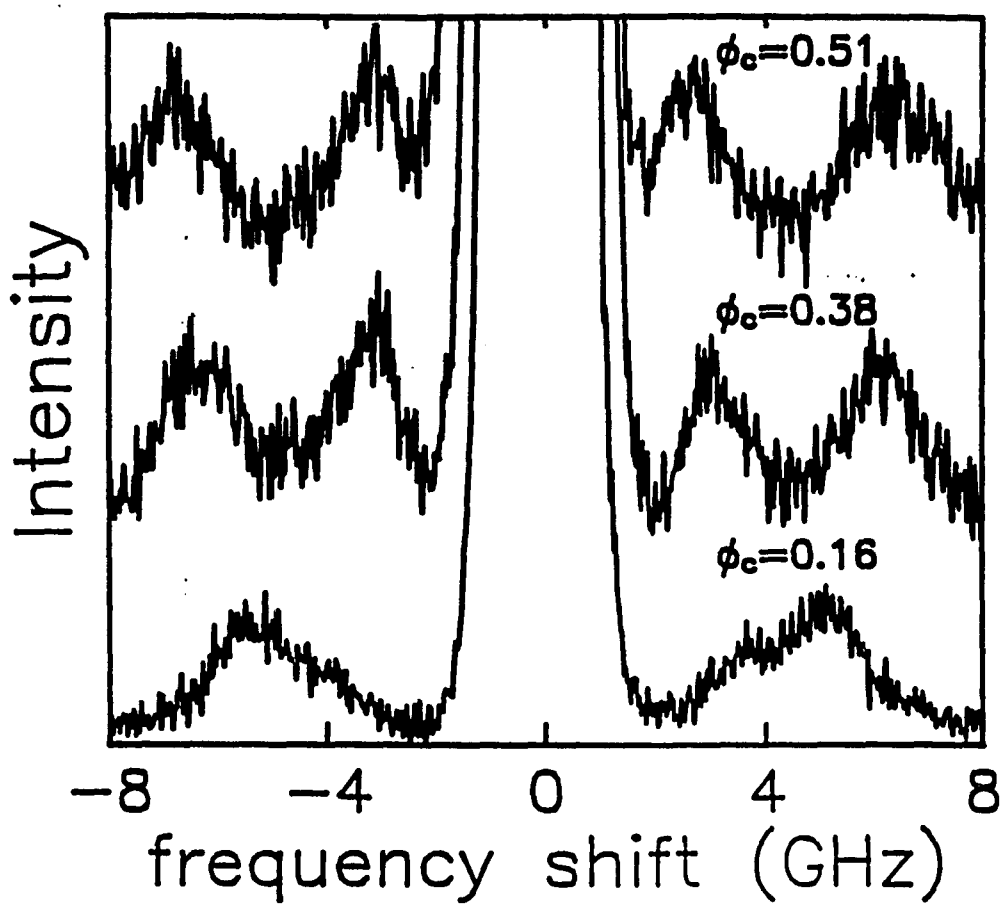

6.3 Brillouin spectra for three different volume fractions of 370 nm diameter spheres measured at $q = 0.026\ nm^{-1}$, corresponding to $qd = 4.1\pi$. The two distinct modes are clearly observed for the two higher volume fractions.

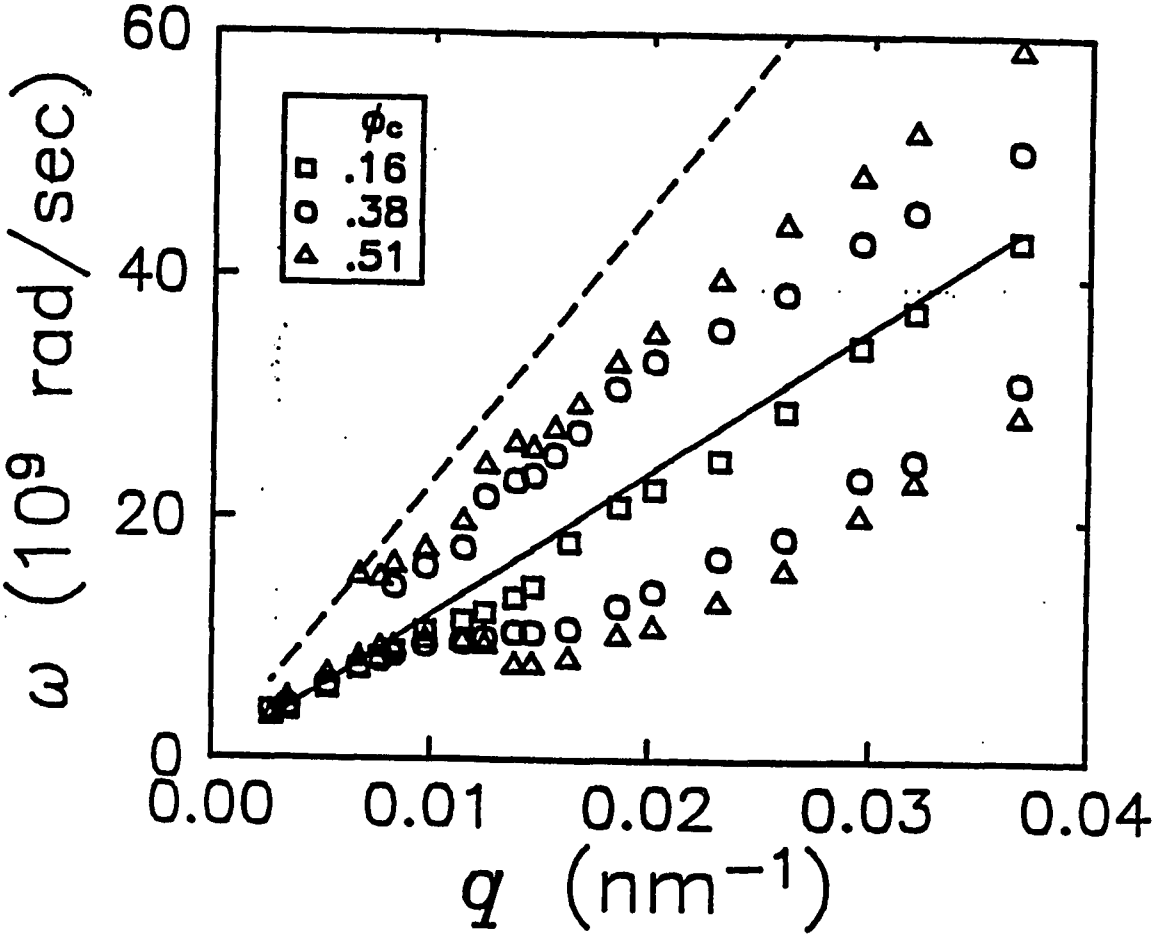

6.4 The dispersion curves for the longitudinal acoustic modes for three different volume fractions of the 370 nm diameter spheres. The lowest volume fraction exhibits only a single mode, while the two higher volume fractions exhibit two modes above $q \approx .009\ nm^{-1}$. The splitting between the modes increases with volume fraction. The solid line is the dispersion curve for the longitudinal mode in the pure index-matching fluid, while the the dashed line is the dispersion curve for pure PMMA.

mode is nearly unchanged from that of the index matching fluid.

At higher volume fractions, two distinct modes are resolved for q above 0.009 nm^{-1}, corresponding to $qd > \pi$. The velocity of the higher frequency mode lies between the velocities of the pure liquid and solid phases. In addition, its velocity increases with increasing volume fraction. This behavior is expected for a mode that is characteristic of an effective medium. By contrast, the behavior of the lower frequency mode is much more unusual and unexpected. Its velocity lies below that of the slowest velocity of any pure phase that makes up the medium. In addition, its velocity *decreases* with increasing volume fraction. Finally, the frequencies of both modes for all three volume fractions soften around the peak in the static structure factor, which occurs at $q \approx 0.015\ nm^{-1}$, corresponding to $qd \approx 2\pi$. The softening of the lower frequency mode is considerably more pronounced, and the degree of softening increases with volume fraction.

To investigate the behavior at even larger values of qd, and to compare the behavior for different sphere sizes, we also measured the dispersion curves with the larger spheres. These are shown in Fig.6.5 for core volume fraction of $\phi_c = 0.10$, 0.36 and 0.57. The overall trend of the dispersion curves are the same as for the smaller spheres. At the very lowest value of q only a single mode is observed, while for all larger values of q, two distinct modes are again observed. In addition, the splitting between the two modes again increases with increasing ϕ_c.

To compare the behavior of the different sphere sizes, we scale the two sets of data together. This is accomplished by multiplying each axis by the sphere diameter, d. Thus, on the horizontal axis, we plot qd, which is a dimensionless quantity, while on the vertical axis, we plot ωd, which has units of velocity. The vertical axis could be made dimensionless as well by normalizing by velocity. This scaling ensures that the dispersion curves of the pure phases exhibit the proper scaling behavior. The two sets of scaled dispersion curves are shown in Fig.6.6,

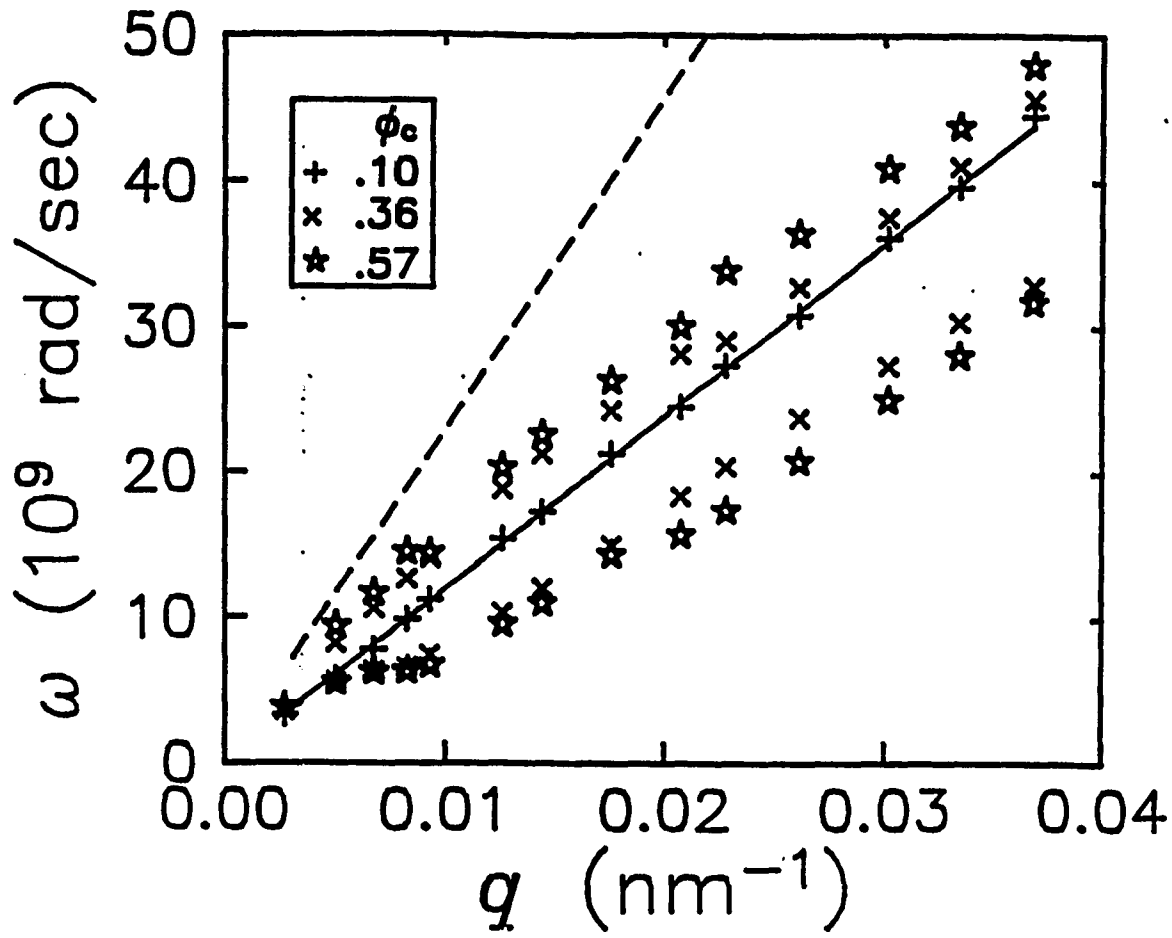

6.5 The dispersion curves for the longitudinal acoustic modes for three different volume fractions of the 680 nm diameter spheres. The lowest volume fraction exhibits only a single mode, while the two higher volume fractions exhibit two modes above $q \approx .005\ nm^{-1}$. The splitting between the modes increases with volume fraction. The solid line is the dispersion curve for the longitudinal mode in the pure index-matching fluid, while the the dashed line is the dispersion curve for pure PMMA.

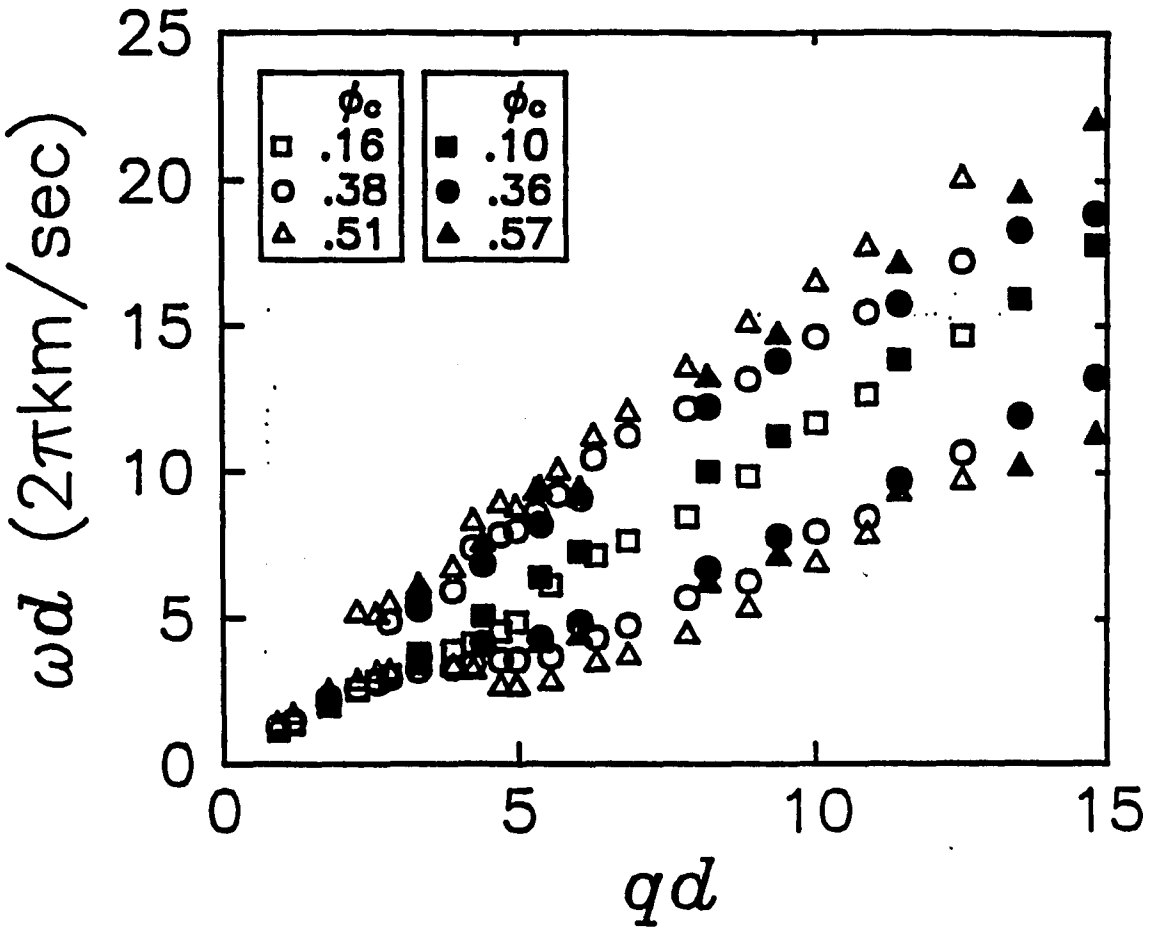

6.6 Scaled dispersion curves for the two different sphere sizes. Each axis is scaled by the core diameter of the spheres, 340 and 650 nm. The scaled data exhibit similar but not identical behavior.

where we only plot the region of qd for which overlapping data is available. The solid points refer to the data for the larger spheres, while the open points refer to the data for the smaller spheres. As expected, the scaled data for the two sphere sizes do exhibit the same trends: the splitting of the modes occurs at the same point, $qd \approx \pi$, for both data sets, and both sets of data exhibit a softening around $qd \approx 2\pi$. However, the scaling of the data is not exact. The degree of softening of the modes at $qd \approx 2\pi$ is substantially less pronounced for the larger spheres than for the smaller spheres. Furthermore, the splitting between the normalized frequencies of the two modes is consistently less pronounced for the larger spheres than for the smaller spheres. Thus, the high frequency mode of the larger sized spheres always has a lower normalized frequency for a given value of qd and ϕ_c than that of the smaller sized spheres. Similarly, the low frequency mode of the larger spheres always has a larger normalized frequency for a given value of qd and ϕ_c than that of the smaller spheres. Furthermore, a larger volume fraction of spheres is required for the larger sized spheres to clearly resolve the two modes.

In addition to the inexact scaling of the data of the different sized spheres, the dispersion curves of the larger spheres exhibit a clear trend as qd increases. To illustrate this more clearly, we plot the phase velocities, $v = \omega/q$, of the two modes for several volume fractions of the larger sized spheres in Fig.6.7. The velocity for $\phi_c = 0.10$ is again almost indistinguishable from that of the index matching fluid. By contrast, for higher volume fractions, the velocity of the higher frequency mode is initially much greater than that of the fluid, but as qd increases, the velocity decreases, and in fact appears to asymptotically approach that of the pure fluid. In addition, the velocity of the lower frequency mode displays a softening at $qd \sim 2\pi$, but as qd increases, it seems to approach a constant value that is well below that of the index-matching fluid.

Finally, at the highest values, $qd \approx 25$, an additional mode appears in the

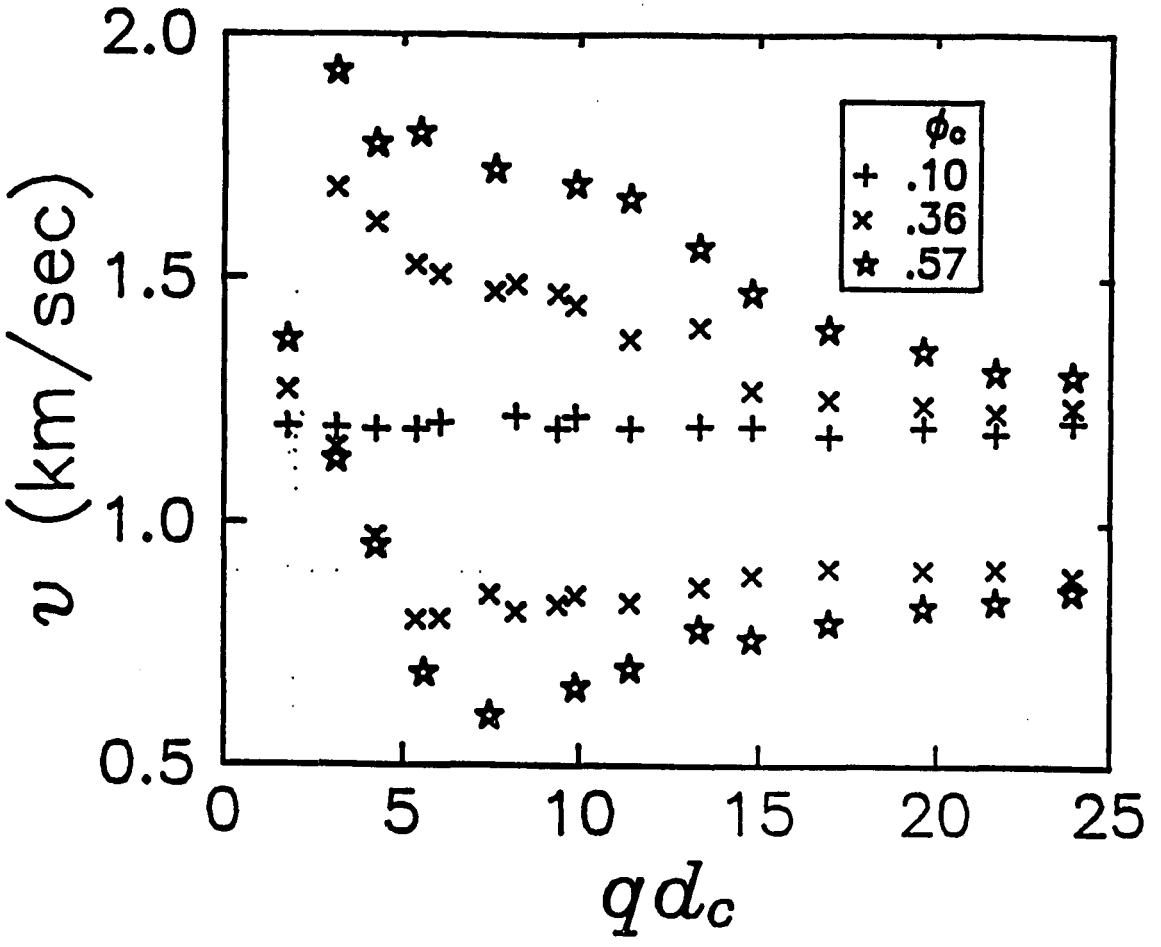

6.7 **The phase velocities of both modes for three different volume fractions of the 680 nm diameter spheres, plotted as a function of** qd. **Only one mode is present for the lowest volume fraction, and its velocity is nearly identical to that in the pure index-matching fluid. The two higher volume fractions exhibit two modes. The velocity of the faster mode is highest around** $qd \approx 2\pi$, **and then decreases as** qd **increases, ultimately asymptotically approaching that of the index-matching fluid. The slower mode exhibits a decreasing velocity as** qd **approaches** 2π, **but then the velocity increases at higher** qd, **ultimately becoming roughly constant, at a value equivalent to that expected for a Stonely wave at a flat interface.**

spectra, at higher frequencies. This new mode is quite broad and its intensity is very weak. We attribute this new mode to the propagation of sound in the bulk solid. The velocity of this mode is close to that measured for solid PMMA, and thus is consistent with sound propagation within the bulk of the spheres. This is expected at these high values of qd, where several wavelengths of sound can fit into each sphere. It is not surprising that the velocity of sound is somewhat different than bulk PMMA, as the fabrication process of the colloids presumably produces somewhat a different polymer. However, since qd is so high, this new mode probably does not reflect a wave that propagates between adjacent spheres, but rather reflects propagation confined within a single sphere.

Further insight into the behavior of the acoustic propagation is obtained from the damping of the Brillouin modes, determined from the measured full widths at half maximum intensities, $\delta\omega$. We characterize the damping by means of the quality factor, $Q = \omega/\delta\omega$, which reflects the number of wavelengths the mode propagates until it no longer couples to the light. We plot the quality factors measured for the smaller spheres as a function of qd in Fig.6.8. As qd approaches zero, the lower frequency mode is very well defined, as indicated by a large value of Q. However, by the time qd reaches about π, the value of Q for the lower frequency mode has decreased and remains constant at about 2, independent of qd. By contrast, the Q of the higher frequency mode exhibits a pronounced resonance around $qd \sim 2\pi$, reflecting a decrease in the damping of the mode. The behavior of Q for the larger spheres consistent with that shown for the smaller spheres in Fig.6.8, but the resonance at $qd \sim 2\pi$ for the higher frequency mode is not as pronounced, since the resolution in qd is not as high with the larger spheres.

6.4 Discussion

The most surprising feature of the dispersion curves for the suspension of

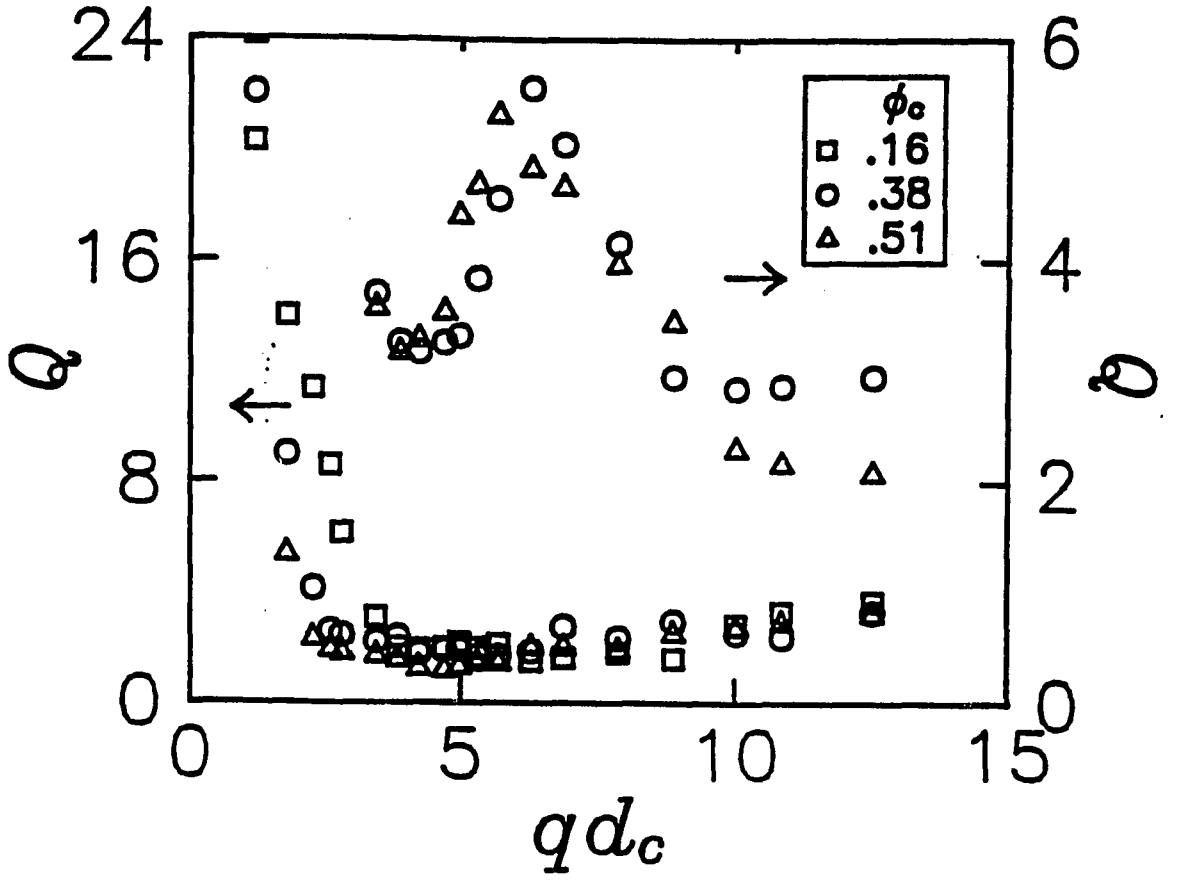

6.8 The quality factors, $Q = \omega/\delta\omega$, for the two modes for three different volume fractions of the 370 nm diameter spheres plotted as a function of qd. The higher frequency mode exhibits a pronounced peak around $qd \approx 2\pi$.

hard sphere colloids is the existence of two distinct modes. For these systems, the continuous phase is a fluid, which has no long range rigidity, and thus can not support shear. Thus, only a single longitudinal mode is expected. In fact, at very long sound wavelengths, this can be rigorously shown to be the case[4]. This same behavior is typically expected to persist to shorter wavelengths as well[1]. Therefore, the observation of two distinct modes when the wavelength of sound becomes comparable to the diameter of the spheres is unexpected.

The closest analogy to this behavior is that first proposed theoretically by Biot[6]. He considered the propagation of sound in a porous medium at long wavelengths and high frequencies. The characteristic frequency required is determined from the viscous penetration length, defined as $\ell = \sqrt{\rho/\eta\omega}$, where ρ is the density of the solid and η is the viscosity of the fluid. This is the length scale of viscous coupling of transverse waves from the solid into the fluid. When the frequency is sufficiently high that ℓ is less than the pore size, the Biot theory applies. Then, the solid and the fluid become decoupled, with one sound mode propagating through the solid phase, and a second, new mode propagating through the fluid phase. This new, slow mode is a wave that propagates predominantly in the fluid, but its velocity is slower than that in the pure fluid phase because of the tortuosity of its path. The veracity of Biot's prediction has been confirmed, both for sound propagation in some porous media structures[7] and for sound propagation through super fluid helium in a porous medium[8]. However, for the Biot theory to apply, the solid phase of the porous medium must be a contiguous, rigid structure and the solid and fluid must form interconnecting phases. This is not the case for a suspension of hard sphere colloids. Because of the grafted polymer stabilizing layer, the solid spheres are not interconnected, even at the highest volume fractions studied. Furthermore, while the fluid phase is clearly completely interconnected, its tortuosity is very nearly unity[9], so the decrease in the sound velocity of the

lower frequency mode can not be ascribed to a Biot slow wave. Thus, the Biot approach can not describe the behavior that we observe.

The data suggest an alternate physical picture of the origin of the two modes. The higher frequency mode has a velocity that lies between that of the solid PMMA and the index-matching fluid. Furthermore, the frequency of this mode increases with increasing volume fraction. Thus the solid PMMA spheres must play an important role in the sound propagation for this mode. However, this mode is only observed when $qd > \pi$, suggesting that the sound propagates through the solid spheres only when it can excite internal resonances of the spheres. This will occur when a half wavelength of the sound can fit inside the sphere, or when $qd \sim \pi$. Since the velocity of sound in the solid is nearly twice that of the fluid, when the acoustic excitation involves a larger proportion of solid spheres due to an increased ϕ, the velocity will increase.

As qd increases still further, the solid and liquid regions can behave increasingly independently, as more sound wavelengths fit into each region. The sound velocity of the higher frequency mode decreases, approaching the velocity in the pure liquid phase. This suggests that the velocity of this mode is increasingly dominated by that of the fluid, implying that the excitation is trapped to a grater extent in the fluid by the large impedance mismatch with the solid. Ultimately, at very large qd, a sufficient number of sound wavelengths can fit into each of the individual phases, and two distinct modes can be expected, corresponding to the velocities in the pure solid and pure fluid phases. This is exactly what is observed with the larger spheres at the largest scattering angles, corresponding to $qd \sim 25$. Presumably the dominant contribution to the Brillouin scattering is from the portion of the excitation in the liquid, where the compressibility is larger, leading to a larger scattering amplitude.

While the high frequency mode reflects sound propagation through both the

liquid and the solid as might be expected for a composite medium, the lower frequency mode can not reflect this type of behavior. Its frequency corresponds to a sound velocity that is even lower than that of the index-matching fluid, the lowest sound velocity in a pure phase of the composite system. Furthermore, the frequency decreases as the volume fraction increases. The only slower propagating sound mode in a system comprised of a solid and a fluid is a Stonely wave, which is a propagating mode confined to an interface between a solid and a fluid[10]. It is analogous to a Raleigh wave which is a propagating mode confined to the interface of a solid and a vacuum. The existence of a Stonely wave requires a shear modulus in the solid. It consists of both longitudinal and transverse components in the solid with a purely longitudinal component in the fluid. Its magnitude decays exponentially away from the interface, both in the fluid and in the solid. Using the known longitudinal and transverse velocities in bulk PMMA and the measured velocity in the fluid, we calculate the velocity of the Stonely wave on a flat interface to be about 950 m/sec. As shown in Fig.6.7, this corresponds remarkably well to the velocity measured at high qd for the larger spheres, where the interface is nearly flat. At smaller qd, where the wavelength is more nearly comparable to the size of the spheres, the measured value of Q implys that the excitation propagates over distances larger than a single sphere. Thus, at low qd, this mode must represent some form of coupled Stonely wave where the longitudinal component in the fluid couples the excitation between adjacent spheres. This accounts for the fact that the splitting between the two modes is less for a given volume fraction of the larger spheres than for the same volume fraction of the smaller spheres. The average distance between the spheres scales with the sphere size, and thus the coupling between adjacent spheres through the exponentially decaying longitudinal fluid portion becomes more difficult with increasing sphere size. This accounts for tha inexact scaling of the data from different sphere sizes. Finally, in the region of low

qd, the scattering of the wave from the different spheres becomes more significant. This accounts for the softening of the mode around $qd \sim 2\pi$, near the peak in the structure factor. Furthermore, the large degree of scattering of this mode is also reflected in the low values of the Q factor, as shown in Fig.6.8.

There have been some previous experimental studies of sound propagation in similar systems, usually using glass rather than polymer spheres[1]. Typically these studies used ultrasonic techniques to measure the actual propagation of sound through the system, and usually they were restricted to sound wavelengths that were small compared to the size of the spheres. Thus, two modes were never seen. In addition, there have been some theoretical treatments of sound propagation through hard sphere systems that used multiple scattering formalism[11]. and were intended to extend into the qd regime studied here. However, these studies did not include a shear modulus for the solid spheres, and thus did not predict the existence of two modes, since a shear modulus is required for a Stonely wave to exist. More recently, numerical calculations on a two dimensional system of disks embedded in a fluid have included the shear modulus for the solids[12]. They have predicted the existence of two modes, in remarkable agreement with the experimental observations reported here. Furthermore, the predicted behavior of the two modes is similar to that observed: the lower frequency mode is predominantly an interfacial mode comprised of a transverse component in the solid, while the higher frequency mode is an longitudinal mode that extends through the bulk of both the fluid and the solid, and is increasingly confined to the fluid at higher qd.

6.5 Conclusion

In this paper, we have presented the results of a study of sound propagation through a suspension of hard sphere colloids. We use PMMA spheres immersed in an index-matching fluid, eliminating any multiple scattering of light. This enables

us to use Brillouin scattering to measure the thermally excited sound waves in the system. By varying the scattering angle, as well as the sphere size, we are able to probe the frequency of the propagating acoustic modes over values of qd extending from about 1 to 25, corresponding to sound wavelengths that are much larger than the size of the spheres, to those that are equal to the size of the spheres, finally to those that are much smaller than the size of the spheres. Surprising results are obtained. Even though the continuous phase is a fluid, and thus can support only single propagating longitudinal mode, two distinct acoustic modes are found for $qd > \pi$. The velocity of the higher frequency mode lies between that of the pure solid and the pure liquid phases, and increases with the volume fraction of spheres. By contrast, the velocity of the lower frequency mode lies below that of the slowest velocity of a pure phase, that of the index-matching fluid, and the velocity *decreases* as the volume fraction of the spheres increases. As qd increases still further, the velocity of the higher frequency mode decreases, asymptotically approaching that of the pure fluid at very high qd. In addition, at these high qd, a weak new mode appears in the spectra corresponding to the velocity of sound in the pure solid PMMA phase. By contrast, at high qd, the velocity of the lower frequency mode is approximately constant. Finally, in all cases, the modes are longitudinal, as confirmed by the absence of any depolarized Brillouin scattering.

We interpret the higher frequency mode as an excitation that propagates within both the liquid and the solid phases, as expected for a composite medium. As the volume fraction of solids increases, the excitation is increasingly within the solid phase, accounting for the increase in the velocity with increasing ϕ. However, as qd increases, more wavelengths of sound can fit into each of the individual phases, and the acoustic impedance mismatch between the liquid and the solid forces the excitation to be increasingly confined to the liquid phase, thus decreasing the velocity as qd increases.

We interpret the lower frequency mode as an interface or Stonely wave, which is the only mode that can propagate at a velocity slower than the velocity in the pure fluid. This mode is confined to an interface between a solid and a fluid, and consists of longitudinal components in both the liquid and the solid as well as a transverse component in the solid. Its amplitude decays exponentially away from both the solid and the liquid interfaces, confining the excitation to the surface. However, this excitation must propagate between adjacent spheres and thus must be coupled through the longitudinal portion in the fluid.

These hard sphere colloid systems have been of great interest recently because of their fascinating phase behavior. The results of this paper suggest that their high frequency dynamic properties, as evidenced by the propagation of acoustic waves through the systems, also exhibits fascinating behavior.

References

[1] L. Shwartz and T. J. Plona. **J. Appl. Phys.** 55, 3971 (1984)

[2] P. N. Pusey and W. Van Megen. **Nature.** 320, 340 (1986)

[3] J. Liu, L. Ye, D. A. Weitz and P. Sheng. to be published.

[4] Z. Hashin. **J. Appl. Mech.** 29, 143 (1962)

[5] P. Sheng. in **Homogenization and Effective Modulii of Materials and Media** ed. J.L. Ericksen, D. Kinderleher, R. Kohn and J.L. Lions (*Springer – Verlag, N.Y.*) p.196 (a983)

[6] M. A. Biot **J. Acoust. Soc. Am.** 28, 168 (1956); 28, 179 (1956);

[7] T. J. Plona **Appl. Phys. Lett.** 36, 259 (1980)

[8] J. Beamish, A. Hikata and C. Elbaum. **Phys. Rev.** B27, 5848 (1983)

[9] M. Y. Zhou and P. Sheng. **Phys. Rev.** B39, 1202 (1989); P. Sheng and M. Y. Zhou. **Phys. Rev. Lett.** 61, 1591 (1988)

[10] L. M. Brekhovskikh. **Waves in Layered Media.** *Academic Press, N.Y.*, (1980)

[11] L. M. Shwartz and D. L. Johnson. **Phys. Rev.** B30, 4302 (1984)

[12] X. D. Jing, P. sheng and M. Y. Zhou. to be published.

Chapter 7

RELAXATION

OF OPTICAL PHONONS IN C-Ge

We report here the use of time resolved Raman scattering[1] to measure the decay rate, $1/\tau$, of the population of nonpolar optical phonons in a crystal[2,3]. The relaxation rate $1/\tau$ of a nonequilibrium population of zero center TO phonons in crystal germanium is obtained by measuring the decay of the intensity of spontaneous anti-Stokes Raman scattering from two picosecond laser pulses as the pulse separation is increased. Also the $1/\tau$ is the difference between the rate, $1/T_1'$, of the breakup of optical phonons into two or more phonons and the inverse processes which replenish the phonon populatoin. The lifetime contributions to the Raman linewidth, $\Delta\nu$, is $\Delta\nu = 1/2\pi T_1'$. A comparison of the temperature dependence of linewidth $\Delta\nu_l$ measured by Menendez and Cardona[4] with $\Delta\nu$ shows that the line is homogeneously broadened and is the sum of a lifetime and pure dephasing contributions due to scattering of the phonon k vector by isotopic disorder, $\Delta\nu = \Delta\nu_l + \Delta\nu_d$. The ability to resolve various contributions to the Raman linewidth can clarify the nature of phonon interactions.

Anharmonic interactions and disorder lead to phonon damping and to a distribution of frequency shifts which broaden the Raman scattering line. The damping itself has lifetime and pure dephasing contributions in which the phonon respectively scatters out of or within the homogeneous bandwidth produced by phonon relaxation. The direct measurements of phonon relaxation presented here demonstrate that, in general, time domain measurements are required to determine the contribution of various phonon relaxation processes to the Raman linewidth.

The detection of nonequilibrium optical phonons and the comparison of time resolved and steady state Raman scattering results is greatly facilitated by the

selective excitation of optical phonons near the zone center by optically excited electrons and holes. Young, Wan and Van Driel[3] have carried out measurements of phonon relaxation in Ge which are consistent with our results. They have pointed out that, even though the matrix element for the electron-phonon interaction via the deformation potential is independent of phonon k vector, the contraints of energy and momentum conservation result in the production of a sharply peaked distribution of phonons near the Γ point. The distribution is qualitatively similar to the distribution of polar phonons produced via the Frohlich interaction with a matrix element $\sim 1/q$. Thus, though the weighted average of the increase in the occupation n of optical phonons is less than .3 for a single pair of pulses at the highest powers used in our experiments, the change in n, Δn, near the Γ point can be as large as 5 at low temperatures and is readily observable. On the other hand, the phonon lifetime measured in the pulse experiment is due to anharmonic processes involving lower energy phonons far from the Γ point, for which Δn is much less than the thermal occupation. The lifetime measurements should therefore not depend upon phonon excitation levels and indeed $1/\tau$ is found to be independent of laser power up the highest powers used in these experiments. The lifetime broadening is therefore determined by the thermal distribution of phonons and can be compared to the low power cw Raman scattering linewidth. By contrast the total Raman scattering linewidth is expected to be power dependent over the range of powers used, though power broadening of the linewidth measured with a picosecond laser was not observed with the low resultation used here.

In light of our results, we examine the widely held assumption that the Raman scattering linewidth of optical phonons in crystals directly yields the lifetime of the zone center phonons via the uncertainty relation. This assumption is consistent with time resolved spontaneous Raman scattering measurements in GaAs at 77 K° performed by Von der linde, Kuhl and Klingenberg[1]. They found that the

relaxation rate of the nonequilibrium phonon population, $1/\tau$, is proportional to the full Raman linewidth at half maximum $1/\tau = 2\pi\Delta\nu$. Moreover, an uncertainty relation holds generally in the case of coherent scattering from coherently excited vibrations, such as is observed in stimulated Raman scattering[5,6] or in coherent anti-Stokes Raman scattering (CARS)[7,8]. In such experiments the scattered wave following a short excitation pulse is the coherent sum of the scattered components of the Raman line and is thus the Fourier transform of the line.

In contrast to longstanding usage, our results demonstrate that lifetime broadening is proportional to $1/T_1'$, the rate of scattering of phonons out of the zone center: $\Delta\nu_l = 1/2\pi T_1'$ [9]. It has a different temperature dependence than $1/\tau$ which includes the inverse process involving the scattering of thermally occupied phonons into the Γ point phonon and thus reduces the overall decay rate. However, the inverse process does not contribute to the Raman linewidth since it is incoherent and cannot, therefore, restore phase coherence.

The experiment is performed using a cavity dumped rhodamine 6G dye laser synchronously pumped by a Kr^+ laser. The appratus set up is shown in Fig 2.3. The laser pulse at photon energy E=2.08 eV has an autocorrelation half-width at half maximum of 2.3 ps. The laser output is split into two beams of equal intensity, one of which is delayed using a computer controlled translation stage. The beams have the same polarization and are focused onto the $< 111 >$ surface of Ge with a spot diameter of 15 μm. The orientation of the light polarization relative to the crystal axes is not known. The Raman scattered light is polarized with a ratio of 8 : 1 along the direction of polarization of the incident beam. The overlap and focus of the beams was confirmed using a pinhole. The total back-scattered light is collected and dispersed in a Spex Triplemate monochromator. An optical multichannel analyzer is used to determine the Raman spectrum which is identical to that observed in cw Raman scattering within the 5 cm^{-1} resolution of the

spectrometer. The relaxation of phonon population is monitored by detecting the anti-Stokes Raman intensity with photon counting electronics as the delay between the pulses is varied. The relaxation rate is found to be independent of pulse energy incident on the sample which was varied from 0.05nJ to 2nJ both by using neutral density filters and by changing the cavity dumping rate from 0.8 to 40MHz.

Photo-excited electron-hole pairs have an excess energy above the bandgap of $E - E_g = 1.3$ eV, which is 35 times the optical phonon energy of $h\nu_o = 36$ meV. Assuming that the carriers give up all their excess energy to optical phonons, and neglecting diffusion effects the average phonon occupation number can be estimated as

$$n = (\frac{\Phi\alpha}{N})\frac{E - E_g}{h\nu_o}(1 - R) \tag{7.1}$$

Where Φ is the photon fluence of a single pulse, $\alpha = 10^5$ cm^{-1} is the absorption coefficient, N is the density of optical phonon modes and R =0.36 is the reflectivity. For a 2nJ incident pulse, this estimate gives $n \simeq 0.3$. From the ratio of Stokes to anti-Stokes Raman scattering intensity $\frac{n+1}{n}$ we determine that $n \geq 5$ at 105 K° and $n \simeq 2.5$ at room temperature, indicating that n is indeed peaked near the Γ point. The lifetime observed at T = 105 K° is independent of excitation pulse energy over a range corresponding to initial carrier densities from 1×10^{18} to 2×10^{20} cm^{-3}. The density would be due by diffusion out of the excitation region. This indicates that neither heating nor carrier screening and scattering affect the measured lifetime over this range.

The Raman spectrum consists of the TO phonon mode at 303 cm^{-1} and a weak background. This background does not depend on pulse separation and is presumably hot luminescence. The interaction between the two beams is used to monitor the nonequilibrium phonon population. The anti-Stokes Raman intensity as a function of pulse delay is a single symmetric peak, as shown in Fig.7.1. As the pulse separation increases the anti-Stokes Raman intensity decays exponentially

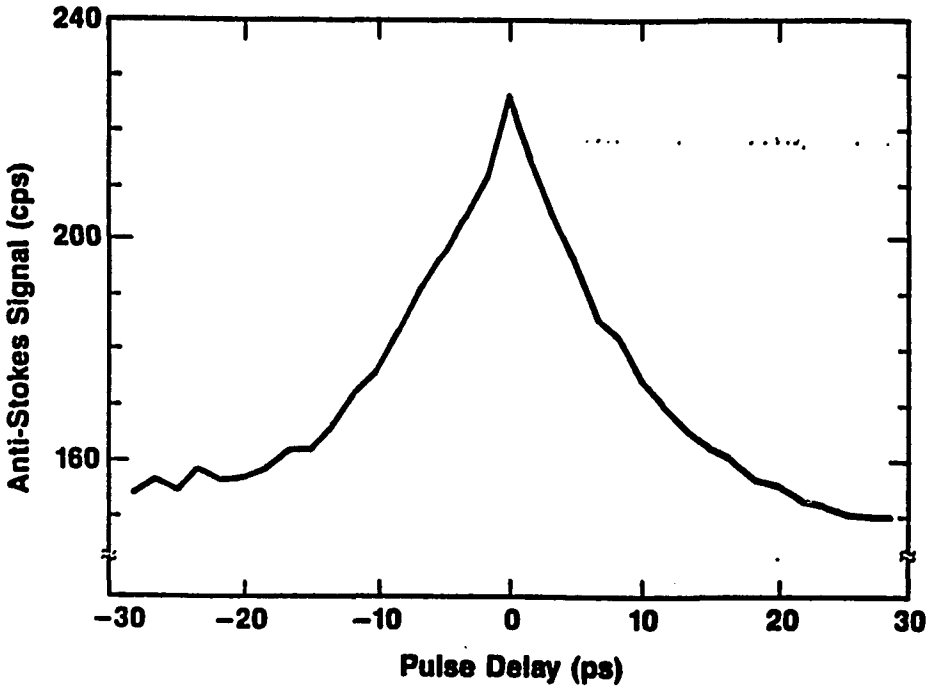

7.1 The intensity of anti-Stokes Raman signal as a function of probe pulse delay in ps.

towards a constant background caused by scattering from each of the pulses independently. This decay is plotted for 105 K° and room temperature in Fig.7.2.

Also shown as the dashed curve is the autocorrelation profile of the excitation pulse. The solid lines are fits to the data obtained by convolution of the excitation profile with exponentials with decay times $\tau = 8$ ps at 105 K° and $\tau = 5$ ps at 300 K°. These times are the best fit to the data to within an uncertainty of 0.5 ps and represent the time in which the excess optical phonon population at the Γ point decays. A larger uncertainty is found between different runs at the same temperature. The values of $1/\tau$ verses T and the total uncertainty are plotted in Fig.7.3.

The temperature dependence of phonon relaxation can be estimated by assuming that it is dominated by three phonon processes in which Γ point phonons at ν_o couple to phonons with combination frequency $\nu_1 + \nu_2 = \nu_o$, which corresponds to the largest peak in the joint density of states. The neutron scattering data of Nilsson and Nelin[10] indicates that the main contribution comes from pairs of LA-LO phonons belonging to the Q branches and from nearby regions of the Brillouin zone with $\nu_1 = 0.35\nu_o$ and $\nu_2 = 0.65\nu_o$ [4]. The relaxation of net phonon population is described by

$$\frac{dn_o}{dt} = \frac{-1}{\tau(0)}[n_o(1+n_1)(1+n_2) - n_1 n_2(1+n_o)] \qquad (7.2)$$

Where n_i is the occupation of phonons with energy $h\nu_i$ and $1/\tau(0)$ is the relaxation rate at $T = 0$. The equilibrium rate for n is the factor multiplying n on the r.h.s. of eq. (6.2)

$$\frac{1}{\tau(T)} = \frac{1}{\tau(0)}(1 + n_1 + n_2) \qquad (7.3)$$

Using the thermal equilibrium values for n_1 and n_2, eq. (7.3) is fit to the experimental results shown as the lower curve in fig. 6.4 with $\tau(0) = 12 \pm 1 ps$.

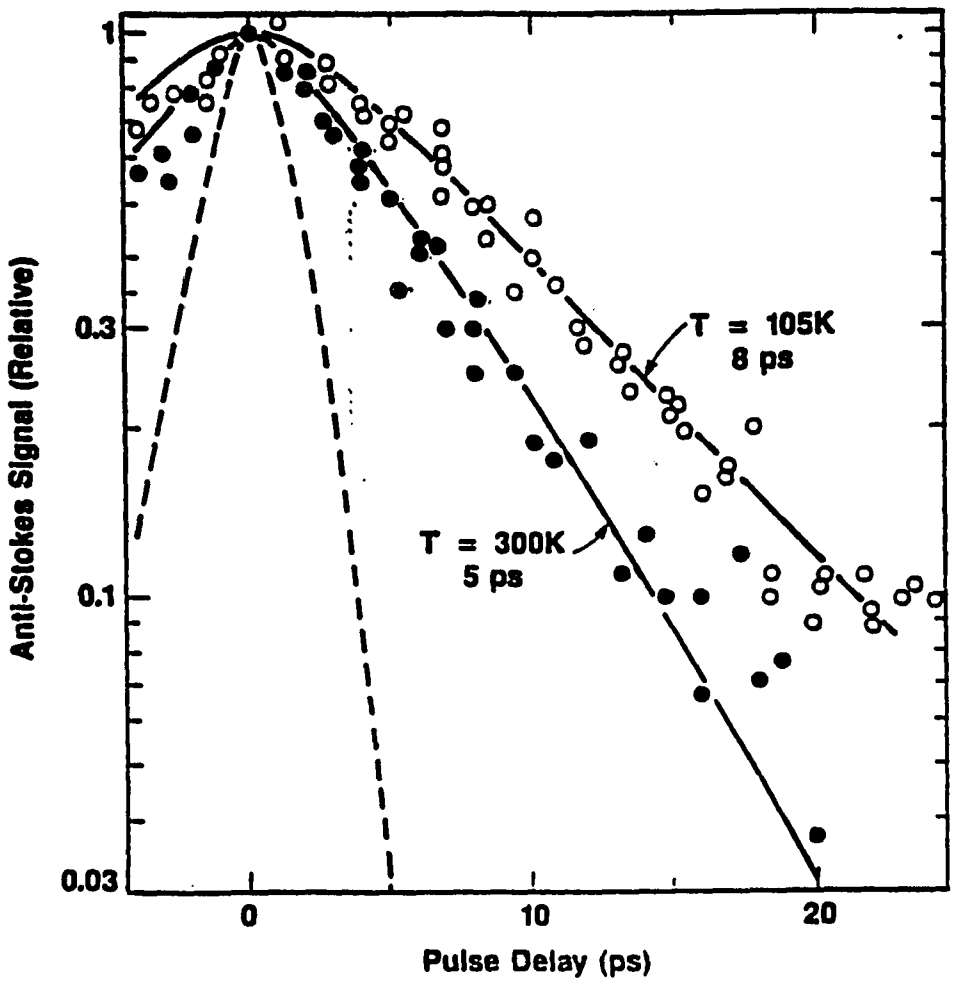

7.2 Difference between anti-Stokes signal and background at $105K°$ and $300K°$. The difference signal at the peak is as large as 50% of the background. The dashed line is the measured excitation pulse autocorrelation profile. The solid lines are convolutions of this profile with exponential decays of the lifetime shown.

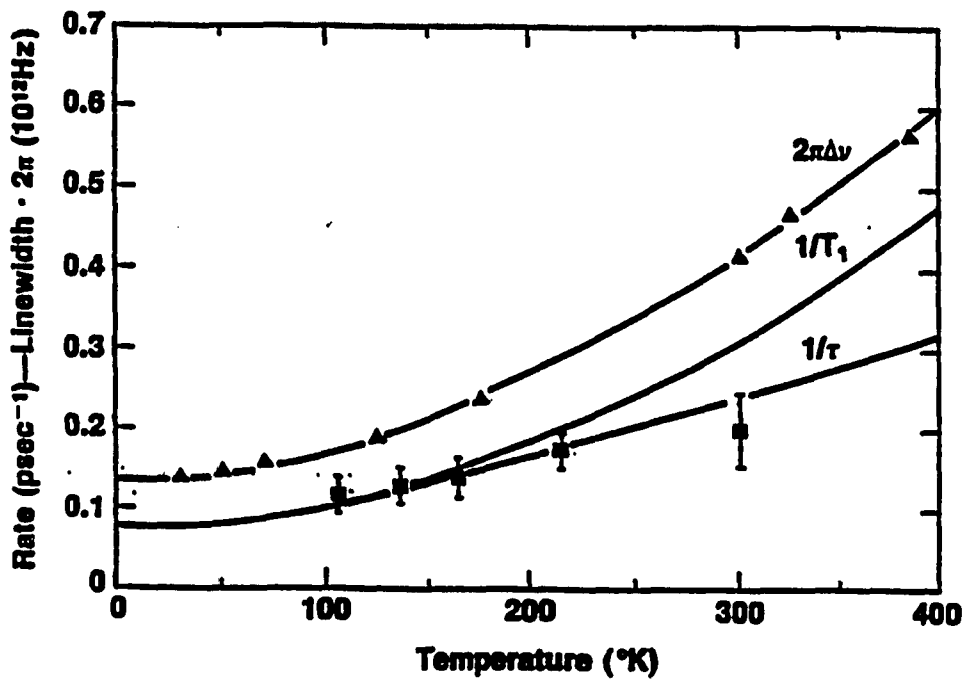

7.3 The squares are measured values of the population decay rate $1/\tau$ and the triangles are $2\pi\Delta\nu$ using the Raman scattering linewidth from ref. 4. The lower line is a fit of $1/\tau$ to eq. (7.3), the middle line is a plot of $1/T_1'$ given by eq. (7.4), and the upper line is a fit of $2\pi\Delta\nu = 2/T_2$ to eq. (7.6).

This lifetime is an order of magnitude longer than calculated by Cowley[11] who used a shell model description of the harmonic Hamiltonian. The use of a more accurate adiabatic bond charge model by WebeR[12], which is in good agreement with phonon dispersion measured by neutron scattering, would improve the calculation of the phonon relaxation time[4].

The scattering rate of phonons out of the Γ point, $1/T_1'$, does not include the reverse process and is given by

$$\frac{1}{T_1'} = \frac{1}{\tau(0)}(1+n_1)(1+n_2) \tag{7.4}$$

This is plotted as the middle curve in Fig.7.3 and is proportional to the lifetime contribution to the Raman linewidth. The triangle in Fig. 7.3 corresponds to $2\pi\Delta\nu$ where $\Delta\nu$ is the Raman linewidth measured by Mendez and Cardona[4]. A comparison of phonon relaxation rates and the Raman linewidth in Fig.7.3 reveals that the Raman linewidth may be expressed as the sum of $\Delta\nu_l$ and a weakly temperature dependent contribution which corresponds to an additional broadening of the Raman line of 0.31 cm^{-1} at T=0.

Inhomogeneity due to impurities ($10^{16}/cm^3$) or to crystal defects are at too low a level in these Ge samples to cause observable broadening. Nor can the relaxation of wavevector conservation, which allows the photon to probe a larger portion of the Brillouin zone, account for the broadening observed. Though broadening in semiconductors can be as large as 10 cm^{-1} for 50 Å microcrystallities[13–15], it is expected to drop as $1/L^2$, where L is the spatial extent of the region probed, because the band is parabolic near Γ point. Assuming $L \simeq \alpha^{-1} \simeq 1000$Å, this source of broadening should be smaller than 0.1 cm^{-1} in Ge.

A significant broadening mechanism is the isotopic mixture of naturally occuring Ge (Ge^{70} 20.5%; Ge^{72} 27.4%; Ge^{73} 7.8%; Ge^{74} 36.5%; Ge^{76} 7.8%). This can be calculated from the variation in the local vibration frequency which

has approximately the same fractional variational as $M^{-\frac{1}{2}}$, where M is the sum of the atomic mass in a unit call. This gives a structured distribution of local mode frequencies due to isotopic disorder for the optic mode which can be crudely characterized by a half width, D=6 cm^{-1}. Since the phonon bandwidth of 2B=150 cm^{-1} is much larger than the disorder, the vibrational mode is extended and substantial averaging of the disorder occurs. Consequently, disorder broadening is dynamical in origin, related to the rate of phonon scattering by local disorder, rather than static and related to the broad distribution of local mode frequencies.

The presence of structural and isotopic disorder in molecular crystals at low temperature has been shown to give rise to asymmetrical line shapes[16] and a non-exponential decay of CARS signals[7] from Frenkel excitons. Such asymmetry disappears at high temperatures and should not be significant in the Raman linewidth of Ge because of substantial lifetime broadening even at T=0, but the influence of disorder still contributes to the linewidth. Disorder leads to scattering of phonons into states of different k vector but the same energy. Such scattering is sometimes referred to as pure dephasing because it does not influence τ since all k vector states at the same energy are presumably equally populated by the initial incoherent excitation.

Klafter and Jortner[17] calculated the optical lineshape for a Gaussian distribution of site energies with standard deviation D at the edge of a band. In the framework of this theory, the disorder broadening, $\Delta\nu_d$, in the case that $\Delta\nu_l \geq \Delta\nu_d$ is given by perturbation theory as $\Delta\nu_d = 2\pi D^2\rho(\nu)(n_o + 1)$ where $\rho(\nu)$ is the density of phonon states. The Raman scattering linewidth is then the sum of lifetime and disorder contribution, $\Delta\nu = \Delta\nu_l + \Delta\nu_d$.

The density of states at the Γ point vanishes in the absence of broadening. However, phonon broadening smears the density of states to give a finite value at the Γ point, which can be approximated by averaging the density of states for

a parabolic band, $\rho(\bar{\nu}) = 3\nu^{-\frac{1}{2}}/4B^{\frac{3}{2}}$, where $\bar{\nu}$ is the frequency offset from the Γ point, over a frequency range $\Delta\nu$. The effective density of states, including the threefold degeneracy at the Γ point, is thus, $\bar{\rho} \simeq \frac{3}{\Delta\nu}\int_0^{\Delta\nu} \rho(\bar{\nu})d\bar{\nu} - (\Delta\nu)^{\frac{1}{2}}/B^{\frac{3}{2}}$. The contribution to the linewidth of isotopic disorder can then be approximated by substituting $\bar{\rho}$ for $\rho(\nu)$. This gives

$$\Delta\nu_d \simeq \frac{2\pi D^2(\Delta\nu)^{\frac{1}{2}}(n_o+1)}{B^{\frac{3}{2}}} \tag{7.5}$$

Taking D = 6 cm^{-1}, B = 75 cm^{-1} and the linewidth at T=0, $\Delta\nu = 0.75$ cm^{-1} gives $\Delta\nu_d = 0.3$ cm^{-1}, which is fortuitously close to $(\Delta\nu - \Delta\nu_l) = 0.31$ cm^{-1}. Broadening due to disorder depends upon temperature through the factor $(\Delta\nu)^{\frac{1}{2}}(n_o+1)$ in eq. (6.5). The total linewidth in the limit $B >> D$ and $\Delta\nu_l \geq \Delta\nu_d$ is the sum of lifetime and disorder broadening and may be expressed as

$$\Delta\nu = \Delta\nu_l + A(\Delta\nu)^{\frac{1}{2}}(n_o+1) \tag{7.6}$$

The fit of this equation to the Raman scattering linewidth data is shown in Fig.7.3 with A = 0.37 $cm^{-\frac{1}{2}}$. This result shows that the Raman scattering linewidth is dynamically broadened. It can therefore be expressed as $\Delta\nu = 1/\pi T_2$ where $1/T_2$ is the relaxation rate of vibrational phase coherence given by $1/T_2 = 1/2T_1 + \gamma$ [9], where $\gamma = \pi\Delta\nu_d$ is the rate of pure dephasing associated with scattering of the k vector of phonons near the Γ point by isotopic disorder.

It still remains to explain the observation of a lifetime limited Raman scattering linewidth in GaAs. The influence of disorder is smaller in GaAs than in Ge because As has a single isotope and Ga has two isotopes (Ga^{69} and Ga^{71}) with a difference in mass which is less than the width of the distribution in Ge. The discrepancy between lifetime broadened linewidth and the total linewidth is therefore small and within the uncertainty in the experimental value of $\tau = 7\pm1$ ps in GaAs at 77 K^{o}[1].

In conclusion measurements of the temperature dependence of phonon population relaxation in Ge show that the Raman scattering linewidth is dynamically broadened and can be separated into a lifetime limited component and a component due to pure dephasing resulting from wave vector scattering by isotopic disorder. The lifetime limited component is shown to be strictly proportional to $1/T_1$ rather than the measured rate $1/\tau$. Since isotopic broadening can be significant, the phonon lifetime can only be inferred from measurements of the Raman scattering linewidth of isotopically pure crystals.

References

[1] D. Von der Linde, J. Kuhl and H. Klingenberg. **Phys. Rev. Lett.** 44, 1505-1508 (1980)

[2] L. Ye, C. B. Roxlo and A. Z. Genack. **Bull. Amer. Phys. Ksoc.** 32, 934 (1987)

[3] J. F. Young, K. Wan and H. M. Van Driel. **Soli. Sta. Elec.** 31, 455-458 (1988)

[4] J. Menendez and M. Cardona. **Phys. Rev.** B29, 2051-2059 (1984)

[5] R. R. Alfano and S. L. Shapiro. **Phys. Rev. Lett.** 26, 1247-1251 (1971)

[6] A. Lauberau, D. Von der Linde and W. Kaiser. **Phys. Rev. Lett.** 27, 802-806 (1971)

[7] I. I. Abram, R. M. Hochstrasser, J. E. Kohl, M. G. Semack and D. White. **J. Chem. Phys.** 71, 153-162 (1979)

[8] T. J. Kosic, R. E. Cline, and D. D. Dlott. **Chem. Phys. Lett.** 103, 109-115 (1983)

[9] R. M. Macfarlane, A. Z. Genack and R. G. Brewer. **Phys. Rev.** B17, 2821-2826 (1978)

[10] G. Nilsson and G. Nelin. **Phys. Rev.** 3, 364-369 (1971)

[11] R. A. Cowley. **J. Phys.** (Paris) 26, 659-665 (1965)

[12] W. Weber. **Phys. Rev.** B15, 4789-4803 (1977)

[13] G. Kanellis, J. F. Morhange and M. Balkanski. **Phys. Rev.** B21, 1543-1548 (1980)

[14] Z. Iqbal, Seprek, A. P. Webb and P. Capezzuto. **Solid State Comm.** 37, 993-996 (1981)

[15] H. Richter, Z. P. Wang and L. Ley. **Solid State Comm.** 39, 625 (1981)

[16] D. M. Burland. **J. Chem. Phys.** 59, 4283 (1973)

[17] J. Klafter and J. Jortner. **J. Chem. Phys.** 68, 1517-1526 (1978)